Characterization of two eukaryotic cytoskeletal proteins horizontally transferred to a cyanobacterium

DISSERTATION

zur Erlangung des akademischen Grades

doctor rerum naturalium

(Dr. rer. nat.)

im Fach Biologie

eingereicht an der

Mathematisch-Naturwissenschaftlichen Fakultät I

der Humboldt-Universität zu Berlin

von

Diplom-Biologe Arthur Guljamow

Präsident der Humboldt-Universität zu Berlin:
Prof. Dr. Jan-Hendrik Olbertz

Dekan der Mathematisch-Naturwissenschaftlichen Fakultät I:
Prof. Dr. Andreas Herrmann

Gutachter:
1. Prof. Elke Dittmann-Thünemann
2. Prof. Conrad W. Mullineaux
3. Prof. Harald Saumweber

Tag der mündlichen Prüfung: 21. Oktober 2011

Abstract

The cyanobacterium *Microcystis aeruginosa* PCC 7806 expresses two unique proteins that show a very high degree of sequence identity with key components of the eukaryotic cytoskeleton. One is actin itself, the building block of microfilaments, the other is profilin, an important actin binding protein. Both proteins are remnants of a rarely observed horizontal gene transfer from eukaryotes to bacteria and their functions are unknown.

By employing a wide range of *in vivo* and *in vitro* methods in complementary experimental approaches, both proteins were characterized in great detail during the course of this work. The purification of both proteins after heterologous expression in *E.coli* allowed for the determination of key biochemical and structural parameters and the comparison with the eukaryotic archetype. In contrast to *bona fide* actin, for instance, its cyanobacterial counterpart does not inhibit DNase I. It forms polymers that can be visualized with labeled phalloidin, resembling eukaryotic actin in that respect. However, confocal laser scanning microscopy reveals key differences between polymers of eukaryotic and cyanobacterial actin. Whereas the former appear as thin cylindrical filaments about 100 µm in length, the latter are shorter and wider arresting polymerization at 5-10 µm. A more refined structural elucidation was achieved by Small-angle X-ray scattering showing that polymers of cyanobacterial actin are more ribbon-shaped.

Furthermore, this work shows fundamental differences between cyanobacterial and eukaryotic profilin. Restricted to actin monomer binding in eukaryotes, a number of experiments described herein show that cyanobacterial profilin decorates actin filaments. Additionally, confocal microscopy and SAXS suggest that cyanobacterial profilin mediates the bundling of cyanobacterial actin polymers into extended heteropolymeric sheets.

These co-polymers may be the basis of the large hollow enclosures observed in *E.coli* cells co-expressing GFP-labeled cyanobacterial profilin and actin. These hollow structures resemble the shell-like distribution of actin in *Microcystis aeruginosa* PCC 7806 and in colonies sampled from its original habitat, as shown in this work.

The findings of this work show that as part of the proteome of a natural bacterial community, both cyanobacterial proteins have gained properties unknown from their eukaryotic ancestors. Furthermore, the results have led to the hypothesis that the adaptation to the confined space of a bacterial cell devoid of binding proteins usually regulating actin polymerization in eukaryotes has driven the co-evolution of cyanobacterial actin and profilin, giving rise to an intracellular entity of potential structural relevance.

Deutsche Zusammenfassung

Das Cyanobakterium *Microcystis aeruginosa* PCC 7806 kodiert zwei Proteine, welche einen ungewöhnlich hohen Grad an Sequenzverwandschaft mit essentiellen Komponenten des eukaryotischen Zytoskeletts aufweisen. Bei einem dieser Proteine handelt es sich um Aktin, den Grundbaustein der Mikrofilamente, das andere ist Profilin, ein wichtiges Aktinbindeprotein. Beide Proteine resultieren aus einem selten beobachteten horizontalen Gentransfer von Eukaryoten zu Bakterien.

Unter Anwendung einer Reihe von *in vivo* und *in vitro* Methoden in einander ergänzenden experimentellen Ansätzen wurden beide Proteine im Verlauf dieser Arbeit detailliert charakterisiert. Die heterologe Expression in *E.coli* und die anschließende Aufreinigung beider Proteine erlaubten die Bestimmung charakteristischer biochemischer und struktureller Parameter sowie deren Vergleich mit bekannten eukaryotischen Vertretern. So inhibiert das cyanobakterielle Aktin im Gegensatz zu seinem eukaryotischen Verwandten zum Beispiel nicht das Enzym DNase I. Hingegen ähnelt es „echtem“ Aktin in der Hinsicht, dass es Polymere bildet, welche mit farbmarkiertem Phalloidin visualisiert werden können. Konfokale Laserscanning Mikroskopie offenbart jedoch grundlegende Unterschiede in den Polymerstrukturen. Filamente von eukaryotischem Aktin sind zylindrisch und erreichen typische Längen von 100 µm, wohingegen Polymere cyanobakteriellen Aktins eine Länge von 5-10 µm nicht überschreiten und zudem breiter sind. Detailliertere Strukturaufklärungen mittels Röntgen-Kleinwinkelstreuung zeigen, dass cyanobakterielle Aktinpolymere in ihrer Form am ehesten einem Band mit annähernd viereckigem Querschnitt ähneln. Desweiteren förderte diese Arbeit grundlegende Unterschiede zwischen eukaryotischem und cyanobakteriellem Profilin zu Tage. Während Profilin in Eukaryoten ausschließlich monomerisches Aktin binden kann, bestätigen verschiedene hier durchgeführte Experimente, dass sich cyanobakterielles Profilin an Aktinfilamente anlagert. Zudem deuten Erkenntnisse aus konfokaler Mikroskopie und Kleinwinkelstreuung darauf hin, dass

cyanobakterielles Profilin die Bündelung von cyanobakteriellem Aktin zu ausgedehnten Heteropolymeren vermittelt.

Diese Co-Polymere bilden möglicherweise die Grundlage für die verhältnismäßig großen, hohlen Einschlüsse, welche in genetisch modifizierten Stämmen von *E.coli* beobachtet werden konnten. Diese Zellen exprimierten sowohl ein Fusionsprodukt aus cyanobakteriellem Profilin und dem grün fluoreszierenden Protein GFP, als auch cyanobakterielles Aktin. Die dort beobachteten hohlen Strukturen erinnern an die hüllenartige Lokalisation von Aktin, welche sowohl für den *Microcystis aeruginosa* Stamm PCC 7806, als auch für *Microcystis* Kolonien aus dessen ursprünglichen Habitat in dieser Arbeit gezeigt wurden.

Die Erkenntnisse dieser Arbeit verdeutlichen, dass beide cyanobakteriellen Proteine als Teil der Proteinausstattung einer natürlich vorkommenden Bakterienpopulation Merkmale erworben haben, die ihre eukaryotischen Vorläufer nicht zeigen. Darüber hinaus konnte anhand der hier gewonnenen Ergebnisse folgende Hypothese aufgestellt werden: Die Anpassung an die begrenzten räumlichen Bedingungen einer Bakterienzelle, welche außerdem keine der für die Regulierung der Polymerisation notwendigen Aktinbindeproteine enthält, war offenbar die Triebkraft für eine Co-Evolution von cyanobakteriellem Aktin und Profilin. Dieser Prozess gipfelte möglicherweise in der Entstehung eines neuartigen intrazellulären Gebildes von potentiell struktureller Bedeutung.

Abbreviations

aa	amino acid
ABP	actin binding protein
ADF	actin depolymerizing factor
Amp	ampicillin
APS	ammonium persulfate
Arp	actin related protein
bp	base pair(s)
BSA	bovine serum albumin
CIAP	calf intestine alkaline phosphatase
Cm	chloramphenicol
CTAB	cetyl-trimethyl-ammonium-bromide
DTT	1,4-dithiothreitole
DMF	dimethylformamide
DNA	deoxyribonucleic acid
dNTP	any triphosphates of the naturally occurring coding deoxy-nucleosids
E. coli	*Escherichia coli*
EDTA	ethylene diamine tetra-acetic acid
EM	electron microscopy
F-actin	filamentous actin
FITC	fluorescein isothiocyanate
Fts	filamentous temperature sensitive protein
G-actin	globular, monomeric actin
HEPES	[4(2-hydroxyethyl)-1-piperazino]-ethanesulfonic acid
HGT	horizontal gene transfer
IFM	immunofluorescence microscopy
hsp	heat shock protein
IGS	intergenic spacer
IPTG	isopropyl β-D-1-thiogalactopyranoside
kb	kilo base pairs
kDa	kilo Dalton
Mbp	mega base pairs
mre	murein cluster e

MW	molecular weight
NCBI	The National Center for Biotechnology Information
nt	nucleotide
OD	optical density
ORF	open reading frame
PAA	polyacrylamide
PAGE	polyacrylamide gel electrophoresis
PCC	Pasteur Culture Collection
PCR	polymerase chain reaction
PEG	polyethylenglycol
pI	isoelectric point
PIP_2	phosphatidylinositol (4,5) bisphosphate
PMSF	phenyl-methyl-sulphonyl-fluoride
PVP	polyvinyl-pyrrolidon
RING-FISH	recognition of individual genes – fluorescence *in situ* hybridization
RNA	ribonucleic acid
rpm	rounds per minute
RT	room temperature
SAXS	small-angle X-ray scattering
SDS	sodium dodecyl sulfate
SSC	salt-sodium-citrate
TAE	tris-acetate-EDTA buffer
TEMED	*N*',*N*',*N*',*N*'-tetramethyl-ethylene-diamine
Tris-HCl	tris-(hydroxymethyl)-aminomethane-hydrochloride
UTR	untranslated region
UV	ultraviolet light
WASp	Wiskott-Aldrich-Syndrome protein
WT	wild type
X-Gal	5-bromo-4-chloro-3-indolyl-β-D-galactopyranoside

Table of contents

1 Introduction

The actin family of proteins is an evolutionarily ancient group whose ancestral genes can be traced back to the origins of life on Earth (Erickson, 2007; Pollard & Cooper, 2009). The first actins have presumably arisen from a primal protein marked by a bi-lobed, flexible structure and the ability to catalyze nucleotide hydrolysis. These, indeed, are the characteristics contemporary actins share with their distant relatives, the sugar kinases and the hsp70 heat shock proteins widely distributed throughout the tree of life (Bork et al, 1992). However, actins diverged from this line rather early in evolution by developing a substantially new trait: the self-aggregation into polymeric filaments. Being one of their signature features, it forms the basis for the remarkable functional versatility and the resultant extensive prevalence of actins in the living world. The adjustability of actin filament assembly, stability and outward appearance has consequently led to actins being utilized by numerous evolutionarily remote organisms for a multitude of key physiological processes.

1.1 Cytoplasmic actin in eukaryotes

1.1.1 General features

Eukaryotic actin is an essential protein that, apart from its prominent role in muscle contraction, is the building block of what is known as the microfilament cytoskeleton. Microfilaments are found in every eukaryotic cell where actin frequently is the most abundant protein species, typically found in concentrations between 0.2 mM and 0.5 mM (8 µg/µl – 20 µg/µl), making up 1-5% of the total protein amount of non-muscle cells (Lodish et al, 2000; Purich & Allison, 1999). Whereas unicellular eukaryotes usually encode and express only one actin gene, most vertebrates possess three tissue-specific isoforms, α-actin in muscle cells and the "non-muscle" β- and γ-actins, constituents of the cytoplasmic microfilaments (Bhattacharya & Weber, 1997; Drouin et al, 1995). Multicellular organisms usually encode multiple isoform

variants, quite frequently amounting up to 10 functional actin genes (Chang et al, 1984; Engel et al, 1982; Engel et al, 1981; Ponte et al, 1983). Warm-blooded vertebrates, for instance, typically express four different α-actins from a single copy gene each and contain multiple copies (totaling four to six) of the β and γ isoforms. Actins are among the most conserved proteins in evolution; α-actins from human, mouse, rat, rabbit and chicken are identical, sharing a 90% sequence identity with fission yeast actin. Plant actins tend to show a higher degree of sequence diversion with many plants possessing up to 100 different actin isoforms. The basis for this exceptional situation is poorly understood (An et al, 1999; Diaz-Camino et al, 2005; Kandasamy et al, 1999; McDowell et al, 1996).

The actin polypeptide is usually composed of about 375 amino acids and has a molecular weight of 43 kDa. After its discovery in skeletal muscle, a high-resolution structure of actin had long remained elusive, mainly because of difficulties obtaining crystals suitable for X-ray crystallography. Therefore, taking from low-resolution data, the monomeric, or "globular", form is referred to as "G-actin". However, as detailed atomic models have eventually become available, the organization of actin into one large and one small domain, forming a deeply divided, roughly "U-shaped" protein has become apparent (see **Figure 1.1A**) (Kabsch et al, 1990; Otterbein et al, 2001). Each of the two domains is further divided into two subdomains, with subdomain 1 and 2 forming the small domain and subdomains 3 and 4 representing the large domain (Kabsch et al, 1990). A nucleotide binding pocket and the binding site for a catalytic cation (Mg^{2+} *in vivo*) - both required for nucleotide hydrolysis - are situated at the bottom of the major cleft where the domains are connected by a flexible hinge region (Kabsch et al, 1990; Otterbein et al, 2001). Owing to this flexibility and in response to its association with its many binding partners, the actin molecule shows a great variability in surface structure and three-dimensional appearance, the most common of which being referred to as the "open" and the "closed" state (Dedova et al, 2002; Fujii et al, 2010; Pollard, 1999; Schutt et al, 1993; Schutt et al, 1995).

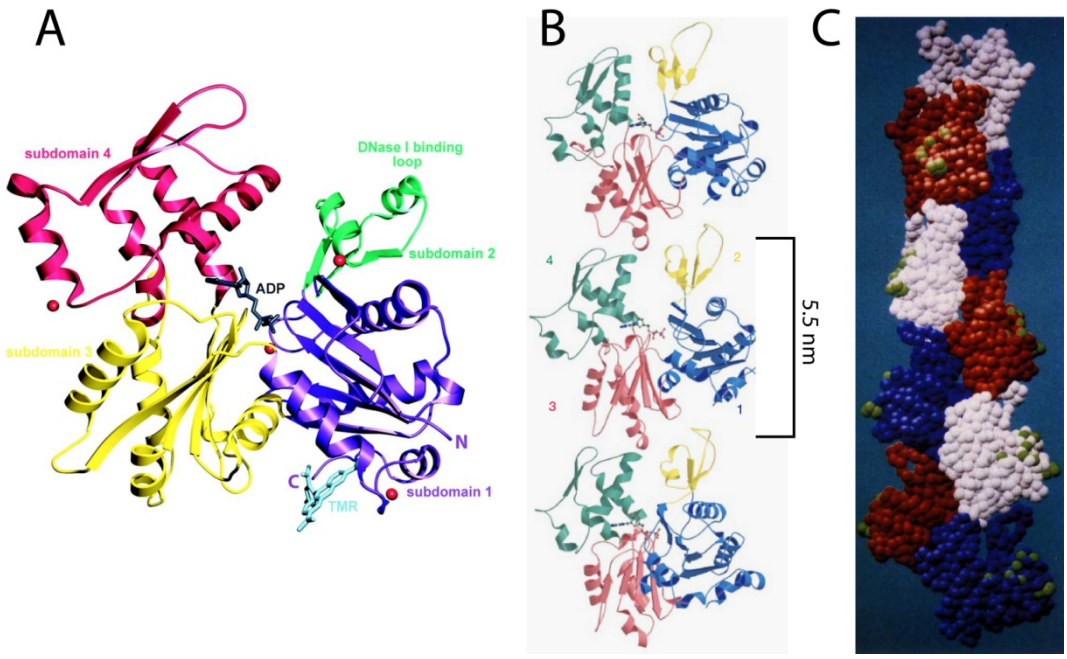

Figure 1.1. Atomic models of monomeric and filamentous actin.
A: Crystal structure of uncomplexed actin from rabbit skeletal muscle in the "conventional view". The four subdomains of actin are represented in different colors. The polypeptide chain termini are indicated. Four Ca^{2+} ions bound to the actin monomer in the crystals are represented as red spheres. Tetramethylrhodamine-5-maleimide (TMR) covalently attached to Cys374 binds in a hydrophobic pocket near the C-terminus. Adapted from Otterbein, 2001.
B: "Holmes" model of one F-actin protofilament. Subunit numbers and the axial repeat are indicated. Adapted from van den Ent et al, 2001.
C: The original "Holmes" model of F-actin as published in 1990 (Holmes et al, 1990) can be interpreted as two protofilaments winding around each other in a two-start right handed helix. Actin monomers are shown in individual colors. Each amino acid is represented as a sphere of 27 nm radius, green spheres represent potential myosin binding regions.

It has been know since its early description that solutions of G-actin spontaneously adopt a gelatinous, highly viscous state under physiological ion concentrations (Straub, 1942). This process can be reversed in a low-salt environment. Closer investigations have shown that these changes in viscosity are brought about by a dramatic reorganization of the actin structure: the linear assembly into polymeric fibers with a diameter of 7-9 nm (Cowieson et al, 2008; dos Remedios et al, 2003). Although the fibrous nature of so called "F-actin" has been established very early in the history of actin research, the determination of the exact physical dimensions and the orientation and conformation of the monomers in the filament pose a challenge to scientists even today. Structural data from low-resolution analyses such as small angle X-ray scattering (SAXS) of F-actin can be fit conveniently to a cylindrical model (Lepault et al, 1994; Norman et al, 2005). More refined low-resolution

models show that the cylindrical surface of the filament is periodically interspersed with structural entities protruding from the main longitudinal axis, confirming findings that were long known from electron microscopy data (Fujii et al, 2010; Hanson & Lowy, 1963; Moore et al, 1970). Although this information was taken as a clear indication for the helical nature of F-actin, definite experimental proof with atomic detail was long unavailable. The main obstacle in obtaining high-resolution structural data from crystallized filamentous material is the lack of precise contacts between filaments (dos Remedios et al, 2003; Hanson & Lowy, 1963). This inherent irregularity of oriented gels of F-actin does, on the one hand, produce characteristic fiber diffraction patterns which are, on the other hand inconclusive with regard to the atomic details of the structure. Therefore, the currently accepted atomic model of F-actin has originally been devised by combining the high-resolution structure of monomers and finding the best fit between its calculated fiber diffraction data and experimental findings (Holmes et al, 1990; Lorenz et al, 1993). According to this model, the actin filament consists of two protofilaments which align in parallel in the same orientation to wind together in a right handed helix forming a polar filament (see **Figure 1.1B and C**). Although this "Holmes model" has gained wide acceptance, a competing model based on crystallization data of G-actin and the actin binding protein profilin has been vibrantly discussed for a number of years (Schutt et al, 1993; Schutt et al, 1995). The observed co-crystals revealed a ribbon-shaped filamentous structure with actin-actin interactions that were proposed to be a representation of those found in F-actin. The "ribbon model" has mostly been regarded as biologically irrelevant and inferior to the helix model, however, with the lack of high-resolution structural data it could not be easily dismissed (Egelman, 1994; Orlova et al, 1994). Thus, it was only with the recent availability of high-resolution structures of F-actin that the helix model was ultimately confirmed (Fujii et al, 2010; Oda et al, 2009). Refinement of the fiber diffraction approach has yielded the first high-resolution model demonstrating that the actin monomers are in a flat and closed conformation in the filament as opposed to being twisted as in the G-actin crystals (Oda et

al, 2009). Another model obtained through cryoEM experiments is very similar and provides additional invaluable insight into the monomer-monomer contact sites showing, for instance, that the axial interactions are stronger than inter-strand bonds (Fujii et al, 2010).

The aggregation of G-actin *en route* to the filament always occurs in a specific head-to-tail fashion that seals the bound nucleotide inside the actin molecule. The formation of dimers and trimers is a comparably slow and rare process, however, if the assembly reaction is nucleated by pre-existing polymer ends, polymerization is rapid and consumes most of the free G-actin (Pollard & Cooper, 2009). Another important feature of the aggregation process is that the addition of subunits preferentially occurs at the end of the growing polymer that does not expose its bound nucleotide to the medium. This has two critical implications. First, actin filaments are polar structures and second, they have considerable differences in terminal elongation rates. This can be illustrated with the S1 globular head domain of myosin that binds to F-actin in a specific, tilted manner, yielding a characteristic arrowhead-like appearance with a "barbed" and a "pointed" end, as observed via electron microscopy (Woodrum et al, 1975). By conducting such "decoration" experiments with growing actin filaments it was shown that the assembly of monomers at the barbed end occurs up to 10 times faster than it does at the pointed end, where monomers dissociate from the polymer. This leaves the impression of a filament of roughly constant length moving in one direction (see **Figure 1.2**) (Pollard & Borisy, 2003; Pollard & Cooper, 2009). Moreover, as ATP-G-actin has a higher affinity for elongating filament ends than ADP-G-actin and the ATPase activity is activated upon polymerization, ADP-bound subunits are predominately situated towards the pointed end. The structural changes in ADP-actin monomers entail a lower affinity for the filament and they subsequently dissociate from its pointed end.

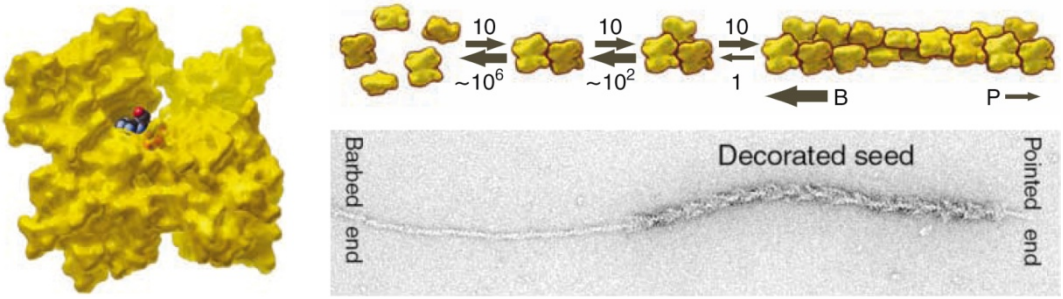

Figure 1.2. Nucleation, polymerization and treadmilling of polar actin filaments.
Model of G-actin (left) in the "conventional view" with the "barbed end" of the molecule facing down. Cartoon diagram of the spontaneous nucleation and polymerization dynamics of actin (top right). Dimers and trimers are very unstable, numbers and widths of arrows indicate relative equilibrium constants of respective reactions. Monomers are added much faster to the barbed end (B) than to the pointed end (P). Electron micrograph of F-actin decorated with myosin heads and elongated with ATP-G-actin (bottom right). Adapted from Pollard & Cooper, 2009 and Pollard & Borisy, 2003.

Free ADP-G-actin is then available for nucleotide exchange and another round of polymerization (Pantaloni et al, 2001; Pollard et al, 2000). This feature of actin filaments is known as "treadmilling" and it provides a means for the cell to generate directed force and do mechanical work (Theriot & Mitchison, 1991; Wang, 1985). The structural flexibility of actin filaments and the dynamic nature of the polymerization process provide an excellent foundation to regulate the overall appearance of the microfilament network. Consequently, actin filaments adopt a variety of higher-ordered structures and form an extended intracellular network essential for many fundamental cellular processes revolving around the two main tasks of maintaining a rigid scaffold and ensuring cell motility (Pollard & Cooper, 2009).

1.1.2 The functions of the eukaryotic actin cytoskeleton

1.1.2.1 The role of microfilaments in cell stabilization

Although the dense system of cellular actin filaments appears to be randomly distributed in the cytosol, close examination reveals a principal organization. *In situ* fluorescent labeling of F-actin shows bundled fibers aligned in a parallel fashion, spanning the cell's periphery where they play a structural role in maintaining cell shape (see **Figure 1.3A**). Special actin bundles, termed "stress fibers," provide mechanical support in cells that are in direct

contact with a solid substratum (Walcott & Sun, 2010). Such cells are attached to the external surface by special cortical regions called "focal adhesions" which are connected to the actin cytoskeleton through direct contact with the end of stress fibers. From the bundles at the cell's periphery, the network of microfilaments fans out into the cytosol to form a less dense three-dimensional network that gives the cytoplasm its gel-like properties.

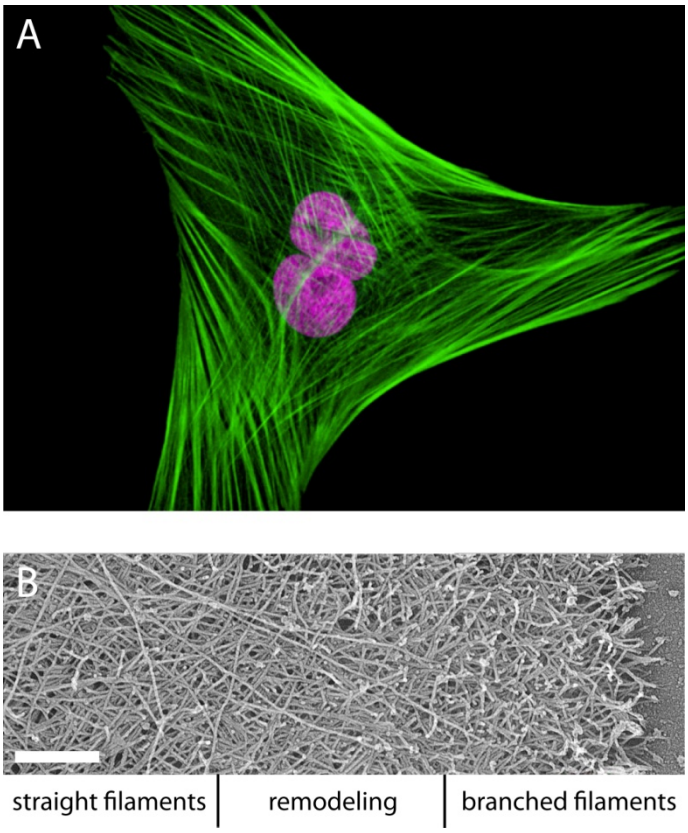

Figure 1.3. Visualizations of the microfilament network.
A: Fibroblast labeled with probes for actin and the nucleus. The actin cytoskeleton was visualized using phalloidin conjugated with green-fluorescent Alexa Fluor 488. The nucleus (purple) was stained with the TO-PRO-3 reagent. Adapted from www.invitrogen.com/site/us/en/home/References/Molecular-Probes-The-Handbook/.html
B: Transmission electron micrograph of the cortical region of a motile keratocyte. Regions with different filament organizations are indicated, branched filaments face the cell membrane. Scale bar: 500 nm. Adapted from Pollard & Borisy, 2003 and Svitkina & Borisy, 1999.

A much higher concentration of actin polymers is found in close vicinity to the inner face of the cell membrane (see **Figure 1.3B**). In this narrow cortex of the cell, microfilaments form a complex three-dimensional network which excludes most cytosolic organelles and is closely connected to the cell membrane via membrane-microfilament binding proteins (Svitkina & Borisy,

1999). These integral membrane proteins serve as attachment sites for the membrane to the cytoskeletal framework, thereby determining the distinctive shape of each cell (Kabsch & Vandekerckhove, 1992; Lodish et al, 2000).
Notwithstanding its essential structural role in determining and maintaining cell shape, the most intriguing property of the actin cytoskeleton is undoubtedly its ability to confer what has become known as "cell motility".

1.1.2.2 Cell motility

The term "cell motility" encompasses a variety of cellular processes involving the generation of mechanical force to move the whole cell or objects within. In eukaryotic cells, movement is generated in two principle ways: either by harnessing the force generated through the regulated assembly and disassembly of cytoskeletal elements or by employing motor proteins which move along filaments, carrying various cellular components along these tracks. The only known actin motor proteins belong to the large myosin family (Hodge & Cope, 2000). These multi-chain proteins share a specific overall structure, organizing the myosin complex into three characteristic functional units. The actin binding head domain harbors an ATPase activity, the adjacent neck domain plays a regulatory role for the head domain's function and the tail domain mediates myosin binding to various cellular structures. Myosins can "walk" along actin filaments in discrete steps harnessing the energy of ATP hydrolysis by the head domain. The most prominent example of force generation by actin and myosin is the process of muscle contraction in muscle tissue achieved by making long polar filaments of actin and myosin slide past each other in opposite directions. The same principle is applied in myosin-containing contractile stress fibers of non-muscle cells. During cytokinesis, actin and myosin accumulate at the cell's equator to form a contractile ring which forms the cleavage furrow and whose ingression into the cell's interior eventually leads to the separation of the two daughter cells (Scholey et al, 2003). While long distance intracellular transport of large cargo, such as organelles, is achieved by the microtubule system, short distance transport of smaller load such as membrane coated vesicles, proteins

and even nucleic acids within the peripheral regions of the cell is carried out by myosins moving along actin filament tracks (Boldogh & Pon, 2006; Estrada et al, 2003; Pollard & Cooper, 2009; Takizawa & Vale, 2000).

A remarkable property of many eukaryotic cells is the ability to move across a surface in an "amoeboid crawling" motion. Essentially, this is a three-step process of controlled rapid change of cell morphology: first, the membrane extends to form protrusions known as "pseudopodia". In the second phase, the pseudopodium attaches to the surface via focal adhesions and the protruding compartment rapidly fills with cytosol. Finally, the rear of the cell is detached from the surface and retracts in the direction of the cell's movement. The key event in cell locomotion is the directed forward movement of a defined patch of the membrane. This is achieved by a rapid elongation of the actin filaments of the cortical network of the respective region. Although the cortex filaments form a complex, cross-linked three-dimensional network, each fiber is generally oriented in the same way, with the barbed end facing the membrane. Upon stimulation, the cell initiates rapid addition of new subunits at these ends, generating enough mechanical force to push forward large portions of the membrane. To allow the interior of the pseudopodium to be filled with cytosol shortly after its attachment to the substratum, the underlying actin network quickly decondenses from the pointed ends. The same principle mechanism is employed by eukaryotic cells to engulf and absorb extracellular objects during endocytosis (Pollard & Borisy, 2003; Pollard & Cooper, 2009; Welch & Mullins, 2002).

The actin network's contrasting tasks of conferring both stability and motility are reconciled by the multitude of mechanisms eukaryotic cells have developed for precisely controlling the rapid rearrangement of well-defined portions of the network in space and time. It is apparent that these rearrangements cannot be provided by the chance fluctuations of the dynamic filaments alone. Instead, a concerted effort and interplay of many factors of control and regulation is required. That, essentially, is the task of the many actin binding proteins.

1.1.3 Actin binding proteins

For the control of the actin network architecture, eukaryotes employ more than 100 actin binding proteins (ABPs) (dos Remedios et al, 2003; Winder & Ayscough, 2005). These proteins are involved in virtually every step of the assembly process leading from single actin monomers to the specific shape of the filamentous network required to carry out its multiple functions. Generally, ABPs can be classified according to their capacity to either bind to actin monomers or filaments, although some ABPs are able to bind both (Winder & Ayscough, 2005).

1.1.3.1 Actin monomer binding proteins

1.1.3.1.1 Inhibitors and activators of actin polymerization

Under physiological conditions, free G-actin quickly polymerizes into F-actin (Pollard & Borisy, 2003). However, filaments near the leading edge of protruding membrane regions were found to elongate up to 250 times faster than observed at typical steady-state conditions while G-actin concentrations generally remain constant (Pollard & Borisy, 2003). Thus, cells must maintain a pool of "silent" actin monomers that can be rapidly recruited to elongate filaments if circumstances necessitate such. The protein thymosin β4 is believed to be the principal actin-monomer-sequestering protein, binding as much as 70% of all cellular monomeric actin, inhibiting nucleotide exchange and blocking polymerization (Hertzog et al, 2004; Paavilainen et al, 2004). Acting in a way similar to thymosin β4, the protein twinfilin suppresses nucleotide exchange and the inherent tendency of G-actin to polymerize (Palmgren et al, 2002).

To circumvent the thermodynamically unfavorable nucleation of polymerization by the formation of actin trimers, the cell utilizes nucleation factors such as Arp2/3 and formin. The Arp2/3 complex contains two actin related proteins that are believed to have evolved from an ancestral actin (Machesky et al, 1994; Mullins et al, 1996; Mullins et al, 1997; Schroer et al, 1994). Binding one actin monomer, the Arps form a stable trimeric nucleus

and a free barbed end primed for polymerization. The Arp2/3 complex also binds laterally to F-actin and is the main factor responsible for the generation of characteristical 70° branched filaments (Mullins et al, 1998). The nucleation activity of the Arp2/3 complex needs to be activated by members of the WASp family of proteins (Wiskott-Aldrich-Syndrome protein) which also bind G-actin and stimulate polymerization (Miki et al, 1998; Paavilainen et al, 2004; Pollard et al, 2000). Because of their multiple interactions with numerous proteins, WASp proteins are major intermediaries between the signaling pathways triggered by internal and external stimuli and the microfilament network (Paavilainen et al, 2004).

While the Arp2/3 complex mainly produces branched F-actin networks, formin is responsible for the formation of straight, unbranched actin filaments (Evangelista et al, 2003; Pollard & Cooper, 2009; Yang et al, 2007). Like most ABPs, formin contains multiple sites of interaction for many proteins. Binding two actin monomers, it nucleates filament formation and elongation. After that, it remains bound to the barbed end, prevents its capping and recruits further actin monomers (Xu et al, 2004).

1.1.3.1.2 Profilin

Another key G-actin-binding protein is profilin. Like thymosin β4 and twinfilin, this ubiquitously expressed protein specifically binds G-actin in a strict 1:1 molar ratio (Yarmola et al, 2008). However, profilin differs in one crucial aspect as it is a nucleotide exchange factor, facilitating the replacement of G-actin-bound ADP with ATP (Goldschmidt-Clermont et al, 1991; Witke, 2004). Since ATP-G-actin has a higher affinity for the elongating ends of filaments, the nucleotide exchange activity of profilin further promotes barbed end growth of F-actin (Vinson et al, 1998). Profilin very effectively recruits G-actin from the silent thymosin β4 pool and keeps it in a polymerization-prone state (Pantaloni & Carlier, 1993; Pollard & Borisy, 2003; Yarmola & Bubb, 2009). In fact, its name derives from its tendency to keep actin pro-filamentous (Carlsson et al, 1977). In the absence of free filament barbed ends, profilin merely sequesters G-actin and inhibits

spontaneous polymerization (Pantaloni & Carlier, 1993). The crystal structure of the 12-16 kDa profilin has been solved both in the uncomplexed and in the actin:profilin heterodimeric state (Chik et al, 1996; Eads et al, 1998; Schutt et al, 1993; Vinson et al, 1993). The residues involved in actin binding are well established, consistent with its high affinity for G-actin, profilin was found to make extensive contact with a hydrophobic cleft situated opposite the nucleotide binding site at the barbed end of the actin molecule (see **Figure 1.4A**) (Chik et al, 1996; Schutt et al, 1993). Profilin also interacts with the membrane-anchored phospholipid phosphatidylinositol (4,5) bisphosphate (PIP_2) and with poly-L-proline sequences found on many proteins (see **Figure 1.4B**) (Paavilainen et al, 2004; Pollard & Quirk, 1994; Schmidt & Hall, 1998; Witke, 2004). PIP_2-bound profilin is unable to bind G-actin, thus facilitating the release of actin monomers to the cortical regions which usually display high polymerization activity.

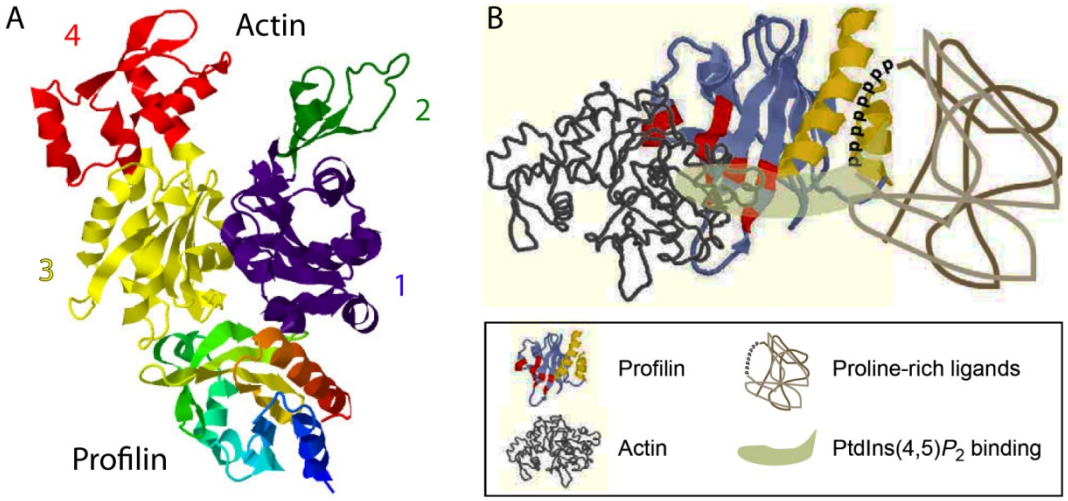

Figure 1.4. The crystal structure of profilin and its binding sites.
A: Crystal structure of a β-actin:profilin complex. Actin is shown in the "conventional view", numbers and colors indicate the subdomains. Modified from Chik et al, 1996, PDB code 1HLU.
B: Molecular model of the major binding sites on the profilin molecule. The binding sites for actin (red) and poly-L-proline (yellow) are distinct, whereas the phosphatidylinositol (4,5)-bisphosphate-binding area occupies a larger part of the surface of the molecule (light green). Adapted from Witke, 2004.

Phosphorylation of PIP_2 is regulated by a kinase/phosphatase system which is controlled by various signaling cascades responding to a broad range of stimuli. However, profilin also inhibits hydrolysis of PIP_2 by phospholipase C,

thereby providing a possible mechanism for feedback auto-regulation and further signal transduction to other target systems (Machesky et al, 1990). To accelerate F-actin polymerization in the cortical region, G-actin-profilin complexes are directed to the plasma membrane by high-affinity binding to a large number of membrane-associated signaling proteins through their poly-L-proline regions (Mahoney et al, 1997; Perelroizen et al, 1994; Witke, 2004). This is possible because the actin-profilin binding is not influenced by the interaction with poly-L-proline (Paavilainen et al, 2004; Witke, 2004). To date, more than 50 profilin ligands are known and this figure is steadily increasing. Thus, in addition to its crucial binding to G-actin, profilin is also one of the principle signal integrators and mediators at the interface of the cellular signaling system and the actin cytoskeleton (see **Figure 1.5**).

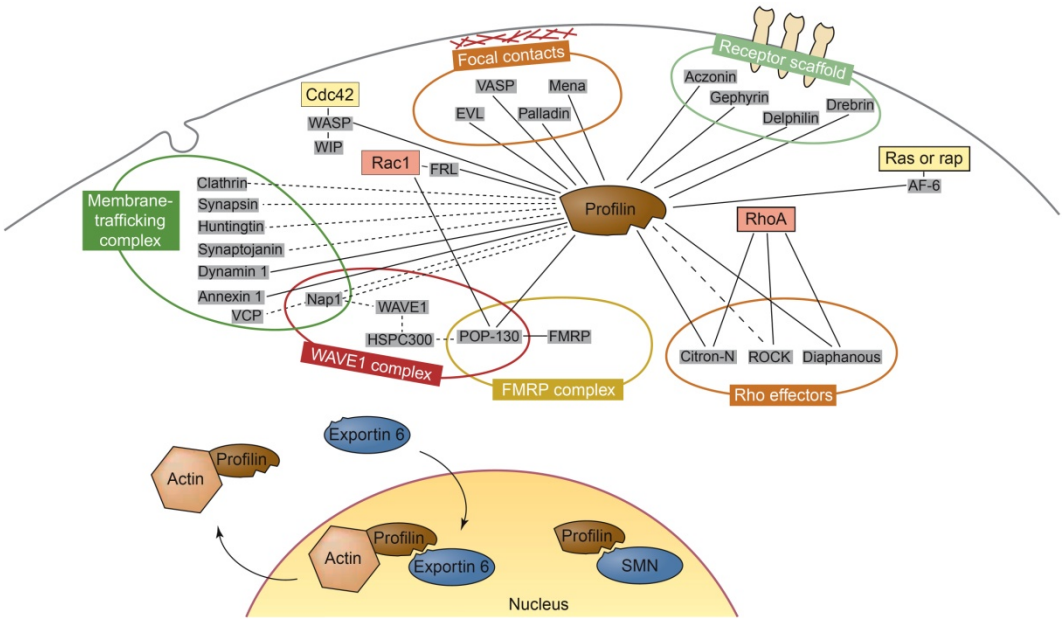

Figure 1.5. Network of molecular interactions of profilin.
Proteins that are known to interact with profilin are grouped according to their cellular location or the complexes in which they are found. Several links exist to small GTPases such as Rac1, RhoA, cdc42, Ras and Rap that are part of pathways that signal to the actin cytoskeleton. Direct interactions between profilin and the ligands are indicated by unbroken lines, whereas potentially direct interactions are indicated by broken lines. Abbreviations: AF-6, All-1 fusion partner from chromosome 6; EVL, Ena VASP like; FMRP, fragile X mental retardation protein; FRL, formin-related gene in leukocytes; HSP, heat-shock protein; Mena, mouse homolog of Drosophila enabled; POP, partner of profilin; SMN, survival of motor neuron; VCP, valosine-containing protein; WIP, WASP-interacting protein. Adapted from Witke, 2004.

1.1.3.1.3 DNase I

The enzyme deoxyribonuclease I (DNase I) is a secretory protein highly conserved in vertebrates. Its most prominent function is the endonucelolytic cleavage of DNA. However, the extracellular distribution throughout many tissues suggests additional functions (Lazarides & Lindberg, 1974; Peitsch et al, 1993; Yonezawa et al, 1990). Most intriguingly, DNase I specifically binds G-actin with a very high affinity (dos Remedios et al, 2003). The crystal structure of the actin:DNase I complex has been solved at high resolution (see **Figure 1.6**) (Kabsch et al, 1990). DNase I tightly binds to the eponymous loop on subdomain 2 at the pointed end of actin, thereby inhibiting the nuclease activity of DNase I (Hitchcock, 1980; Lazarides & Lindberg, 1974).

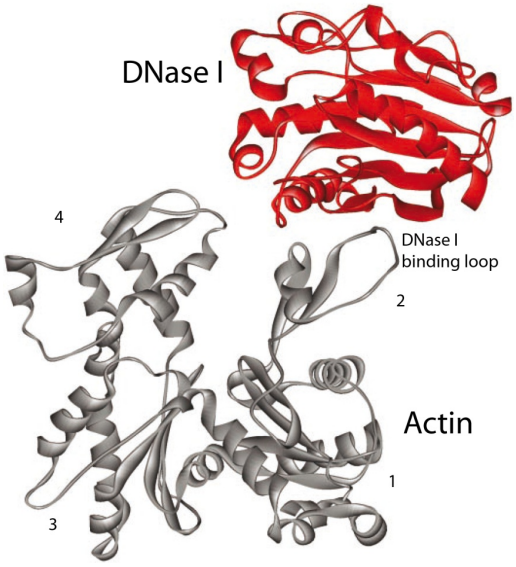

Figure 1.6. The crystal structure of actin in complex with DNase I.
The actin molecule (grey) is shown in the conventional view, the DNase I binding loop and subunit numbers are indicated. DNase I (red) binds to subdomain 2 at the pointed end of actin. Modified from Kabsch et al,1990.

This interaction has made DNase I an important analytical tool, as measuring the inhibition of DNase I allows the determination of the ratio of G-actin to F-actin with high precision (Blikstad et al, 1978; Malicka-Blaszkiewicz, 1986). Fluorescently labeled DNase I is frequently used to visualize G-actin in live cells (Cramer et al, 2002). Remarkably, the physiological relevance of the actin:DNase I interaction is still largely unknown. As the major fraction of

DNase I is found in extracellular space where actin is scarce, it has been discussed that actin plays a role in protecting the cell from uncontrolled DNA degradation by intracellular DNase I prior to its secretion (dos Remedios et al, 2003).

1.1.3.2 Actin filament binding proteins

Once a specific manifestation of the microfilament cytoskeleton has been established, the cell must be able to control its stabilization or its quick remodeling, depending on the given situation. To stabilize filaments of constant lengths, proteins such as CP (capping protein) or tropomodulin are employed (Winder & Ayscough, 2005). While the former caps barbed ends, the latter is a potent pointed-end-capper. Moreover, capped filaments are frequently stabilized by the highly conserved tropomyosins which bind laterally over an extended range of the whole filament and protect it from the influence of depolymerizing, severing and branching factors (Blanchoin et al, 2001; Maciver et al, 2000).

Stable single filaments can be shaped into a dense network both by Arp2/3 mediated branching and by proteins such as filamin, spectrin and transgelin. These cross-linking factors create a very dense, intricate meshwork of actin filaments (Winder & Ayscough, 2005). The parallel alignment and lateral stabilization of filaments into bundles and cables is brought about by bundling proteins. While α-actinin and fascin are responsible for the formation of loose filamentous bundles, other proteins, such as plastin and fimbrin produce bundles with higher stiffness and rigidity (Bartles, 2000; Claessens et al, 2006; Winder & Ayscough, 2005).

F-actin interacting proteins also play an important role in the connection and anchoring of filaments to the other major cytoskeletal elements and the cytoplasmic membrane. Spectrin and plectin, for instance, link F-actin to intermediate filaments and microtubules. Anchoring to lipid membranes can occur by the binding to integral membrane proteins, mediated e.g. by dystrophin, vinculin and talin (Le Rumeur et al, 2010; Xu et al, 1998). Alternatively, some proteins (e.g. annexins) can connect actin filaments

directly to phospholipids of the membrane (Hayes et al, 2004).

The importance of the rapid initiation of polymerization and the stabilization of existing filaments is equaled by the regulated disassembly of distinct portions of the actin network. To this end, cells usually follow a three-way approach of removing the tropomodulin cap, accelerating depolymerization at the pointed end and severing filaments. The major proteins facilitating the depolymerization of F-actin belong to the highly conserved ADF (actin depolymerizing factor)/cofilin (cosediments with filamentous actin) family of proteins that bind to F-actin and induce the dissociation of ADP-bound monomers from the pointed end (Lappalainen et al, 1998; McGough et al, 1997). While ADF/cofilins also exhibit a weak filament-severing activity, the main protein employed to break actin filaments in two is gelsolin. This highly flexible multi-domain protein is a very potent regulator of filament assembly and disassembly (Sun et al, 1999). After severing a filament, gelsolin caps the newly generated barbed end and prevents its elongation. Additionally, this activity of gelsolin is regulated through the interaction with various intracellular factors (Chou et al, 2002; Hartwig et al, 1995).

Many F-actin binding proteins do not directly influence the structure of the filamentous network, they rather interact with signaling pathways and mediate reconstruction by the interaction with other shape-modulating ABPs. VASP (vasodilator stimulated phosphoprotein), for instance, is often found in cellular regions with a high actin turnover rate. It interferes with capping proteins thus ensuring the availability of free barbed ends for continuous polymerization (Bear et al, 2002). Through the interaction with profilin, VASP recruits polymerization-competent ATP-G-actin (Reinhard et al, 1995). Another important signal intergrator is WIP (WASp interacting protein). It was discovered via its regulation of the WASp mediated control of filament nucleation, effectively blocking actin polymerization (Martinez-Quiles et al, 2001; Vetterkind et al, 2002). This activity can be reversed by the interaction with cortactin (Kinley et al, 2003). Covering F-actin along its entire length, cortactin connects many actin related signaling pathways to the filament network through its multi-domain modular organization (Pant et al, 2006).

Recently, cortactin has been found to modulate the appearance of actin filaments on its own by initiating the formation of flat sheets of F-actin (Cowieson et al, 2008).

1.1.3.3 Concluding remarks on actin binding proteins

A recurring theme of ABPs is their modular polypeptide structure and their ability to interact not only with actin but also with a number of other cellular factors creating a complex system of functional interdependence, cross-talk and feedback regulation. The most potent proteins responsible for dramatic changes of the network architecture are particularly well-embedded in signaling and regulatory networks. Profilin, the Arp2/3-WASp system and formin as the main factors promoting actin polymerization are tightly regulated, multi-modular proteins. The same holds true for the potent F-actin disassemblers, ADF/cofilin and gelsolin and also for the large class of myosin motor proteins. The involvement of actin in a multitude of protein-protein interactions exerts significant evolutionary constraint on its structure and sequence. Indeed, the observation that no other known protein participates in more protein-protein interactions than actin (Dominguez, 2004) and the fact that actin is among the most conserved proteins in evolution are intimately related (Erickson, 2007). This notion has even been further substantiated in the last decade by the discovery and characterization of prokaryotic actins.

1.2 Prokaryotic actins

Long believed to be restricted to eukaryotes, prokaryotic actin homologs have been discovered by the identification of conserved amino-acid residues derived from structure-based alignments of core motifs comprising what is now called the "actin fold" (Bork et al, 1992). This ground-breaking study was initiated bearing in mind the observation that the similarity actin shares with sugar kinases and hsp70 chaperones is immediately recognizable at the structural level while being virtually undetectable in amino acid sequence comparisons. Therefore, a database search based on three-dimensional structural alignments was performed (Bork et al, 1992). Prokaryotic proteins identified to be structurally related to actin were FtsA, MreB and ParM. The first two were then known to be involved in the regulation of cytokinesis and in cell shape determination of rod-shaped cells, respectively. ParM had been found necessary for the faithful replication and segregation of the *E. coli* plasmid R1. Early investigations into the newly discovered actin-like proteins, primarily, the elucidation of high-resolution crystal structures, revealed that all three proteins are true actin homologs (see **Figure 1.7**). Despite only showing a degree of sequence identity of about 14% with each other and eukaryotic actin, each of the three bacterial actin candidate proteins adopts the typical bi-lobed actin fold with 4 clearly distinguishable subunits. Thus, their homology with actin was widely accepted. This finding soon triggered the search for the roles these newly found actins played in their host organisms.

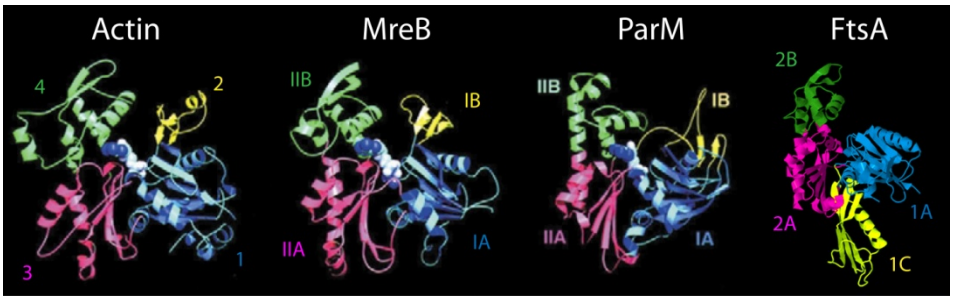

Figure 1.7. Crystal structures of actin, MreB, ParM and FtsA.
Structures are shown in the conventional view, corresponding subdomains are in the same color, subdomain classifications are given. Data are from Otterbein et al, 2001 (actin); van den Ent et al, 2001 (MreB); van den Ent et al, 2002 (ParM) and van den Ent & Löwe, 2000 (FtsA).

1.2.1 Bacterial cytokinesis: FtsA

Although FtsA shows the typical bi-lobed actin structure, subdomain 2 (here termed 1C) is misplaced when compared to the actin archetype, apparently having "swung out" towards the barbed face of the protein (van den Ent & Löwe, 2000). In many bacteria, FtsA is involved in positioning the Z-ring during cytokinesis. The main component of the Z-ring is FtsZ, a bacterial homolog of the eukaryotic microtubule-forming protein tubulin (see **Figure 1.8A**) (Ben-Yehuda & Losick, 2002; Erickson, 1998; van den Ent et al, 2001a). FtsZ is targeted to the future site of cell constriction through an elaborate cascade of many protein-protein interactions. Being part of that cascade, FtsA bridges FtsZ to the cytoplasmic membrane and possibly to other components of the cytokinesis machinery (see **Figure 1.8D**) (Pichoff & Lutkenhaus, 2005; van den Ent & Löwe, 2000; Yan et al, 2000). Despite clear indications that FtsA monomers interact with each other, the question whether polymeric filaments are formed is still unresolved. There have been reports of corkscrew-like aggregations formed *in vitro,* however, their physiological relevance remains speculative and no FtsA polymers have been confirmed *in vivo* (see **Figure 1.8B and C**) (Lara et al, 2005; van den Ent & Löwe, 2000).

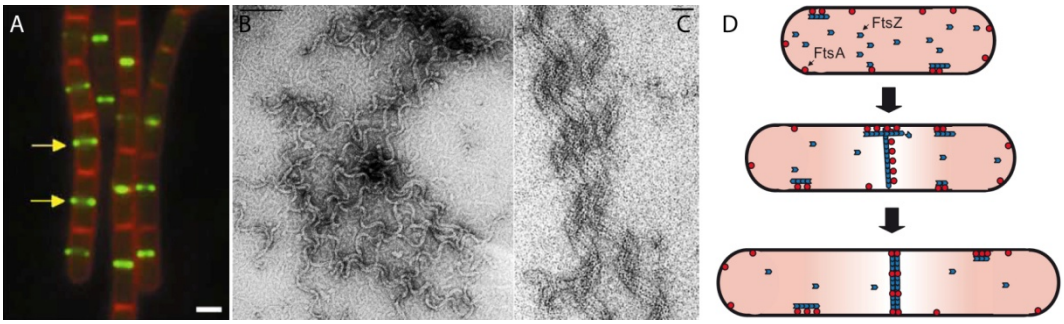

Figure 1.8. FtsA and the cell division protein FtsZ.
A: GFP-tagged Z-rings at the division site in *Bacillus subtilis*. The membrane is stained red, scale bar: 1 µm. Adapted from Ben-Yehuda & Losick, 2002.
B and C: Electron micrographs of FtsA polymers formed *in vitro*. **B** shows an overview, scale bar: 100 nm. **C** shows filaments in detail, scale bar: 20 nm. Adapted from Lara et al, 2005.
D: Model for the role FtsA plays in the assembly of the Z-ring. FtsZ polymers are linked to the membrane through FtsA. Elongation of membrane-linked polymers is subject to an elaborate control system. Growth is restricted to the division plane and to a direction perpendicular to the long cell axis. Adapted from Pichoff & Lutkenhaus, 2005.

1.2.2 Plasmid segregation: ParM and AlfA

By the time of its identification as a putative bacterial actin, ParM was known to be essential for the faithful segregation after replication of the *E.coli* plasmid R1. The crystal structure of ParM and its ability to polymerize into double-stranded helical filaments have demonstrated some similarities with eukaryotic actin (van den Ent et al, 2002). In analogy to actin, ATP-ParM shows a higher tendency to polymerize than ADP-ParM. Also, ATPase activity is induced by filament formation and ADP-ParM rapidly dissociates from filament ends (Garner et al, 2004). Further analyses have shown, however, that the evolutionary distance between actin and ParM is reflected in a number of fundamental differences. The spontaneous nucleation of ParM filaments, for instance, occurs rather rapidly and is believed to constantly take place *in vivo*. Moreover, ParM filaments have, in contrast to eukaryotic actin, a left-handed helical twist, they grow bidirectionally at equal rates and show a length adaptation to the bacterial cell, terminating elongation at about 1.5 µm *in vitro* (Garner et al, 2004; Garner et al, 2007; Orlova et al, 2007). Three plasmid loci are required for the partitioning after replication: *parM* (the "partition motor"), *parR* and *parC*.

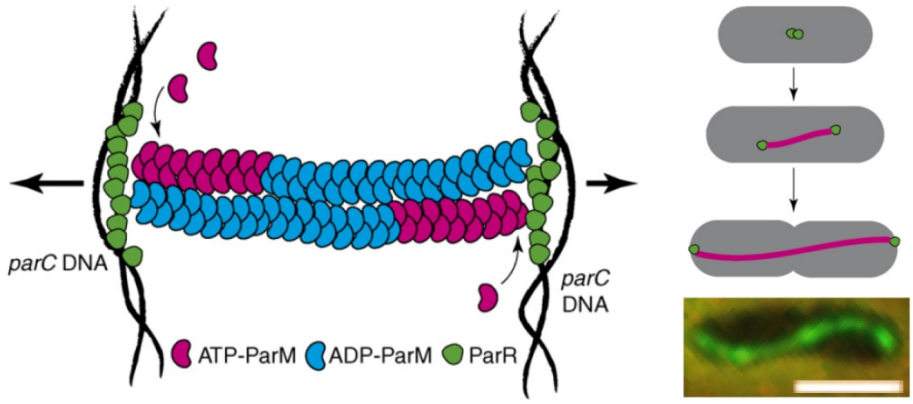

Figure 1.9. ParM filament formation and plasmid DNA segregation.
ParM forms a filament bundle in-between duplicated plasmids that elongates as plasmids segregate towards the poles. Filaments are bound through ParR (green) to a specific site on the plasmid, *parC*. Insertion of ATP-ParM (red) at the growing tip of filaments is proposed to exert force on the plasmids, pushing the copies apart (arrows). Owing to its hydrolysis activity ADP-ParM (blue) accumulates in the filament. The right hand side shows an *in vivo* model (top) and an anti-ParM immunofluorescence image of an *E.coli* cell (bottom, scale bar: 2 µm). Modified from Dye & Shapiro, 2007 (schematic models) and Møller-Jensen et al, 2002 (micrograph).

The ParR protein binds to ParM filament ends thus terminating depolymerization while actively adding new ParM monomers, displaying a "formin-like" activity (see 1.1.3.1.1 Inhibitors and activators of actin polymerization, p10) (Garner et al, 2004; Garner et al, 2007; Moller-Jensen et al, 2002). Additionally, ParR binds to the centromer-like locus *parC* forming a simple analog to the eukaryotic mitotic spindle (see **Figure 1.9**) (Dye & Shapiro, 2007; Møller-Jensen & Gerdes, 2004; Møller-Jensen et al, 2002).

The recently discovered AlfA protein from *Bacillus subtilis* has some properties strongly resembling ParM and apparently segregates plasmids in a very similar way. However, AlfA filaments show considerable structural differences compared to ParM (see **Figure 1.10**) (Becker et al, 2006; Polka et al, 2009; Popp et al, 2010a). Recently, the plasmid encoded loci *alfB* and *alfC* were discussed to perform functions similar to ParR and *parC*, respectively (Popp et al, 2010b).

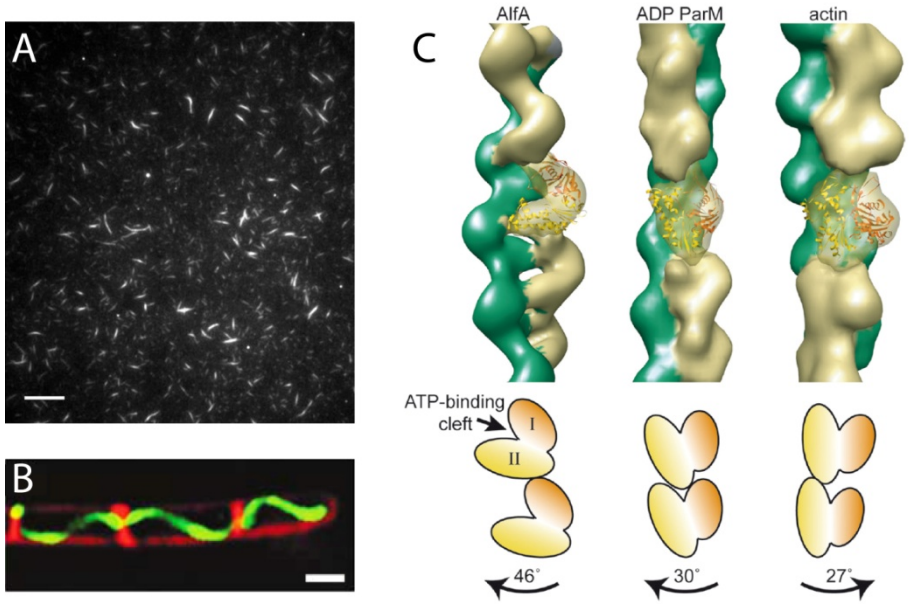

Figure 1.10. Filaments formed by AlfA.
A: TIRF micrograph of Cy3-labeled AlfA showing stable filamentous bundles. Scale bar: 10 µm.
B: GFP-AlfA filaments (green) formed in *Bacillus subtilis* cells. Membranes are stained with FM 4-64 (red). Scale bar: 1 µm.
C: Architecture of filaments of AlfA (left), ADP-ParM (middle) and actin (right). AlfA and ParM are left-handed, actin is right-handed. A single filament subunit is transparent, with the crystal structure of ParM fitted into the model. Cartoons (bottom) indicate the orientations of subunits in the filaments; the magnitude and direction of the rotation between subunits moving up each strand are indicated by labeled arrows. **A** and **C** modified from Polka et al, 2009, **B** adapted from Becker et al, 2006.

1.2.3 Wide-spread and multifunctional: MreB

MreB was originally characterized as part of the *mre* (murein cluster e) locus involved in cell shape regulation in *E.coli* (Doi et al, 1988). Although it had been identified as a potential actin homolog, research interest had long been hesitant owing to MreB's low sequence similarity to actin. A dramatic turnaround was brought about by the discovery that MreB forms filaments in a nucleotide dependent manner (Jones et al, 2001; van den Ent et al, 2001b). Many laboratories have since worked at uncovering the functions and molecular mechanisms connected with MreB. A thorough understanding of MreB similar in extent to the comparably simple ParM system is impeded by the fact that MreB is the most prevalent prokaryotic actin involved in a broad range of sometimes species-specific cellular processes (Shaevitz & Gitai, 2010).

1.2.3.1 General features of MreB

An *mreB* gene is found in the vast majority of non-spherical bacteria, with some species, mainly gram-positives, encoding multiple homologs (Cabeen & Jacobs-Wagner, 2010; Daniel & Errington, 2003). While some rod-shaped bacteria (e.g. Rhizobiae, Mycobacteria, Mycoplasmas) lack MreB, it is found in some spherical members of the Cyanobacteria and Planctomycetes (Shaevitz & Gitai, 2010). The considerable sequence variation of MreBs commands caution in generalizing its function. Rather, the view has emerged that some very basic properties of MreB are applied by different bacteria to specific cellular processes. The unifying feature, of course, is the ability to form filamentous polymers. MreB protofilaments seem to assemble in a straight fashion rather than exhibiting the typical actin twist and have the tendency to spontaneously align into bundles and ribbons with mixed polarities (Shaevitz & Gitai, 2010; van den Ent et al, 2001b). Depending on the polymerization conditions, MreB can also form ring-like assemblies and sheets of diagonally interwoven filaments of about 1-5 µm (see **Figure 1.11A**) (Esue et al, 2005; Popp et al, 2010c). Finally, a general feature of MreB essential for its physiological function is its high turnover rate with the tendency to treadmill (Carballido-Lopez & Errington, 2003a; Defeu Soufo &

Graumann, 2004; Defeu Soufo & Graumann, 2006; Jones et al, 2001; Kim et al, 2006; Srinivasan et al, 2007).

1.2.3.2 MreB and cell shape determination

Mutational studies have shown that an MreB knock-out is either lethal or severely impairs cell viability (Cabeen & Jacobs-Wagner, 2010; Daniel & Errington, 2003). At any rate, *mreB* mutants usually display aberrant cell shapes, such as the formation of spherical cells in rod-shaped bacteria (Graumann, 2004; Hu et al, 2007). Many insights into the role of MreB cell shape determination stem from *Bacillus subtilis* where two additional proteins with homology to MreB are found: Mbl and MreBH. All three assemble *in vivo* into dynamic helical "cables" that are, much as the filaments formed by actin, being constantly remodeled by treadmilling, moving with a velocity of about 0.1 µm per second just beneath the cellular surface (see **Figure 1.11B and C**) (Amos et al, 2004; Carballido-Lopez & Errington, 2003a; Defeu Soufo & Graumann, 2005; Graumann, 2004; Jones et al, 2001). The helical superstructures formed by the individual MreB homologs in *Bacillus subtilis* show variations in length, pitch and cellular localization suggesting that they control different aspects of growth and cell shape (Daniel & Errington, 2003; Defeu Soufo & Graumann, 2004; Graumann, 2004; Jones et al, 2001).

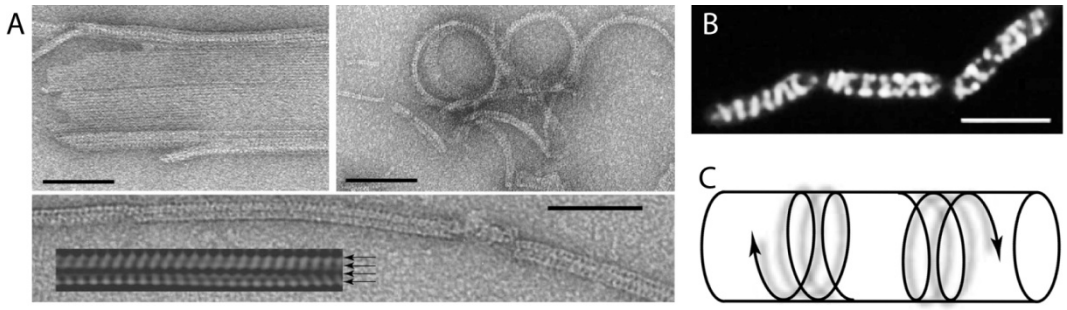

Figure 1.11. MreB filaments *in vivo* and *in vitro*.
A: Electron micrographs of MreB filaments formed *in vitro*. Single protofilaments assemble into pairs but do not twist around each other (bottom), the inset is an enlarged filtered image, the arrows show surface borders of individual filaments. Protofilaments can form flat sheets (top left) or ring-like structures (top right). Scale bars: 100 nm; adapted from Amos et al, 2004.
B: Dynamic GFP-Mbl helices in *Bacillus subtilis*. Scale bar: 4 µm; adapted from Carballido-Lopez & Errington, 2003a.
C: Schematic representation of dynamic MreB helices in rod-shaped bacteria. Adapted from Graumann, 2004.

MreB and Mbl are thought to exert their influence on cell shape mainly through the regulation of the synthesis of new cell wall material whose insertion into a growing cylindrical peptidoglycan layer also follows comparable helical patterns (Carballido-Lopez & Errington, 2003b; Daniel & Errington, 2003; Figge et al, 2004; Kruse et al, 2005; Scheffers et al, 2004; van den Ent et al, 2010). Similar observations were made with MreB in *E.coli* and *Caulobacter crescentus* suggesting a general role in cell shape determination (Kim et al, 2006; Takacs et al, 2010; Uehara & Park, 2008; Varma et al, 2007a; Varma & Young, 2009). It has been shown recently that in addition to its influence on cell wall synthesis the inherent stability of the helical MreB bundles mechanically contribute to the bending stiffness of *E.coli* cells (Wang et al, 2010).

1.2.3.3 The role of MreB in DNA replication and segregation

Knock-out strains have shown that MreB is required for proper segregation of chromosomes after replication (Gitai et al, 2004; Kruse et al, 2003; Soufo & Graumann, 2003). However, this matter remains controversial as its exact function and the underlying mechanisms are still unclear. Since they bind to chromosomal origins of replication, MreB filaments have been proposed to actively push chromosomes apart in a ParM-like fashion (Gerdes et al, 2004; Gitai et al, 2005; Graumann, 2004). Alternatively, MreB filaments may recruit the segregation machinery to the vicinity of the chromosome (Defeu Soufo & Graumann, 2005; Kruse et al, 2006). An example of this may be the suggested motor-like DNA segregating function of RNA polymerase that interacts with and is localized by MreB (Kruse et al, 2006). It is difficult, however, to directly attribute segregation defects in MreB-deficient cells to a primary role MreB plays in chromosome partitioning, as it is also involved in DNA replication (Defeu Soufo & Graumann, 2005; Munoz-Espin et al, 2009; Shebelut et al, 2009). Additionally, MreB regulates DNA decatenation through the interaction with topoisomerase IV (Madabhushi & Marians, 2009).

1.2.3.4 Additional functions of MreB and unresolved issues

MreB was shown to be involved in a number of further physiological processes. A recurring role appears to be the recruitment of cellular components that require an exact localization to fulfill their functions (Shaevitz & Gitai, 2010). Among these are chemotactic receptors of *E.coli* as well as gliding motility proteins in *Myxococcus xanthus*, type-IV pilus associated factors in *Pseudomonas aeruginosa*, intracellular organelles such as inclusion bodies (*E.coli*) or carboxysomes (*Synechococcus elongatus*) and various polar protein markers in *Caulobacter crescentus* and other bacteria (Bowman et al, 2008; Cowles & Gitai, 2010; Gitai et al, 2004; Mauriello et al, 2010; Rokney et al, 2009b; Savage et al, 2010; Shih et al, 2005). In some actinomycetes, MreB is required for sporulation (Mazza et al, 2006). It has been suggested that MreB cannot execute its multiple functions unaided by other cellular factors (Shaevitz & Gitai, 2010). In analogy with eukaryotic ABPs, a network of MreB interacting and regulating factors has been proposed. However, their existence and identity remain speculative.

1.2.4 More actins: MamK, BARP, Alps and Ta0583

In addition to MreB, some magnetotactic bacteria contain an additional actin homolog, MamK. It is required for the correct alignment of intracellular magnetic vesicles and also forms polymeric filaments that have the ability to form bundles (see **Figure 1.12**) (Komeili et al, 2006; Taoka et al, 2007). Although the involvement of auxiliary proteins in magnetosome positioning is suggested, only one protein, MamJ, is known that possibly interacts with MamK filaments *in vivo*, connecting them to membrane-clad magnetic particles (Scheffel et al, 2006).

The myxobacterium *Haliangium ochraceum* contains an actin homolog termed BARP (bacterial actin-related protein). Intriguingly, BARP shows about 40% sequence identity with eukaryotic actin while only being about 25% identical to bacterial actins (Wu et al, 2009). While the expression of BARP in *Haliangium ochraceum* was shown, its function is unclear.

Recently, more than 35 highly divergent families of actin-like proteins (Alps)

were uncovered in some bacterial genomes (Derman et al, 2009). Although these proteins share no more than 15% sequence identity with other actins, signature sequence motifs have been identified and at least three Alps form filaments. One, Alp7A from *Bacillus subtilis,* apparently shows properties reminiscent of AlfA (see **Figure 1.12**) (Derman et al, 2009).

One archaeal actin homolog, Ta0583 from *Thermoplasma acidophilum*, has been discovered and studied in detail. Its crystal structure reveals the common actin fold, it shows structural properties of eukaryotic actin but also of MreB and ParM (see **Figure 1.12**) (Roeben et al, 2006). It is able to hydrolyze various nucleotide triphosphates and forms bundles of helical filaments that resemble F-actin (Hara et al, 2007). Although its function is unclear, the resemblance of Ta0583 with ParM has prompted the suggestion that it has entered the archaeal lineage via a shuttling plasmid while having retained ancient features of today's eukaryotic actin.

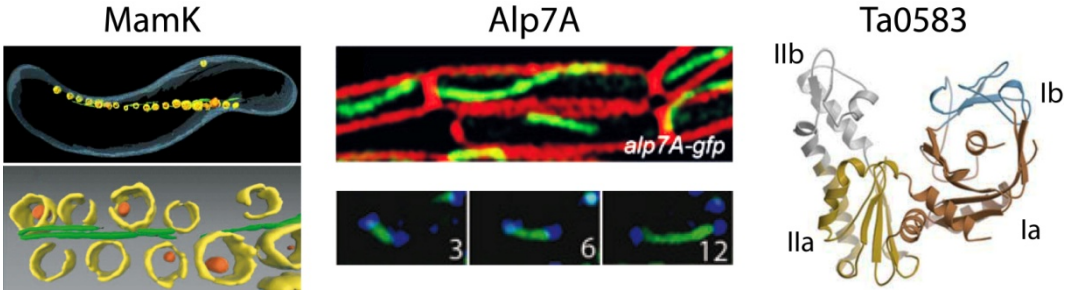

Figure 1.12. Prokaryotic actin homologs MamK, Alp7A and Ta0583.
Left: Three-dimensional surface-rendered reconstructions of MamK filaments (green) *in vivo*. MamK aligns membrane-covered vesicles (yellow) containing magnetite crystals (red). Bottom image shows magnification. Adapted from Scheffel et al, 2006 and Komeili et al, 2006.
Middle: GFP-tagged Alp7A (green) forms filaments in *Bacillus subtilis* (top). Membranes are stained with FM 4-64 (red). An Alp7A-GFP filament (green) is attached to CFP-tagged plasmids (blue) and pushes them apart (bottom). Numbers give time interval in seconds after first image capture. Adapted from Derman et al, 2009.
Right: Crystal structure of Ta0583 in the conventional actin view. Subdomains are indicated according to bacterial nomenclature. Adapted from Roeben et al, 2006.

1.3 Concluding remarks on actins

The combined results of classical eukaryotic actin biochemistry and of the revitalized field of bacterial Cell Biology have led to the emergence of a

1.4 Horizontal gene transfer

Over the last decades, horizontal gene transfer (HGT, also called lateral gene transfer, LGT) has steadily gained acceptance as a significant factor in evolution (Doolittle, 1999; Gogarten & Townsend, 2005; Syvanen & Kado, 2002; Tepfer et al, 2003). Being recognized now as a potent evolutionary force, accumulating evidence of HGT events has prompted the reevaluation of prokaryotic genome shaping and speciation (Jain et al, 1999; Jain et al, 2002; Koonin et al, 2002; Smets & Barkay, 2005; Thomas & Nielsen, 2005). By means of horizontal gene transfer, prokaryotic communities are able to

dynamically rearrange their genetic equipment in order to respond to environmental conditions and to invade ecological niches. Prokaryotes have evolved a number of mechanisms to execute the exchange of genetic material between cells and even across species barriers. The most prominent are the conjugative transfer of mobile genetic entities, the shuttling of genes by the transduction of prokaryotic viruses and the uptake and incorporation of naked extracellular DNA molecules (referred to as "transformation" through "natural competence"). Intracellular mobile genetic elements such as transposons, insertion elements, genomic islands (GEIs) or integrons are frequently found to be involved in HGT events. Due to their tendency to relocate within the genome of their host organism, they are likely to associate with and be mobilized by genomic regions involved in extracellular DNA transfer (Frost et al, 2005; Mazel, 2006; Sorensen et al, 2005). Some of these elements, most prominently genomic islands (also known as pathogenicity islands), frequently contain advantageous clusters of functionally related genes that confer a specific trait and are rapidly spread throughout prokaryotic communities (Dobrindt et al, 2004; Schubbe et al, 2003). Indeed, a significant portion of the genetic diversity and adaptive flexibility observed in microbial populations can probably be attributed to HGT (Brown et al, 2002; Koonin et al, 2002; Palenik et al, 2009). The interdomain exchange (that is, between eukaryotes and prokaryotes) of genetic material is less common and mostly directed towards eukaryotes (Andersson, 2005; Doolittle, 2002; Koonin et al, 2002). A reason for this is the incompatibility of eukaryotic nucleotide sequences in prokaryotic contexts mainly because of the interruption by introns. Their removal is therefore a prerequisite for eukaryotic genetic information to manifest itself in a bacterium. Given the instability of mRNA, reverse transcripts of processed messengers must be viewed as one major source for eukaryotic DNA suitable for uptake, utilization and propagation (Da Lage et al, 2004). What with the general rare occurrence of reverse transcripts and the tendency of reverse transcriptases to produce incomplete copies of the original sequence, the low frequency of observed events of HGT from eukaryotes to prokaryotes is not surprising. Additionally, out of the three

major ways of DNA-uptake by prokaryotes, only transformation by natural competence can provide a direct route of entry for eukaryotic genes.

Rare as they are, reports of eukaryote-to-prokaryote HGT are mostly met with heightened interest. In a recently reported example, genes for the microtubule forming tubulin α and β isoforms have apparently found their way from a eukaryote into some species of the bacterial genus *Prosthecobacter* to encode for the BtubA/B proteins, respectively (Jenkins et al, 2002). They are more similar to eukaryotic tubulin than to the ubiquitous prokaryotic tubulin homolog FtsZ, which seems to have been replaced by the eukaryotic proteins in some *Prosthecobacter* species (Jenkins et al, 2002; Pilhofer et al, 2007). In another fascinating case of interdomain transfer, genes for a plastid-targeted fructose bisphosphate aldolase (FBA) of undisputed eukaryotic origin were found in the genomes of several isolates of the cyanobacteria *Prochlorococcus* and *Synechococcus* (Rogers et al, 2007). The eukaryotic gene, derived from red algae, is encoded directly adjacent to a cyanobacterial non-homologous FBA gene and most likely fulfills a function in its new prokaryotic host.

1.5 Cyanobacteria

1.5.1 General aspects

Despite their early descriptions as "blue-green algae", cyanobacteria are phototrophic eubacteria generally classified as gram-negative, even though their cellular envelope differs in some aspects from that archetype (Rippka, 1988). Owing to their ability to sustain life in the most diverse environments, cyanobacteria occur in a multitude of morphotypes. Members of that group may be halophilic, cryophilic or thermophilic; they can exist in a unicellular shape, they can form filaments of various appearances or complex colonies with intricate architecture. To adapt to harsh environmental conditions, cyanobacteria can differentiate into specialized cells such as motile hormogonia, nitrogen-fixing heterocysts or durable resting spores called akinetes. Many taxa of cyanobacteria are commonly found in close symbiotic

association with marine sponges, fungi and plants but also with bacteria and a multitude of other organisms (Steward et al, 1983; Usher et al, 2007).

Presumably having inhabited the earth for about 3.5 billion years, cyanobacteria are "ancient" organisms. The cyanobacterial "innovation" to combine the two PS1 and PS2 photosystems of the other phototrophic bacteria (ancestors of green and purple bacteria, respectively) with light harvesting complexes did not only provide the means for cyanobacteria to compete for resources by augmenting photosynthesis efficiency. The transfer of electrons to water by the thylakoid electron transport chain and the subsequent release of oxygen as a "byproduct" formed the atmosphere as we know it today and provided, as it were, the fuel which drove the explosive evolution of the quantum leap of life towards eukaryotes and multicellularity (Madigan et al, 2002; Willmotte, 1994).

Today, cyanobacteria are as ecologically relevant on a global scale as they have ever been. They represent the most abundant marine life form and are responsible for the major part of net primary bio-production on Earth (Field et al, 1998). Their nitrogen-fixing capabilities in combination with their occurrence in soil, freshwater and as symbionts of many plants assign cyanobacteria a vital role in fertilization and vegetation sustainability (Montoya et al, 2004; Peters, 1991). Cyanobacteria, in their capacity as carbon fixing organisms, have recently gained prominence in light of the search for CO_2-neutral, food-crop-independent providers of biomass as an energy source.

Since it is now generally appreciated under the endosymbiotic theory on the origin of eukaryotic cell organelles that cyanobacteria and plant chloroplasts share a common ancestor, cyanobacteria are model organisms for photosynthesis-related studies (Douglas, 1998; Giovannoni et al, 1988). Finally, the capability of many cyanobacteria to produce a plethora of secondary metabolites is another field of scientific interest. While the function of many of these metabolites is unknown, some are involved in cyanobacterial cell-cell communication, in neutralizing competing organisms or in intracellular stress response (Jenke-Kodama et al, 2008; Meissner, 2010;

Zilliges et al, 2008). Yet for the human they are notoriously known to be toxic compounds in cyanobacterial blooms of large freshwater bodies (Utkilen et al, 1996). However, for some of these secondary metabolites a pharmaceutical applicability has been shown and many more yet undiscovered metabolites are thought to be of similar benefit (Gustafson et al, 1997; Huskens et al, 2010; Kehr et al, 2006).

1.5.2 Cyanobacterial actins

Screening the available genome data bases for prokaryotic actins reveals that FtsA appears to be absent from cyanobacteria while MreB is widely spread (Cabeen & Jacobs-Wagner, 2010). Most genomes of non-spherical cyanobacteria and of those able to form multicellular colonies or filamentous assemblies contain an *mreB* gene (Shaevitz & Gitai, 2010). *Synechocystis*, which is strictly unicellular and spherical, lacks *mreB*. The only study aimed at elucidating the function of a cyanobacterial MreB was conducted with the filamentous, heterocyst-forming *Anabaena*. In this organism, MreB is non-essential and is involved in cell-shape regulation but does not play a role in chromosome segregation (Hu et al, 2007).

1.5.3 *Microcystis aeruginosa*

The spherical, colony-forming cyanobacterium of the genus *Microcystis* is commonly found in aquatic habitats. As it lacks a nitrogen fixing machinery, it does not form heterocysts (Kaneko et al, 2007; Rippka et al, 1979). *Microcystis* does, however, occur in a broad spectrum of colony morphotypes by the characteristics of which it has generically been grouped into "species" such as *Microcystis aeruginosa*, *M. ichtyoblabe, M. wesenbergii* etc (Via-Ordorika et al, 2004). Although this arbitrary clustering is not supported by molecular biological data, it is still widely used. The ability to form variously shaped colonies stems from the propensity of *Microcystis* to produce a complex mucilaginous sheath. *Microcystis aeruginosa* is among the most dominant bloom forming species probably owing to the production of toxins, the most prominent of which is the hepatotoxic microcystin (Dittmann et al,

1997). A commonly used laboratory strain had been isolated from the Braakman freshwater reservoir in the Netherlands in 1972 and was subsequently added to the Pasteur Culture Collection at the Pasteur Institute in Paris, France, under the classification "PCC 7806". Its genome sequence has been made available to the public in 2008 (Frangeul et al, 2008).

1.6 Eukaryotic actin and profilin in *Microcystis aeruginosa*

The genome of *Microcystis aeruginosa* PCC 7806 encodes the 39 kDa protein ActM that shares a 67% sequence identity with eukaryotic actins from Cnidaria and Echinodermata and is 65% identical with mammalian actins. A second protein (designated PfnM), encoded about 280 nucleotides downstream of *actM*, shows an 83% identity to profilin from *Hydra magnipapillata* (see **Figure 1.13A**). The 15 kDa PfnM is the only known profilin homolog (see 1.1.3.1.2 Profilin, p11) to be reported from a prokaryote (Guljamow et al, 2007). The *actM-pfnM* region is flanked by short inverted repeats and a tRNA gene in an organization reminiscent of the GEI class of bacterial mobile genetic elements (see **Figure 1.13A**). The high degree of sequence identity, the conservation of signature sequence stretches and the GEI-like organization of the *actM-pfnM* genomic region are strong indications that both proteins have not arisen in *Microcystis aeruginosa* but were transferred from a eukaryote (Guljamow et al, 2007). However, the property of GEIs to facilitate the rapid spreading of genes across bacterial species and the fact that both genes show bacterial-type patterns in GC content and codon usage suggest that *Microcystis* was not necessarily the primary recipient of the original genes and might have acquired *actM* and *pfnM* from some other bacterium. Nonetheless, there is no doubt that both ultimately are of eukaryotic, most likely marine invertebrate, origin.

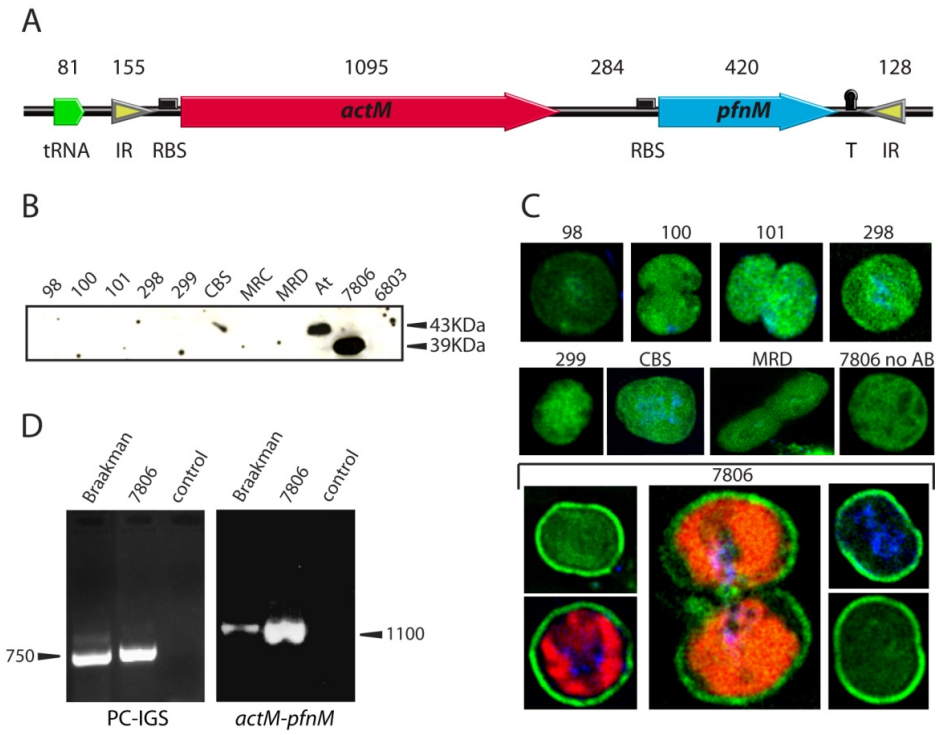

Figure 1.13. Actin and profilin in one strain of *Microcystis aeruginosa*.
A: *ActM-pfnM* GEI. Inverted repeats (IR), a tRNA gene (tRNA), ribosome binding sites (RBS) and a transcription terminator (T) are indicated. Numbers refer to nucleotide lengths.
B: Anti-actin Western blot. *Arabidopsis thaliana* ('At') and *Synechocystis sp.* PCC 6803 ('6803') were used as controls. *Microcystis aeruginosa* strains are indicated.
C: Immunofluorescence micrographs of *Microcystis aeruginosa* strains. ActM is FITC-stained (green), DNA is blue. Red and green autofluorescence is also visible. Cells denoted '7806 no AB' show background intensities of green autofluorescence. Strains are indicated above respective images.
D: PCR of field samples from the Braakman habitat. PCC 7806 and water controls were prepared in parallel. Specific primers show the presence of cyanobacterial DNA ('PCIGS' (Neilan et al, 1995)). *ActM–pfnM* specific primers yielded the expected fragment ('*actM-pfnM*'). Modified from Guljamow et al, 2007.

Interestingly, the two genes were so far only found in the genome of the PCC 7806 lab strain of *Microcystis aeruginosa* and in recent metagenomic samples taken from the strain's original habitat (see **Figure 1.13B, C, D**). Both genes are actively expressed in *Microcystis aeruginosa* and the ActM protein can be detected on protein immunoblots with an antibody raised against *Arabidopsis thaliana* actin (see **Figure 1.13B**). Immunofluorescence microscopy employing this antibody shows that ActM accumulates in a shell-like layer adjacent to the cell envelope in *Microcystis aeruginosa* (see **Figure 1.13C**). Although this localization tentatively suggests a role in cell stabilization, the exact functions of both ActM and PfnM in *Microcystis aeruginosa* have remained speculative.

1.7 Aims of this study

By the time the present study was initiated, the ActM and PfnM proteins were not characterized biochemically. The most immediate questions regarding the ability of ActM to polymerize, the physical and biochemical properties of possible filaments and the nature of the putative interaction of PfnM and ActM needed to be addressed. Additionally, a number of ecological issues remained to be resolved: the species distribution of the *actM-pfnM* genomic island in the original habitat of *Microcystis aeruginosa* PCC 7806 was of high interest as was the question whether variants of that specific genomic region could be identified in field samples. The attempted clarification of these open questions was the motivation driving the experiments described herein.

2 Materials and methods

2.1 Materials

2.1.1 Chemicals

Substance	Provider
Acetone	Roth, Karlsruhe, Germany
Acrylamide/Bisacrylamide (37.5:1)	Roth, Karlsruhe, Germany
Actin, from rabbit skeletal muscle, 99% pure, AKL99	Cytoskeleton, Denver, USA
Agar	Difco, Sparks, USA
Agarose	Biozym, Hessisch Oldendorf, Germany
Ammonium sulfate	Roth, Karlsruhe, Germany
Ampicillin	Roth, Karlsruhe, Germany
APS	Roth, Karlsruhe, Germany
ATP 10 mM	Fermentas, St Leon-Rot, Germany
β-mercaptoethanol	Roth, Karlsruhe, Germany
Boric acid	Roth, Karlsruhe, Germany
Bradford's reagent	Pierce, Rockford, USA
Bromophenol blue	Merck GmbH, Darmstadt, Germany
BSA	Fermentas, St Leon-Rot, Germany
Calcium chloride	Roth, Karlsruhe, Germany
Chloroamphenicol	Serva, Heidelberg, Germany
Chloroform/Isoamylalcohol 24:1	Roth, Karlsruhe, Germany
Coomassie staining Roti-Blue	Roth, Karlsruhe, Germany
CTAB	Serva, Heidelberg, Germany
DNA from salmon sperm	Fermentas, St Leon-Rot, Germany
dNTPs 10mM solution	Fermentas, St. Leon-Rot, Germany
DTT	Roth, Karlsruhe, Germany
EDTA	Roth, Karlsruhe, Germany
Ethanol	Roth, Karlsruhe, Germany
Ethidium bromide	Sigma, St. Louis, USA
Formaldehyde 37%	Roth, Karlsruhe, Germany
Formamide	Roth, Karlsruhe, Germany

GelCode Blue Stain Reagent	Pierce, Rockford, USA
Glucose	Roth, Karlsruhe, Germany
Glutardialdehyde 25%	Roth, Karlsruhe, Germany
Glycerol	Roth, Karlsruhe, Germany
Glycine	Roth, Karlsruhe, Germany
HEPES	Amersham Life Sciences, Cleveland, USA
Hoechst dye bis-Benzimide H33342	Serva, Heidelberg, Germany
Hydrochloric acid	Roth, Karlsruhe, Germany
IPTG	Roth, Karlsruhe, Germany
Isopropanol	Roth, Karlsruhe, Germany
Magnesium chloride	Roth, Karlsruhe, Germany
Methanol	Roth, Karlsruhe, Germany
Ni-NTA Agarose	Qiagen, Düsseldorf, Germany
PEG 4000 50% (w/v)	Fermentas, St. Leon-Rot, Germany
Phalloidin, labeled, A488 or TRITC	Invitrogen, Carlsbad, USA
Phenol/Chloroform/Isoamylalcohol	Roth, Karlsruhe, Germany
PMSF	Serva, Heidelberg, Germany
Potassium chloride	Roth, Karlsruhe, Germany
Polyvinyl-pyrrolidon 70 kDa	Roth, Karlsruhe, Germany
n-Propylgallate	Roth, Karlsruhe, Germany
SDS	ICN Biochemicals, Meckenheim, Germany
Skim milk powder	Sigma-Aldrich, Buchs, Switzerland
Sodium acetate	Roth, Karlsruhe, Germany
Sodium chloride	Roth, Karlsruhe, Germany
Sodium dihydrogenphosphate	Roth, Karlsruhe, Germany
Sodium hydrogenphosphate	Roth, Karlsruhe, Germany
Sodium hydroxide	Roth, Karlsruhe, Germany
TEMED	Roth, Karlsruhe, Germany
Tris	Roth, Karlsruhe, Germany
Triton X-100	Roth, Karlsruhe, Germany
Trypton	Difco, Sparks, USA
Tween 20	Sigma, Sparks, USA
Urea	ICN Biomedicals, Meckenheim, Germany
UTP, Fluorescein-12 labeled	Roche, Mannhein, Germany
X-Gal	Roth, Karlsruhe, Germany

Yeast extract	Difco, Sparks, USA

2.1.2 Enzymes

CIAP	Fermentas, St. Leon-Rot, Germany
Klenow fragment	Fermentas, St. Leon-Rot, Germany
Lysozyme (chicken egg white)	Sigma-Aldrich, Buchs, Switzerland
Proteinase K	Boehringer, Mannheim, Germany
Restriction endonucleases	Fermentas, St. Leon-Rot, Germany New England Biolabs, Frankfurt/M., Germany
RNase A/T1 Mix	Fermentas, St. Leon-Rot, Germany
T4 DNA Ligase	Fermentas, St. Leon-Rot, Germany
DNase I, RNase-free	Fermentas, St. Leon-Rot, Germany
Taq polymerase	Qiagen, Düsseldorf, Germany
Pfu polymerase	Fermentas, St. Leon-Rot, Germany

2.1.3 PCR primers

Table 2.1. PCR primers.

Name	5'-3' Sequence	Tm [°C]	Target
ActinMicFW	CCGTTTGGACTTAGCAGAG	62	*actM*
ActinMicroFW	AACAAATGAGTGAAATCGTAATTGA	62.2	*actM*
ActinCyanoFW	AGCCCCTGAAGAACATCTCA	63.7	*actM*
ActinMicRV	CGGTGCTAAGGCATTGATTT	63	*actM*
A-P GEI FW	GGTACTGGGAGAGGGTGACA	60	*actM*
A-P GEI RV	GTCGCTTTGTCGAAACCCTA	60	*pfnM*
T7_PfnMFW	TAATACGACTCACTATAGGTTTGTGCGCTC AATCAAATG	62	*pfnM*
T7_PfnMRV	TAATACGACTCACTATAGGGCCGACCGCTT TATTGGTAT	62	*pfnM*
T7_ActMCyanoFW	TAATACGACTCACTATAGGAGCCCCTGAAG AACATCTCA	63	*actM*
T7_ActMMicRV	TAATACGACTCACTATAGGCGGTGCTAAGG CATTGATTT	63	*actM*
ProfilMicFW	GAAAATTGCGCGTATGATGA	63.4	*pfnM*
ProfilMicRV	ACCGCACTTTTGGATTTTTG	63.6	*pfnM*
ProfilinMicroRV	CCACGACTTTCTAAATAATCTGCAA	63.9	*pfnM*

Name	5'-3' Sequence	Tm [°C]	Target
PC(+)	GGCTGCTTGTTTACGCGACA	52	*cpcB*
PC(–)	CCAGTACCACCAGCAACTAA	52	*cpcA*
M13_Fw	GTAAAACGACGGCCAGT	53	M13
M13_Rv	AACAGCTATGACCATG	53	M13
T7_PC (+)	TAATACGACTCACTATAGGGGCTGCTTGTT TACGCGACA	52	*cpcB*
T7_PC (-)	TAATACGACTCACTATAGGCCAGTACCACC AGCAACTAA	52	*cpcA*
T7 Prom	TAATACGACTCACTATAGGG	53	T7 Promoter
T7 Term	TAGTTCCTCCTTTCAGCAAAA	53	T7 Terminator
ActMExFW	CATATGAGTGAAATCGTAATTGATTG	55	*actM*
ActMExRV	GGATCCTTAGAAACATTTTTTATGCAC	55	*actM*
PfnMExFW	CATATGTATTACGACAGTTACATTG	55	*pfnM*
PfnMExRV	GGATCCTTAAATGCCACGACTTTCTA	55	*pfnM*
PfnM_SybrFW	GCAGAAAATTGCGCGTATGA	60	*pfnM*
PfnM_SybrRV	CATCCTCGCGCAAAAATAGA	60	*pfnM*
ActMprobe2FW	GCGGTTATCCGTTTGGACT	60	*actM*
ActMprobe2RV	CCTCTTTGGGACAATAGCTTCA	60	*actM*
ActMprobe9FW	AAATGACGGTCGGGAAATTA	60	*actM*
ActMprobe9RV	CCCTATAAATGCGGGTTGAA	60	*actM*
Pfnprobe161FW	AAAGTGCGGTTGTGATAGGG	60	*actM*
Pfnprobe161RV	CCGACCGCTTTATTGGTATTT	60	*actM*
cpcBA_128FW	TGCGCGAAACCTATGTAGC	60	PC-IGS
cpcBA_128RV	CGGCTTCTTTCATTTTGCTTA	60	PC-IGS
PC_SybrFW	TGAAATTGCCAGCTACTTCGAC	60	PC-IGS
PC_SybrRV	CCCAATAATCTTGCAATAAGTTTCC	60	PC-IGS
GFPuv_XbaFW	TCTAGACTTGAAATGAGTAAAGGAGAA	58	*gfpuv*
GFPuv_EcoRV	GAATTCTTATTTGTAGAGCTCATCCATGC	58	*gfpuv*
GFPuv_FW	TCTAGACTTGAAATGAGTAAAGGAGAA	58	*gfpuv*
GFPuv_RV	GAATTCTTATTTGTAGAGCTCATCCATGC	58	*gfpuv*
GFPEco47Fw	AGCGCTACATGAGTAAAGGAGAA	58	*gfpuv*
GFPEco47Rv	AGCGCTTCGGATTGTAATTT	58	*gfpuv*
ActM_Xba_FW	GGAGTCTAGAATGAGTGAAATCG	62	*actM*
ActM_Xba_RV	CCGCTATAAAACATCTAGAGAAACA	62	*actM*
PfnM_Xba_FW	GTCTAGAATGTATTACGACAGTTACAT	62	*pfnM*
PfnM_Xba_RV	TTGTCTAGAAATGCCACGACT	62	*pfnM*

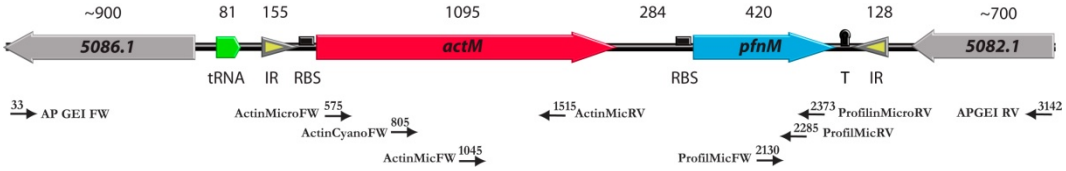

Figure 2.1. Primer binding sites in the *actM-pfnM* genomic region.
The genomic island coding for ActM and PfnM and two flanking ORFs are shown. Numbers above regions refer to nucleotide lengths. Primer binding sites and direction of replication initiation are indicated by small arrows. Numbers refer to 5' primer binding site, 1 being at the leftmost border of the shown region. Abbreviations: IR - inverted repeats; tRNA - tRNA gene; RBS - ribosome binding site; T - transcription terminator.

2.1.4 Plasmid vectors

pACYC184	Fermentas, St. Leon-Rot, Germany
pBLUESCRIPT II SK (+)	Stratagene/Agilent, Santa Clara, USA
pDrive	Qiagen, Düsseldorf, Germany
pET15b	Novagen/Merck, Darmstadt, Germany
pGFPuv	Clonetech, Mountain View, USA

2.1.5 Antibodies

anti-actin (from mouse) clone mAbGEa	Affinity BioReagents, Golden, USA
anti-actin (from rabbit), polyclonal, A2066	Sigma-Aldrich, Buchs, Switzerland
anti-GFP N-terminal (from rabbit), G1544	Sigma-Aldrich, Buchs, Switzerland
anti-mouse (from goat), FITC labeled	Jackson, Hamburg, Germany
anti-mouse Ig (from sheep), horseradish peroxidase conjugated	Sigma-Aldrich, Buchs, Switzerland
anti-PfnM antiserum (from rabbit)	Pineda, Berlin, Germany
anti-poly-histidine (from mouse) clone HIS-1	Sigma-Aldrich, Buchs, Switzerland
anti-rabbit (from goat), TRITC labeled	Jackson, Hamburg, Germany
anti-rabbit Ig (from sheep) horseradish peroxidase conjugated	Sigma-Aldrich, Buchs, Switzerland

2.1.6 Kits

Amicon Ultra concentrator columns	Millipore, Billerica, USA
Copy Control Fosmid Library Production	Epicentre, Madison, USA
Dynal kilobaseBINDER Kit used with MagnaRack magnetic rack	Invitrogen, Carlsbad, USA
FluoroTag FITC Conjugation Kit	Sigma-Aldrich, Buchs, Switzerland
Jetsorb Gel Extraction	Genomed, Löhne, Germany
PCR Cloning Kit pDrive	Qiagen, Düsseldorf, Germany
Plasmid Mini Prep	Qiagen, Düsseldorf, Germany
Qiaquick PCR Purification	Qiagen, Düsseldorf, Germany
MaxiScript T7	Ambion, Austin, USA
RECOMT Thrombin CleanCleave	Sigma-Aldrich, Buchs, Switzerland
Sephadex G-25M prepacked column	Sigma-Aldrich, Buchs, Switzerland
SuperSignal West Pico	Pierce, Rockford, USA
Taq DNA-Polymerase	Qiagen, Düsseldorf, Germany
TaqMan® Fast Universal PCR Master Mix	Applied Biosystems, Foster City, USA
Trizol RNA Isolation Kit	Gibco/BRL, Eggenstein, Germany
Universal ProbeLibrary Set, Arabidopsis	Roche, Mannhein, Germany

2.1.7 Membranes, papers, films and filters

Glass fiber filters GF6	Schleicher & Schuell, Dassel, Germany
Household absorbent paper towels	ReAm, Taucha, Germany
Household cling film	Melitta Haushaltsprodukte, Germany
Hybond-C extra Nitrocellulose membrane	Amersham Pharmacia Biotech, Freiburg, Germany
Hybond-N+ Nylon membrane	Amersham Pharmacia Biotech, Freiburg, Germany
Hyperfilm MP X-ray detection film	Amersham Pharmacia Biotech, Freiburg, Germany
Imaging Screen K	BioRad Laboratories, München, Germany
Sealing film Parafilm M	Pechiney Plastic Packaging Inc., Wisconsin, USA
Whatman 3MM paper	Whatman Paper, Maidstone, U.K.

2.1.8 Technical appliances

Agarose gel electrophoresis chambers	BioRad Laboratories, München, Germany
	PEQLAB, Erlangen, Germany
Autoclave, model 3870 MLV	Systec, Wettenberg, Germany
Centrifuges:	
Refrigerated centrifuge Sorvall RC-5B	Du Pont, Bad Homburg, Germany
	Du Pont, Bad Homburg, Germany
Desktop centrifuge Sorvall MC 12C	Beckmann, München, Germany
Ultra centrifuge L8-M	
Micro-Ultracentrifuge MX-150,	Sorvall/Thermo Scientific, Waltham, USA
Rotor S45-A	Eppendorf, Hamburg, Germany
Centrifuge 5415C	Eppendorf, Hamburg, Germany
Desktop refrigerated centrifuge	Heraeus, Hanau, Germany
Biofuge fresco	
ChemiDoc XRS+	BioRad Laboratories, München, Germany
Desktop heating plate	IKA Werke, Staufen, Germany
Desktop shaker	Renner, Dannstadt, Germany
Electrical power supply, model 1000/500	BioRad Laboratories, München, Germany
Electrophoresis system Mini Protean 3	BioRad Laboratories, München, Germany
Electroporation unit Gene Pulser II	BioRad Laboratories, München, Germany
Freezers, refrigerators	Bosch, Stuttgart, Germany
Glass bead mill, model MM2	Retsch, Haan, Germany
Heating block	Stuart Scientific, Stone, Staffordshire, U.K.
Ice machine	Scotsman, Milano, Italy
Incubation oven	Diagen, Hilden, Germany
Microscopes:	
Deconvolution microscope:	
DeltaVision spectris system	Applied Precision, Issaquah, USA
Confocal microscope:	
Zeiss LSM 710; AxioObserver Z.1	Zeiss, Jena, Germany
Microwave ovens	Toshiba, Tokyo, Japan
Milli-RO 10/Milli-Q Plus water purifiers	Millipore Corp., Bedford, USA

Mini Trans-Blot Cell	BioRad Laboratories, München, Germany
Nanodrop 2000	Thermo Scientific, Waltham, USA
Peltier Thermal Cycler PTC-200	Biozym, Oldenburg, Germany
Real-Time PCR System 7500	Applied Biosystems, Foster City, USA
Scales; precision scales	Sartorius, Göttingen, Germany
Shaking incubator	Kühner AG, Birsfelden, Switzerland
Sonicator Sonopuls HD 60	Bandelin electronic, Berlin, Germany
Spectral photometer UV/Vis	Philips, Hamburg, Germany
Sterile workbench	Nuaire, Plymouth, USA
UV oven GS Gene Linker	BioRad Laboratories, München, Germany
Vacuum concentrator 5301	Eppendorf, Hamburg, Germany
Vacuum pump UNIJET II	Uni Equip, Martinsried, Germany
Vortexer "vortex genie"	Bender and Hobein, Zürich, Switzerland
Water bath	Huber, Offenburg, Germany

2.1.9 Miscellaneous materials

Examination gloves	Roth, Karlsruhe, Germany
Glass beads d=0.11 mm; d=0.18	Sartorius, Göttingen, Germany
Glassware	Schott, Mainz, Germany
	Kinematica, Littau, Switzerland
Magnet stirrers	Roth, Karlsruhe, Germany
Microscopic slides and cover slips	Roth, Karlsruhe, Germany
Petri dishes (disposable; ∅ = 10 cm)	Greiner Bio-One, Frickenhausen Germany
Pipette tips 10 µl, 20 µl, 100 µl, 200 µl, 1000 µl	STARLAB, Ahrensburg, Germany
Pipette tips 1000 µl, 5000 µl	Biozym, Hess. Oldendorf, Germany
Pipettes Pipetman series	Gilson S.A.S., Villiers Le Bel, France
PP-tubes, sterile, 15 ml, 50 ml	Greiner Bio-One, Frickenhausen, Germany
Safe-Lock Tubes 0,5 ml, 1,5 ml, 2,0 ml	Eppendorf, Hamburg, Germany
SafeSeal-Tips 10 µl, 20 µl, 100 µl, 200 µl, 1000 µl	Biozym, Hess. Oldendorf, Germany

2.1.10 Biological material

Escherichia coli BL21 (DE3)	Novagen/Merck, Darmstadt, Germany
Escherichia coli EPI100-T1R	Epicentre, Madison, USA
Escherichia coli XL-1 Blue	Stratagene/Agilent, Santa Clara, USA
Microcystis aeruginosa PCC 7806	Pasteur Culture Collection, Paris, France

2.2 Methods

2.2.1 Cultivation of bacteria

2.2.1.1 Cultivation of *Microcystis aeruginosa*

Cyanobacteria kept in liquid culture were cultivated in BG-11 medium (Rippka et al, 1979) in sealed, aerated 500 ml Erlenmeyer flasks. Environmental conditions were set at a temperature of 23°C, a continuous illumination with a light intensity of 30 $\mu Em^{-2}s^{-1}$ and shaking at 40 rpm. For cultivation of cyanobacteria on petri dishes a medium with final concentrations of 0.7% Bacto-agar (see 2.1.1 Chemicals, p35) and 1 x BG-11 was prepared, 40 ml of which was poured-to-coagulate into sterile petri dishes. Temperature and light conditions were chosen as before.

2.2.1.2 Cultivation of *Escherichia coli*

Escherichia coli cells were cultivated under standard conditions either in liquid LB medium or on LB agar in petri dishes (Sambrook et al, 1989). Cultures for preparation of plasmid vector DNA were incubated in 3-4 ml liquid LB medium at 37°C and shaking at 220 rpm. Corresponding to resistance markers used on respective vector constructs, Amp or Cm were added to either medium to final concentrations of 100 µg/ml and 50 µg/ml, respectively. For co-expression experiments, cells were grown in LB media containing both 50 µg/ml Amp and 12.5 µg/ml Cm.

2.2.2 Collection of field samples

Samples were collected by using conical plankton nets with a 30 µm mesh size which were dragged through the water at a depth of about 1 m. Net samples were either fixed by the addition of ethanol or left untreated and kept at 4°C. Alternatively, 10 l of unfiltered water were collected and subsequently filtered through GF6 glass fiber filters (see 2.1.7 Membranes, papers, films and filters, p40). Filters containing biological material were kept frozen.

2.2.3 Molecular biological techniques

2.2.3.1 Preparation of genomic DNA from cyanobacteria

Cells grown in liquid culture were harvested by centrifugation (4,000 x g, 10 min), washed two times in TE-buffer, resuspended in 0.5 ml of TES-buffer and incubated on ice for 1 h. Lysozyme was added to a final concentration of 2 mg/ml and the suspension was incubated for 1 h at 37°C. Subsequently, EDTA, proteinase K and SDS were added (to a final concentration of 0.05 M, 50 µg/ml and 2 %, respectively) and incubated for 1 h at 37°C. Following that, one volume of phenol/chloroform/isoamylalcohol (25:24:1) was added, the preparation was well mixed and centrifuged for 6 min at 4°C and 4000 x g. The tube was then carefully removed from the centrifuge and the aqueous (top) fraction was transferred into a new tube. Again, one volume of phenol/chloroform/isoamylalcohol (25:24:1) was added, well mixed and centrifuged as before. After centrifugation, the aqueous phase was well mixed – this time with one volume of chloroform/isoamylalcohol (24:1) and centrifuged as before. In the following step 2.5 volumes of isopropanol were added and the preparation incubated for 1 hour at RT to precipitate DNA. Isopropanol was removed by centrifugation at 6000 x g, 4°C, for 10 min and recovery of the resulting pellet, discarding the supernatant. The pellet was washed with 500 µl 70% ethanol by centrifugation at 6000 x g, 4°C, for 10 min and was subsequently left to air-dry completely or transferred to a vacuum-concentrator. Finally, the DNA-pellet was resuspended in 100 µl

water or TE-buffer. To remove RNA from the extract, an RNase A/T1 Mix digestion was performed following supplier's instructions. DNA was stored at -20 °C.

TE-buffer	10 mM Tris-Hcl; 1 mM EDTA, pH 8.0
TES-buffer	25% w/v Saccharose, 50 mM Tris-HCl, 100mM EDTA, pH 8.0

2.2.3.2 Preparation of metagenomic DNA from field samples

Prior to DNA extraction from field samples, frozen freeze-dried glass fiber filters (see 2.1.7 Membranes, papers, films and filters, p40) with adhering biological material were pulverized in liquid nitrogen. Particular care was taken to prevent contamination and degradation of the preparations. Liquid samples collected with plankton nets were pelleted by centrifugation (4000 x g, 10 min). Cellular material remaining afloat after centrifugation was collected by filtration, pulverized in liquid nitrogen and added to the pellet fraction. The pellet was washed in 0.5 ml 5 M NaCl solution by centrifugation as before to remove polysaccharides and other extracellular components. The pellet was resuspended in TE, treated with lysozyme, EDTA, proteinase K and SDS as described above (see 2.2.3.1 Preparation of genomic DNA from , p44). In the following step, one 8^{th} volume of a CTAB/PVP extraction buffer was added and the reaction incubated for 30 min in a water bath at 65°C. DNA was extracted with phenol/chloroform/isoamylalcohol as before, precipitated with isopropanol and washed 3 times with ample amounts of ethanol to remove excess salt.

CTAB/PVP extraction buffer	10% CTAB (w/v); 8% PVP; 0.7 M NaCl; 8% β-mercaptoethanol

2.2.3.3 Preparation of plasmid DNA from *Escherichia coli*

Plasmid DNA from *E. coli* was isolated following the standard procedure of the alkaline lysis (Sambrook et al, 1989). Cells in 3-4 ml liquid LB medium were collected by centrifugation at 3,000 x g for 5 min and the pellet resuspended in 300 µl buffer P1. Buffer P2 (300 µl) was then added and the suspension was mixed gently. Following an incubation time of 5 min at RT, 300 µl of buffer P3 were added and the preparation was kept on ice for 5 min. During these steps the mixture was not vortexed to avoid dissociation of genomic DNA from the membrane fraction. Cellular debris was pelleted by centrifugation step at 15,000 x g, 4°C, for 10 min, leaving the plasmid DNA in the clear supernatant. Nucleic acids were precipitated with 0.7 volumes of isopropanol, the solution was centrifuged at 15,000 x g, 4°C, for 10 min and the pellet was washed with 1 ml 70% ethanol. After centrifugation as before, the pellet was air-dried and resuspended in 100 µl water or TE-buffer.

P1	50 mM Tris-HCl pH 8.0; 10 mM EDTA
P2	200 mM NaOH; 1 % SDS
P3	3 M Potassium acetate, pH 5.0

2.2.3.4 Quantification of nucleic acids by spectro-photometry

The concentration of RNA or DNA in an aqueous solution was determined by measuring the absorption of UV-light of a wavelength of 260 nm in a Nanodrop 2000 photometer (see 2.1.8 Technical appliances, p41).

2.2.3.5 Digestion of DNA with restriction endonucleases

DNA cleavage was performed adhering to manufacturers' instructions (see 2.1.2 Enzymes, p37). Commonly, a reaction volume of 20 µl was chosen and DNA was incubated for 1 hour at 37°C.

2.2.3.6 Agarose gel electrophoresis of DNA

DNA fragments were separated size-wise in agarose gels by electrophoresis (Sambrook et al, 1989). According to the size of the DNA fragments, agarose concentrations of 0.5%-1.0% (w/v) were used, where longer fragments required the lower concentrations. Agarose was dissolved in TAE buffer by heating in a microwave oven, gels immersed in TAE buffer were run at a constant voltage of 100 V. DNA samples were mixed with 1 µl of DNA loading dye prior to loading to visualize progress of run. The genome of the phage λ digested with the restriction endonuclease *PstI* served as a size marker. Gels contained ethidium bromide in a final concentration of 0.05 µg/ml to indicate location of DNA bands under UV illumination. For signal detection and image processing, the ChemiDoc XRS+ system was used in combination with the "Quantity One" software.

TAE	40 mM Tris, 20 mM acetic acid, 1 mM EDTA
DNA loading dye	50 % Ficoll; 1 mM EDTA, pH 8.0; 0.05 % (w/v) Bromophenol blue; 0,05 % (w/v) Xylene cyanol

2.2.3.7 Elution of DNA fragments from agarose gels

DNA fragments were eluted from agarose gels using the Jetsorb Gel Extraction kit (see 2.1.6 Kits, p40) according to manufacturer's instructions.

2.2.3.8 Primer design and polymerase chain reaction

DNA fragments were amplified by PCR using the Qiagen Taq DNA-Polymerase System (see 2.1.6 Kits, p40). Primer sequences and annealing temperatures were deduced using the software program "Primer3" publicly available online at http://frodo.wi.mit.edu/primer3/. Reactions were performed in a total volume of 20 µl with the following composition: 2 µl of 10 x Taq-buffer, 0.5 µM of each primer, 0.15 mM of dNTPs, 1U of Taq

polymerase and 1 µl of template DNA (either 100-200 ng of genomic DNA or approximately 10 ng of plasmid DNA). Probes were then transferred to a thermal cycler and subjected to a specific amplification program. Common steps included the initial denaturation at 95°C for 3 min, normally followed by 35 cycles of a subsequent denaturation at 95°C for 30 sec, a primer annealing at the ambient annealing temperature for 30 sec, an elongation of double-stranded DNA fragments by Taq-Polymerase at 72°C for a period of time dependent on the length of the amplificate (approx. 1 min per kb amplificate length). After 35 cycles a final elongation step at 72°C for 10 min ensured the completion of unfinished synthesis events.
To perform PCR analyses from bacterial cells ("colony PCR") 1 µl of bacterial suspension replaced the template DNA in the initial reaction mixture. Additionally, the initial denaturation step in the cycler program was extended to 10 min at 95°C.

2.2.3.9 Inverse PCR

Inverse PCR was performed according to established protocols (Sambrook et al, 1989). The method allows the characterization and sequence determination of regions of DNA flanking a stretch of known sequence (see **Figure 2.2**). This requires the identification of restriction endonucleases that do not cut in the known part of the DNA (see 2.2.7 *In silico* analyses, p67). In the case of the *actM-pfnM* region the endonucleases *BglII* and *XbaI* meet these criteria. Approximately 750 ng of genomic DNA were digested in a total reaction volume of 20 µl (see 2.2.3.5 Digestion of DNA with restriction endonucleases, p46). Reactions containing genomic DNA from *Microcystis aeruginosa* PCC 7806 and pDrive cloning vectors carrying the complete *actM-pfnM* genomic island were prepared as controls.

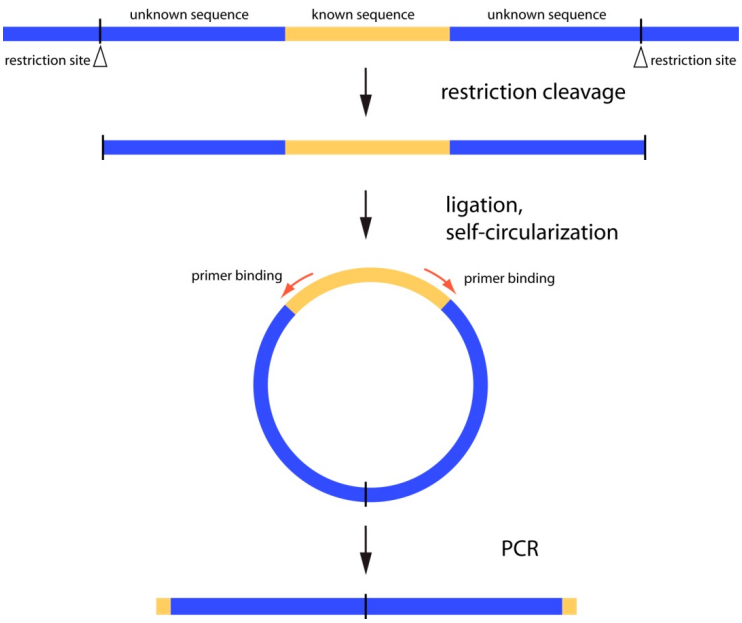

Figure 2.2. Principle of the inverse PCR method.
It is important that the used restriction enzyme does not recognize a site within the known sequence. Self-circularization occurs preferentially at low DNA concentrations.

Digested DNA was extracted with phenol/chloroform, precipitated with isopropanol and washed with ethanol to deactivate the restriction enzyme (see 2.2.3.1 Preparation of genomic DNA from cyanobacteria, p44). To determine conditions optimal for self-circularization, ligation was performed in three dilutions of purified, digested genomic DNA, using either 65 ng, 8 ng or 1 ng in a total reaction volume of 10 µl (see 2.2.3.14 Ligation of linear DNA fragments into plasmid vectors, p51). PCR reactions were performed with ligation reactions using various primers binding within the *actM-pfnM* region (see **Figure 2.1**, p39). Reverse complements of these primers were used to amplify unknown sequences.

2.2.3.10 Biotin pull-down assay

Pull-down assays were performed with the Dynal kilobaseBINDER Kit (see 2.1.6 Kits, p40) according to manufacturer's instructions. 5' biotinylated primers initiating outward-directed linear amplification from the *actM-pfnM* region were used with metagenomic DNA isolates. After 35 cycles of Taq-polymerase mediated amplification, reactions were mixed with streptavidin-coupled magnetic beads. Beads were immobilized with a magnetic tube rack,

beads suspension was either directly used in sequencing reactions or DNA was extracted according to manufacturer's instruction.

2.2.3.11 Quantitative PCR (qPCR)

Assays were designed utilizing the Universal ProbeLibrary Assay Design Center (see 2.2.7 *In silico* analyses, p67), resultant primers generated amplification products of 70 – 100 bp, probes were identified from the Arabidopsis set. Reactions were carried out in a 7500 Real-Time PCR System using the *TaqMan* Fast Universal PCR Master Mix. Each reaction contained 50 ng of DNA, 1 µM of each primer and 100 nm of the particular probe. The cycle protocol was as follows: an initial step at 95°C for 10 min was followed by 40 cycles of 15 s at 95°C and 1 min at 60°C. Each reaction was analyzed in triplicates per experiment. No-template controls (NTC) were included for each primer pair. Results were analyzed using the Sequence Detection Software v1.4.

2.2.3.12 Generation of labeled RNA-probes for RING-FISH

The gene of interest to be visualized by RING-FISH (see 2.2.5.3 RING-FISH of bacterial cells, p63) was PCR-amplified with primers expanded by the 5' addition of a T7 promoter sequence sufficient to drive transcription by the T7 RNA polymerase. To generate labeled probes hybridizing to both sense and anti-sense sequences in downstream applications, both primers of one pair carried a T7 extension. Probes designed to recognize antisense sequences only (genomic DNA) originated from a mix of labeled sense primers and unlabeled anti-sense primers (see **Figure 2.3**). Purified PCR products (see 2.2.3.13 Purification of PCR fragments and other DNA, p51) were used as template for *in vitro* transcription by T7 RNA polymerase with the MaxiScript T7 kit (see 2.1.6 Kits, p40). Following the manufacturer's instructions, reactions contained 1 µg of template DNA and fluorescein-12-labeled UTP (see 2.1.1 Chemicals, p35) and unlabeled UTP in a 1:1 molar ratio.

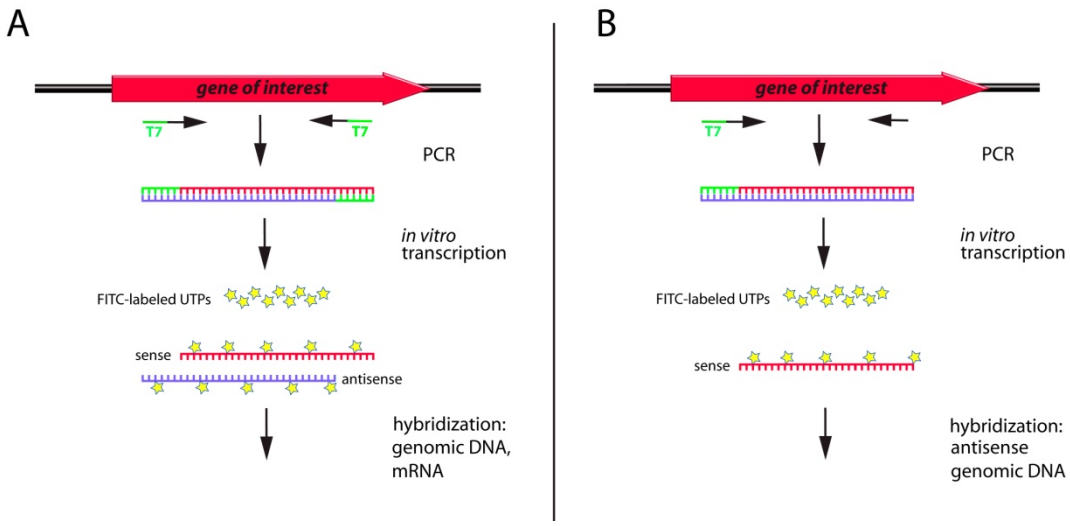

Figure 2.3. Strategies for probe generation for RING-FISH experiments.
T7 promoter sequences are added to PCR amplificates of the gene of interest. Subsequent *in vitro* transcription with T7 RNA polymerase and FITC labeled UTPs generates fluorescent RNA probes.
A: T7 promoter sequences on both primers result in probes recognizing sense and anti-sense targets.
B: T7 promoter sense primers will lead to probes hybridizing to anti-sense sequences only.

2.2.3.13 Purification of PCR fragments and other DNA

To remove primers, unwanted oligonucleotides and other impurities from DNA fragments such as plasmids or PCR products, the Qiagen Qiaquick PCR Purification kit (see 2.1.6 Kits, p40) was used as instructed by the manufacturer.

2.2.3.14 Ligation of linear DNA fragments into plasmid vectors

PCR fragments synthesized by Taq DNA polymerase were ligated into the Qiagen pDrive cloning vector following the instructions of the Qiagen PCR Cloning kit used (see 2.1.6 Kits, p40).
DNA fragments for blunt end ligations were created either directly by cleavage with blunt-cutting restriction endonucleases or by "fill in" of overhangs with Klenow fragment (see 2.1.2 Enzymes, p37). Incubation took place for 30 min at 37°C in a total reaction volume of 30 µl following manufacturer's instructions for the use of Klenow fragment. To remove 5' phosphate DNA overhangs and avoid religation, linearized plasmid vectors were treated with CIAP (see 2.1.2 Enzymes, p37). A reaction volume of 30 µl

was incubated for 30 min at 37°C following the manufacturer's instructions. Ligation was performed with T4 DNA ligase (see 2.1.2 Enzymes, p37) in a 20 µl reaction mix containing linearized vector and respective insert in a molar ratio of 1:2, 0.5 mM ATP and 2.5 % (w/v) PEG 4000. The reaction was incubated overnight in a refrigerator (10°C-14°C).
For sticky-end ligations, PEG 4000 was omitted from the reaction.

2.2.3.1 Transformation of *Escherichia coli*

Cells of *E. coli* were transformed utilizing the $CaCl_2$-induced chemical competence (Sambrook et al, 1989) of the XL-1 strain used (Bullock et al, 1987). 200 µl of XL-1 cell culture was mixed with the respective ligated plasmid vector and kept on ice for 30 min. The mixture was then subjected to a heat shock in a water bath at 42°C for 1 min. Afterwards, 500 µl of SOC medium were added and cells were incubated for 1 hour at 37°C and shaking at 220 rpm. Meanwhile, LB medium agar plates were prepared containing 100 µg/ml ampicillin, 40 µg/ml X-Gal and 0.2 mM IPTG. Positive clones were determined by blue-white selection. For further analysis, single white colonies were picked and transferred into 3-4 ml of liquid LB medium containing 100 µg/ml ampicillin. For co-expression experiments chloramphenicol (12.5 µg/ml) was used for selection in addition to ampicillin.

SOC medium	2% (w/v) trypton; 0.5% (w/v) yeast extract; 20 mM glucose; 8.6 mM NaCl; 25 mM KCl; 10 mM $MgCl_2$; pH 7.0

2.2.3.2 Generation of GFP-fusion proteins

For C-terminal fusion of GFP, the nucleotide sequence for GFPuv was amplified by PCR from the pGFPuv vector using the primers GFPuv_FW and GFPuv_RV (see 2.1.3 PCR primers, p37). The amplicon coded for an N-terminal SRLE-linker peptide and carried an *XbaI* and an *EcoRI*

restriction site at the 5' and the 3' end, respectively. After subcloning into and *XbaI*/*EcoRI* mediated restriction out of the cloning vector pDrive (see 2.2.3.14 Ligation of linear DNA fragments into plasmid vectors, p51), the *gfpuv*-sequence was ligated into the *XbaI*/*EcoRI*-linearised pBLUESCRIPT II SK (+) vector (see 2.1.4 Plasmid vectors, p39). The *actM* and *pfnM* sequences were amplified from purified genomic DNA from *Microcystis aeruginosa* PCC 7806 using primer pairs ActM_Xba_FW/RV for *actM* and PfnM_Xba_FW/RV for *pfnM*. The primers were designed in a way as to add *XbaI* restriction sites to both ends and to remove the stop-codon. After pDrive subcloning and *XbaI* restriction, the thus modified *actM* and *pfnM* sequences were ligated into the GFPuv-carrying, *XbaI* linearized pBLUESCRIPT II SK (+) vector to yield ActM-SRLE-GFPuv and PfnM-SRLE-GFPuv fusion proteins, respectively.

For N-terminal fusion, *gfpuv* was amplified using a proof reading Pfu polymerase and the 5' phosphorylated primer pair GFPEco47Fw/Rv. The PCR product was blunt-ligated (see 2.2.3.14 Ligation of linear DNA fragments into plasmid vectors, p51) into *NdeI* linearized plasmid vectors generated for the heterologous expression of ActM and PfnM (see below).

2.2.3.3 Construction of plasmid vectors for heterologous expression

The primer pairs ActMExFW/RV and PfnMExFW/RV were used in PCR reactions to amplify the *actM* and *pfnM* genes, respectively, from purified genomic *Microcystis aeruginosa* PCC 7806 DNA. In these reactions a proof-reading Pfu polymerase (see 2.1.2 Enzymes, p37) was used according to the manufacturer's instruction; a short incubation with Taq polymerase (10 min, 72 °C) followed to add A-overhangs for TA-cloning. An *NdeI* and a *BamHI* site was added to each amplicon's 5' and 3' end, respectively. After pDrive subcloning and excision with *NdeI* and *BamHI*, the *actM* and *pfnM* genes were ligated into the pET15b expression vector previously linearized with the same restriction enzymes.

2.2.3.4 Generating *E.coli*-strains for co-expression of proteins

GFP-labeled proteins encoded on pBLUESCRIPT II SK (+) derived vectors of the pMB1/ColE1 compatibility group (see 2.2.3.2 Generation of GFP-fusion proteins, p52) were co-expressed in *E.coli* BL21 (DE3) with proteins encoded on pACYC184 derived vectors with a compatible p15A-type origin of replication (see 2.1.4 Plasmid vectors, p39). The latter were constructed as follows: using 5' phosphorylated primers T7 Prom and T7 Term a region sufficient for heterologous expression of proteins encompassing the complete sequence flanked by and including the T7 promotor and T7 terminator sites were amplified with Pfu polymerase (see 2.1.2 Enzymes, p37) from the pET15b derived expression vector constructs carrying the desired gene to be co-expressed with the GFP-fusion protein of interest (see 2.2.3.3 Construction of plasmid vectors for heterologous expression, p53). This amplicon was then ligated into the pACYC184 vector subjected to *HindIII* restriction and subsequent 5' overhang fill-in by Klenow-fragment (see 2.2.3.14 Ligation of linear DNA fragments into plasmid vectors, p51). No inducer of transcription (IPTG) was necessary to produce sufficient amounts of either protein.

2.2.3.5 Construction of genomic fosmid libraries

Fosmid libraries from (meta-) genomic DNA isolates were generated with the Copy Control Fosmid Library Production kit (see 2.1.6 Kits, p40). The fosmid vector used was pCC2FOS. 10 single clones were picked and pooled to grow overnight in liquid LB medium supplemented with 12.5 µg/ml chloramphenicol. Overnight cultures were screened by colony-PCR (see 2.2.3.8 Primer design and polymerase chain reaction, p47). Colonies of positive pools were grown separately and re-screened.

2.2.3.6 Sequencing of DNA fragments

DNA fragments to be sequenced were ligated into the pDrive cloning vector (see 2.2.3.14 Ligation of linear DNA fragments into plasmid vectors, p51) and delivered for automatic sequencing to "SMB Service in Molecular Biology".

The company's instructions for preparing DNA sequence samples were followed.

2.2.4 Proteo-biochemical methods

2.2.4.1 Preparation of proteins from bacterial cells

To generate cell-free extracts, a liquid bacterial cell culture was centrifuged at 3,000 x g for 6 min. Pellets were resuspended in extraction buffer (1 ml per 100 ml cell culture) and 1 volume of glass beads (d=0.11 mm and d=0.18 mm in a 1:1 ratio) were added. This mixture was transferred to liquid N_2 immediately. After thorough freezing, tubes were thawed and transferred to a glass bead mill to grind open bacterial cell walls for 5 min at 4°C at maximum speed. The cycle of freezing, thawing and grinding was repeated another three times, mixtures were then centrifuged at 15,000 x g, 4°C, for 10 min. The cleared supernatant contained cellular protein. Alternatively, cells were disrupted using a sonicator. Cell pellets resuspended in buffer as before were sonicated on ice in six maximum energy bursts of 10 seconds each with 10-seconds-breaks interrupting each burst phase. After sonication treatment, cell debris was pelleted as before and protein fractions were recovered. To recover the insoluble protein fraction, cell pellets remaining after extraction with native buffer were resuspended in denaturating buffer and subjected to another round of mechanical disruption.

native extraction buffer	500 mM Tris-HCl; 50 mM EDTA; 0.5 mM PMSF, pH 8.0
denaturating extraction buffer	100 mM Na_2HPO_4; 10 mM Tris-HCl; 8 M urea; pH 8.0

2.2.4.2 Heterologous expression and purification of proteins

Expression in *E. coli* BL21 (DE3) cells was induced with 0.5 mM IPTG at OD_{600} of 1.0, cells were grown for 4 h at 37°C with shaking at 220 rpm. Cell-free extracts were prepared (see 2.2.4.1 Preparation of proteins from bacterial cells, p55) either in G buffer (approx. 1 ml buffer per 100 ml culture volume) supplemented with 40 mM imidazole and 0.5 mM PMSF for ActM or in native lysis buffer for PfnM. Expressed proteins were purified over a Ni-NTA-agarose matrix following the instructions in the handbook. The matrix was washed twice with the respective lysis buffer containing 60 mM and 20 mM imidazole for ActM and PfnM, respectively. The elution buffer contained 250 mM imidazole. Protein purity was determined by SDS-PAGE analysis (see 2.2.4.5 SDS Polyacrylamide gel electrophoresis of proteins, 57). To estimate the amount of protein aggregated in insoluble inclusion bodies, the pellet remaining after glass bead mill treatment in native lysis buffers was resuspended in an equal volume of denaturating buffer and subjected to another round of disruption. For purification under denaturating conditions, native buffer or G-buffer was replaced with denaturating buffer, respective imidazole concentrations remained as under native conditions. Protein levels were assessed via SDS-PAGE and immunoblots.

G-buffer	5 mM Tris, 0.1 mM $CaCl_2$, 0.2 mM ATP, 1 mM NaN_3, pH 8.0
native lysis buffer	50 mM NaH_2PO_4, 300 mM NaCl, 10 mM imidazole, 0.5 mM PMSF, pH 8.0
denaturating buffer	100 mM Na_2HPO_4, 10 mM Tris-HCl, 8 M urea, pH 8.0

2.2.4.3 Purification and concentration of protein solutions

Solutions of known proteins were concentrated with Amicon Ultra centrifugal filters with a molecular weight cut-off of 10,000 Da (for PfnM) and 30,000 Da (ActM) following the manufacturer's instructions.

2.2.4.4 Quantification of protein extracts after BRADFORD

Concentrations of total protein amounts were determined spectrophotometrically by the method after Bradford (Bradford, 1976) using the BioRad Protein Assay system. 795 µl of bi-distilled water were mixed with 200 µl of the assay reagent and 5 µl of the protein solution to be analyzed. After an incubation time of 10 min, absorptions were measured at λ=595 nm. A series of solutions of varying concentrations of BSA was used to determine a standard calibration curve and individual concentrations were accordingly calculated.

2.2.4.5 SDS Polyacrylamide gel electrophoresis of proteins

Protein samples were electrophoretically separated utilizing the principles of the discontinuous method described by Laemmli (Laemmli, 1970). Depending on molecular weight of the proteins of interest, separating gels contained 10-12.5 % acrylamide while stacking gels contained 4% acrylamide. APS and TEMED were added to final concentrations of 0.5% and 0.05%, respectively. Samples were mixed with 0.25 volumes of 5 x SDS-PAGE loading dye and heated at 95°C for 10 min. Each gel was completely immersed in SDS-PAGE running buffer and run at constant currents of 30 mA in a BioRad Mini Protean electrophoresis chamber (see 2.1.8 Technical appliances, p41). Gels were either stained or kept for further analyses. For staining, gels were floated in either Pierce GelCode Blue Stain Reagent or Roth "Roti-Blue" Coomassie staining for at least 1 hour. Gels were de-stained in distilled water.

Separating gel	10% or 12.5% (v/v) acrylamide/bisacrylamide 37.5:1; 375

	mM Tris-HCl,pH 8.8; 0.1% (w/v) SDS
Stacking gel	4% (v/v) acrylamide/bisacrylamide 37.5:1; 125 mM Tris-HCl, pH 6.8; 0.1% (w/v) SDS
Running buffer	192 mM Glycin; 25 mM Tris; 0.1% (w/v) SDS
5xLoading dye	250 mM Tris, pH6.8; 0.5% bromophenol blue; 10% (w/v) SDS; 50% (v/v) Glycerol; 500 mM DTT

2.2.4.6 "Western blot" – transfer of proteins from PAA gels

After SDS-PAGE, proteins were transferred from PAA gels and immobilized on Hybond C-extra Nitrocellulose membranes for immunodetection (see 2.1.7 Membranes, papers, films and filters, p40). Blotting was performed using the BioRad Mini TransBlot Cell system. Gels and accordingly sized membranes were equilibrated for 10 min in Western blot transfer buffer before blotting "sandwich" was prepared following manufacturer's instructions. Blots were run at a constant voltage of 100 V for 1 hour.

Western blot transfer buffer	15.6 mM Tris; 120 mM Glycine

2.2.4.7 Immunodetection on Western blot membranes

After Western blot transfer, membranes were blocked with 5% (w/v) skim milk powder in TBS-T for at least 1 h. Primary antibodies (see 2.1.5 Antibodies, p39) were used in a dilution of 1:10,000 in blocking solution, except for the anti-actin mouse monoclonal antibody and the anti-PfnM rabbit antiserum which were used at dilutions of 1:3,000 and 1:50,000, respectively. During incubation, membranes were rocked gently for at least 1 h at 4°C. Membranes were rinsed twice for 10 min with TBS-T. Secondary antibodies conjugated with horseradish peroxidase were used in a dilution of 1:10,000. Membranes were incubated in 20 ml of secondary antibody solution for at least 1 h at 4°C. Finally, membranes were washed with TBS-T for 30

min with 4 changes of washing buffer. Visualization of band signals was performed using the Pierce SuperSignal West Pico Chemiluminescent Substrate kit according to manufacturer's instructions in combination with a ChemiDoc XRS+ imaging system or with X-ray films for detection. Films were exposed for 10 min and developed in a dark chamber under standard photographic conditions.

TBS-T	10 mM Tris-HCl; 150 mM NaCl; 0.1% (v/v) Tween 20

2.2.4.8 DNase I assay

5 µl of DNase I (0.1 U/µl) were incubated with 5 µl of purified rabbit actin or ActM (both at 0.5 µg/µl) in G-buffer and incubated for 5 min at RT. Complete reactions were added to 100 µl of salmon-sperm DNA solution (40 ng/µl) in DNase I reaction buffer and absorption at 260 nm was followed over time with a Nanodrop 2000 spectro-photometer.

2.2.4.9 Binding and co-elution assays

Proteins expressed heterologously in *E.coli* from pET15b expression vectors were attached via 6 x His tag to a Ni-NTA agarose matrix and washed as if to be purified (see 2.2.4.2 Heterologous expression and purification of proteins, p56). Instead of elution, an ensuing equilibration of the loaded agarose matrix with G-buffer (containing 10 mM imidazole for matrix--bound PfnM and 40 mM imidazole for matrix-bound ActM) was followed by the addition of native, non-tagged protein extracts of the potential binding partner in the same buffer. Tag-free PfnM was generated by thrombin mediated cleavage (RECOMT Thrombin CleanCleave Kit) of purified 6xHis-tagged PfnM, complete removal of the tag was verified on immunoblots using a monoclonal anti-poly-histidine antibody produced in mouse (see 2.1.5 Antibodies, p39). Untagged ActM was expressed in *E.coli* from the pCC2FOS fosmid vector carrying the *actM-pfnM* region from *Microcystis aeruginosa*

PCC 7806 in its native genomic environment (see 2.2.3.5 Construction of genomic fosmid libraries, p54). The identity of the insert was verified by DNA sequencing (see 2.2.3.6 Sequencing of DNA fragments, p54) and the presence of untagged ActM in native protein extracts was checked on immunoblots. GFP-fusion proteins did not carry a 6xHis-tag and were used directly after protein extraction. Matrixes were washed three times with G-buffer (supplemented with 20 mM and 60 mM imidazole four matrix-bound PfnM and ActM, respectively) and eluted with 250 mM imidazole in G-buffer.

2.2.4.10 PfnM antibody generation

For antibody generation, PfnM was purified under denaturating conditions (see 2.2.4.2 Heterologous expression and purification of proteins, p56), precipitated with 45 % (w/v) $(NH_4)_2SO_4$ for 45 min on ice and pelleted at 12,000 x g for 15 min at 4°C. 1 mg of precipitated protein was used to raise polyclonal antibodies in rabbit serum (Pineda antibody service, Berlin, Germany).

2.2.4.11 Preparation of polymerized actin

Rabbit actin or ActM in G buffer was converted to Mg^{2+}-actin by adding 1/20 volume of conversion buffer (Gershman et al, 1989) prior to polymerization. Polymerization was started with the addition of 1/20 volume of initiation buffer.

conversion buffer	1 mM EGTA, 1 mM $MgCl_2$
initiation buffer	2 M KCl, 40 mM $MgCl_2$

2.2.4.12 Phalloidin staining of actin

4 µl of a solution of polymerized actin or ActM (see 2.2.4.11 Preparation of polymerized actin, p60) were spread on a poly-L-lysine-coated coverslip (see

2.2.5.2 Immunostaining of fixed cyanobacterial cells, p63). After 2 min, excess fluid was removed, actin filaments were fixed with 2.5% glutaraldehyde in PBS for 5 min, washed 3 times 5 min with PBS and incubated with 50 µl of a 0.165 µM (0.25 U) solution of fluorescence-labeled phalloidin in PBS for 30 min. Preparations were washed twice in PBS and mounted for fluorescence microscopy on glass slides in 4% (v/v) n-propylgallate dissolved in 87% (v/v) glycerol.

2.2.4.13 FITC-labeling of PfnM

Purified PfnM (1 mg/ml) was conjugated with FITC according to the FluoroTag FITC Conjugation Kit protocol (see 2.1.6 Kits, p40). Briefly, 125 µg of FITC was added to 1 mg of protein and allowed to react in 0.1 M carbonate-bicarbonate buffer (Delory, 1945) for 1 h at RT. Labeled PfnM was isolated and separated from unincorporated FITC with a Sephadex G-25M pre-packed column. The molar ratio of incorporated FITC to PfnM (F/P) sufficient to provide satisfying fluorescent intensities was determined to be 1.12.

carbonate-bicarbonate buffer 90 mM $NaHCO_3$, 10 mM Na_2CO_3, pH 9.0

2.2.4.14 Co-polymerization of ActM and PfnM

Purified ActM and PfnM (either FITC-labeled or untagged) in G-buffer were brought to a concentration of 75 µM and mixed in different molar ratios. Polymerization of ActM was initiated (see 2.2.4.11 Preparation of polymerized actin, p60) and solutions were kept at 4°C over night. Co-polymerization was assessed either by phalloidin staining and fluorescence microscopy (see 2.2.4.12 Phalloidin staining of actin, p60). Alternatively, reactions were ultra-centrifuged at 100,000 x g, 1 h, 4°C in a Sorvall Micro-ultracentrifuge MX-150 equipped with an S45-A rotor. Pellets were resuspended and analyzed by SDS-PAGE and Western-immunoblots. Protein

bands on Coomassie-stained gels were detected with a ChemiDoc XRS+ detection system running the Image Lab software. For quantification, bands were identified manually and analyzed using the "Volume" tool. Manual band detection and subsequent data analyses were performed in triplicates and averaged.

2.2.5 Fluorescence microscopy

2.2.5.1 Fixation and permeabilization of bacterial cells

To perform whole-cell immunostaining with cyanobacteria, cells were harvested by centrifugation of 25 ml of liquid culture at 2,000 x g, RT for 5 min. Pellets were washed once in PBS and resuspended in PBS by brief vortexing to resolve clumps. Cells were fixed in 3.7% (v/v) formaldehyde in PBS for 1 h on ice. After three PBS washing steps, cells were resuspended in GTE buffer and permeabilized by addition of freshly prepared lysozyme solution (in GTE) to a final concentration of 2 mg/ml. Glass slides were coated with 0.1% (w/v) poly-L-lysine solution by dispersing 10 µl solution and subsequent air drying. After incubation with lysozyme for 3 min at RT, 50 µl of fixed cells were spread on poly-L-lysine treated slides using a cover slip. Glass slides were dipped into methanol for 5 min at -20°C and subsequently into -20°C acetone for 30 seconds. Cells thus prepared were blocked in 2% (w/v) BSA in PBS for 15 min.

PBS	140 mM NaCl; 2.7 mM KCl; 8 mM Na_2HPO_4; 1.8 mM KH_2PO_4; pH 7.4
GTE	50 mM glucose; 20 mM Tris-HCl pH 7.5; 10 mM EDTA, pH 8.0

2.2.5.2 Immunostaining of fixed cyanobacterial cells

After blocking as described above (see 2.2.5.1 Fixation and permeabilization of bacteria, p62), fixed and permeabilized cells were incubated with a primary antibody at a dilution of 1:500 in 2% BSA (w/v in PBS) for 1 hour at RT in a humid chamber. To this end, 20 µl of diluted antibody were pipetted directly onto cells immobilized on poly-L-lysine treated slides and covered with a cover slip. Afterwards, slides were washed twice in PBS in a cuvette for 10 min and subsequently incubated with a fluorescently-labeled secondary antibody diluted 1:100 in 2% BSA (w/v in PBS) for 1 hour in a humid chamber in the dark. To conclude staining, cells were washed twice for 10 min in PBS. If desired, the second wash contained Hoechst DNA dye in a final concentration of 0.05 µg/ml. Cells were mounted in a drop of 4% (v/v) n-propylgallate dissolved in 87% (v/v) glycerol and stored for up to 4 weeks at -20°C.

2.2.5.3 RING-FISH of bacterial cells

Cyanobacterial cells were fixed and immobilized on poly-L-lysine coated glass slides as before (see 2.2.5.1 Fixation and permeabilization of bacterial cells, p62). Slides were incubated in serial steps with 50% (v/v) ethanol, 80% ethanol and 96% ethanol for 2 min each. Concentration of labeled RNA-probes in hybridization buffer (see 2.2.3.12 Generation of labeled RNA-probes for RING-FISH, p50) was adjusted to 5 ng/µl and dried preparations were incubated with 20 µl of probe solution for 80 min at 80°C in the dark in sealed, air-tight wet chambers. To assess influence of hybridization stringency on signal intensity, formamid and SDS concentrations were varied ranging from 20%/0.02% (formamid/SDS), 35%/0.02% to 80%/0.01%. Incubation was continued over night at 46°C. Slides were washed once in pre-warmed washing buffer for 20 min at 46°C. Slides incubated with 80% formamid were not washed. For 35% formamid treated slides, washing buffer composition was adjusted to contain 88 mM NaCl. Finally, slides were washed in water for 5

min at RT, mounted as before and analyzed microscopically (see 2.2.5.2 Immunostaining of fixed cyanobacterial cells, p63).

hybridization buffer	900 mM NaCl, 0.02% SDS, 20 mM Tris, 20% formamide
washing buffer	250 mM NaCl, 0.01% SDS, 20 mM Tris

2.2.5.4 Live-cell imaging

Escherichia coli cells expressing GFP-tagged proteins were observed alive. After thorough vortexing, cells in liquid culture were diluted 1:5 in fresh culture medium and a 15 µl sample was directly pipetted onto agarose-coated glass slides. To generate these, 10 µl of a 1% (w/v) solution of low melting point agarose in LB-medium were spread on the slides, air-dried and used within 16 hours.

2.2.5.5 Image acquisition and processing

Wide-field deconvolution-based fluorescence microscopy, image acquisition and processing were carried out using the DeltaVision spectris system with the pre-installed default softWorx software package. Images were acquired as stacks of z-sections with one image taken every 0.2 µm spanning the whole cell volume. Standard excitation and emission filters were used for visualization: the "DAPI" excitation/emission filter pair (wavelengths of 360 nm and 457 nm, respectively), the "RD-TR-PE" filter pair (555 nm/617 nm) and the "FITC" filter pair (490 nm/528 nm). Acquired raw images were deconvolved by iterative constrained deconvolution using the algorithms implemented in the softWorx software package.

For confocal fluorescence microscopy a Zeiss LSM 710 system with an inverted microscope AxioObserver Z.1 was used. The imaging software ZEN 2009 was used for operating the system, image acquisition and processing.

2.2.6 Small-Angle X-ray Scattering (SAXS)

2.2.6.1 SAXS data acquisition

Small-angle X-ray scattering measurements were performed in collaboration with Friedmar Delißen and Prof. Andreas Thünemann at the BAM Bundesanstalt für Materialforschung- und Prüfung Berlin with a SAXSess camera (Anton Paar, Austria). This Kratky type of camera is attached to a laboratory X-ray generator (PW3830, PANalytical), and is operated with a fine focus glass X-ray tube at 40 kV and 50 mA ($Cu_{K\alpha}$, $\lambda = 0.1542$ nm). A focusing multi-layer optic and a block collimator provide a monochromatic primary beam with low background. ActM/PfnM samples (see 2.2.4.14 Co-polymerization of ActM and PfnM, p61) were filled in a reusable vacuum tight flow cell sample holder. SAXS data (intensity as a function of the scattering vector) was recorded for 1800 s with a CCD detection system in a q-range of 0.08 to 6.0 nm^{-1} (Anton Paar). Thus, the scattering was measured in the size range of $\pi/q_{max} = 0.5$ nm to $\pi/q_{min} = 40$ nm. The scattering vector is defined in terms of the scattering angle, θ and the wavelength, λ of the radiation, thus $q = 4\pi / \lambda\sin(\vartheta)$. For clarity, the angle between incident and scattered beam is 2θ. The two-dimensional intensity data was converted to one-dimensional data with the CCDQuant software. The temperature of 25°C was controlled with a TCS 120 sample holder (Anton Paar) with an accuracy of ± 0.2°C. A reusable capillary was used for all measurements to attain the same scattering volume and background contribution. The resulting scattering curves were corrected for the contribution of the suspension medium (water) and the glass capillary. Furthermore, the data was de-smeared using the length profile of the primary beam (Orthaber et al, 2000) with SAXSQuant.

2.2.6.2 Modeling analysis of SAXS data

The total scattering of ActM filaments could be described as the sum of filament and random-coil scattering as

$$I(q) = I_1(q) + I_2(q).$$

The geometrical model of ribbon shaped filaments is represented by parallelepipeds (Kuchibhatla et al, 2009) of length a, width b and thickness c with $a > b > c$. They have the scattering function (Mittelbach & Porod, 1961)

$$I_1(q) = k_1 \int_0^{\pi/2} \int_0^{\pi/2} \left[\frac{\sin(\tfrac{1}{2} aq \sin\theta\cos\varphi)}{\tfrac{1}{2} aq \sin\theta\cos\varphi} \times \frac{\sin(\tfrac{1}{2} bq \sin\theta\sin\varphi)}{\tfrac{1}{2} bq \sin\theta\sin\varphi} \times \frac{\sin(\tfrac{1}{2} cq \cos\theta)}{\tfrac{1}{2} cq \cos\theta} \right] \sin\theta \, d\theta \, d\varphi$$

The Debye formula describes the scattering of a polymer with a random coil structure:

$$I_2(q) = \frac{2k_2}{R_g^2 q^2} \left[\exp\left(-R_g^2 q^2\right) + R_g^2 q^2 - 1 \right],$$

where R_g is the ensemble average radius of gyration and k_1 and k_2 are scaling factors.

From the radius of gyration for the random-coil contribution to the scattering of $R_g = 0.7$ nm the number of amino acids can be determined with the following equation applicable for linear flexible polymer chains:

$$R_g = R_0 N^{\nu}, \quad (1).$$

Here N is the number of amino acids of the chain, R_0 is a constant and ν is an exponential scaling factor. From eq. (1) the number of amino acids in the random coil segments of polymerized ActM were calculated with reported values of $R_0 = 0.1927$ nm and $\nu = 0.598$ (Kohn et al, 2004).

From these parameters the radius of gyration of the cross section R_c was determined with $R_c = (b^2/12 + c^2 / 12)^{1/2}$.

2.2.6.3 Model-free analysis of SAXS data

To check the consistency of the parameters derived from model-based curves, model-free data evaluation methods are useful (Glatter, 1979). To obtain information related to the cross-sectional dimension of the ActM polymers the cross-section Guinier law was applied to the data (Glatter & Kratky, 1982):

$$\ln(qI(q)) = \ln(qI_0) - \tfrac{1}{2} R_c^2 q^2.$$

A straight line in an $\ln(qI(q)) - q^2$ – plot yields the radius of gyration of the cross-section R_c.

The pair-distance distribution function (PDDF) of the cross-section, $p_c(r)$, as determined by indirect Fourier transformation of $qI(q)$ (Glatter, 1980), was applied as another model-free nethod. To remove the contribution of the unknown polymer length to good approximation, the multiplication of $I(q)$ with q is valid (Schnablegger et al, 1999a; Schnablegger et al, 1999b).

From the $p_c(r)$, the R_c was determined applying:

$$R_c^2 = \int_0^\infty r^2 \rho_c(r)\,\mathrm{d}r \,/\, 2\int_0^\infty \rho_c(r)\,\mathrm{d}r.$$

2.2.7 *In silico* analyses

3D protein models:	
PDB sequence file retrieval	RCBS protein data bank at http://www.rcsb.org/pdb
3D image viewing and analysis	"Chime 2.6", MDL Information Systems, Inc, http://www.mdl.com/products/framework/chime
BLAST analyses	http://www.ncbi.nlm.nih.gov/BLAST
Genomic resources:	http://www.ncbi.nlm.nih.gov
cyanobacteria	"CyanoBase" at http://www.kazusa.or.jp/cyano
Illustrations design	Adobe Illustrator CS3
Image processing	Adobe Photoshop CS3
Literature searches	http://www.ncbi.nlm.nih.gov/pubmed

Microscopic image analysis:	
Deconvolution microscopy	softworx, Applied Precision
Confocal microscopy	ZEN 2009, Zeiss
PCR primer design	http://frodo.wi.mit.edu/primer3/
Proteomics	http://www.expasy.org
Restriction endonucleases analysis tool	http://tools.neb.com/NEBcutter2/index.php
SAXS data acquisition and analysis	"SAXSQuant", "CCDQuant", Anton Paar
Scanning and image processing of blots and gels	"Quantity One" and "Image Lab", BioRad
Sequence analysis:	
alignments	"ClustalX 1.83" ftp://ftp-igbmc.u-strasbg.fr/pub/ClustalX
editing of alignments	"DAMBE 4.2.13" http://dambe.bio.uottawa.ca "BioEdit 7.0.5.3" http://www.mbio.ncsu.edu/BioEdit/bioedit.html "MEGA 3.1" http://www.megasoftware.net
Spreadsheets	Microsoft Excel 2007
qPCR:	
assay design	Universal ProbeLibrary Assay Design Center, http://www.roche-applied-science.com/sis/rtpcr/upl/index.jsp?id=UP030000
data analysis	Sequence Detection Software v1.4, Applied Biosystems
Word processing	Microsoft Word 2007

3 Results

3.1 Characterization of ActM and PfnM *in vitro*

3.1.1 Heterologous expression of ActM and PfnM

To obtain high-purity protein samples for subsequent analyses, ActM and PfnM were heterologously expressed in the *E.coli* strain BL21(DE3) from the pET15b vector optimized for T7 RNA polymerase mediated heterologous expression of proteins (Studier & Moffatt, 1986). Translation of genes ligated into a designated site of pET15b will add an N-terminal 6xHis-tag for immunodetection and purification. For a detailed description of the cloning procedure see 2.2.3.3 Construction of plasmid vectors for heterologous expression, p53.

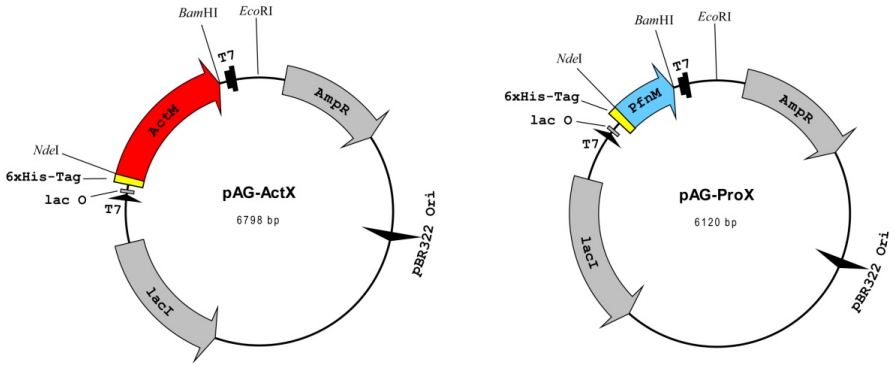

Figure 3.1. Maps of vectors generated for heterologous expression of ActM and PfnM.
The *actM* and *pfnM* genes (red and blue, respectively), the ampicillin-resistance gene ("Amp^{R}"), the lac-inhibitor ("lacI"), the origin of replication ("pBR322 ori"), the lac operator region ("lac O") and the location of the 6xHis-Tag are shown. The maps do not show all restriction sites, T7 promoter and terminator regions are indicated "T7" at the N- and the C-terminus of the inserted gene, respectively.

The successful generation of expression vectors pAG-ActX and pAG-ProX for the expression of *actM* and *pfnM*, respectively (see **Figure 3.1**) was verified by sequencing, PCR and restriction analysis (data not shown). Downstream analytical methods aimed at elucidating protein properties under physiological conditions require heterologous proteins in their native confirmation. Therefore, after induction of expression with 0.5 mM IPTG, cell extracts were prepared and purified based on a native buffer system

containing 10 mM imidazole for lysis, 20 mM imidazole in each of the two washing steps and 250 mM imidazole in the elution fractions. For PfnM, this method yielded satisfactory results for both purity and protein levels (see **Figure 3.2**, right). In contrast to that, purification of ActM was less favorable under these conditions. The elution fractions displayed a high amount of contaminations visible as additional bands in the SDS-PAGE profile (see **Figure 3.2**, left).

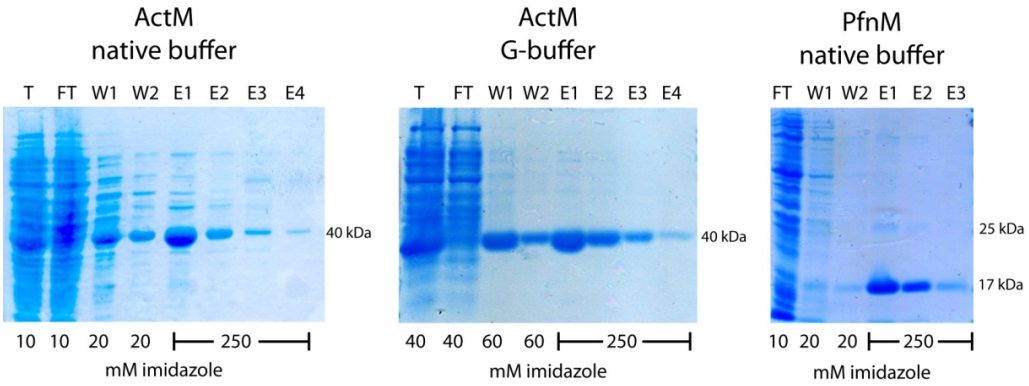

Figure 3.2. SDS-PAGE analysis of ActM and PfnM purifications.
ActM purity using the G-buffer system (middle) is superior to the standard native buffer system (left). PfnM purity (right) was best in standard native buffer. Abbreviations: T: total protein extract; FT: flow through fraction; W1-2: consecutive wash fractions; E1-4: consecutive elution fractions. Imidazole concentrations of fractions in mM are indicated at the bottom.

Therefore, more stringent washes were required and the specificity of the initial binding of proteins to the Ni-NTA-agarose matrix had to be increased. To achieve this, imidazole levels were raised to 40 mM in the lysis buffer and to 60 mM in the wash buffer. The elution buffer remained unaltered. This imidazole pattern significantly increased the purity of the protein and was used in all future preparative rounds.

The buffer recommended for purification under native conditions contains 300 mM NaCl. Salt concentrations in this range are known to induce the polymerization of eukaryotic actin (Pollard & Cooper, 2009). Therefore, to obtain default working preparations of unpolymerized actin, purification of both ActM and PfnM was performed in a buffer known to keep actin in its monomeric state ("G-buffer", see 2.2.4.2 Heterologous expression and purification of proteins, p56) and the results were assessed as before. While

purity and yield of PfnM were entirely unsatisfactory, the ActM quality was as high as with the native lysis buffer system (see **Figure 3.2**, middle). Therefore, ActM purifications were carried out with G-buffer and the imidazole patterns determined before. The buffer system for PfnM adhered to the manufacturers recommendations.

3.1.2 Characterization of PfnM

3.1.2.1 Antibody generation and Western immunoblots

Purified PfnM appears as a band corresponding to 17 kDa on SDS-PAGE gels (see **Figure 3.2**, right). The difference to the predicted PfnM size of 15 kDa can be explained with a 20 amino acid sequence containing the 6xHis-tag and a thrombin cleavage site added by the pET15b expression vector system. Although of much lower intensity than the main 17 kDa band, an additional band of 25 kDa is frequently detectable with SDS-PAGE in PfnM purifications.

For further analyses a specific anti-PfnM antibody was generated (see 2.2.4.10 PfnM antibody generation, p60). After 120 days of immunization the polyclonal rabbit antiserum was suitable for PfnM detection with high specificity and sensitivity, detecting a 17 kDa band in samples of purified PfnM (see **Figure 3.3**, left).

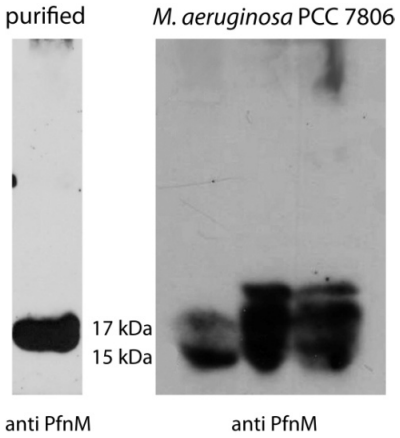

Figure 3.3. Western immunoblot analyses of PfnM from *E.coli* and *Microcystis aeruginosa*.
Purified PfnM, visualized with an anti-PfnM antiserum (left) appears at 17 kDa.
In *Microcystis aeruginosa* PCC 7806, the anti PfnM antiserum shows a dual band with molecular weights of 15kDa and 17 kDa.

Note that the 25 kDa band seen on protein gels is absent from anti-PfnM immunoblots. In immunoblots of *Microcystis aeruginosa* PCC 7806 protein extracts the anti-PfnM antiserum yields two "monomer" bands, one at 15 kDa another at 17 kDa (see **Figure 3.3**). The latter might be the result of posttranslational modifications modifying the electrophoretic properties of the PfnM protein.

3.1.3 Characterization of ActM

On SDS-PAGE gels, purified ActM runs at approximately 40 kDa, a molecular weight slightly above the value of 39 kDa determined for non-tagged ActM from *Microcystis aeruginosa* PCC 7806 (see **Figure 3.2**, p70) (Guljamow et al, 2007). As mentioned before, this weight difference can be attributed to the amino-acids added to the N-terminus in the expression and purification system (see 3.1.2.1 Antibody generation and Western immunoblots, p71). Eukaryotic actin usually runs at 43 kDa.

3.1.3.1 Quantitative Western blot analysis

The 40 kDa band seen on SDS-PAGE gels can be detected with an anti-actin monoclonal antibody in Western immunoblots of heterologously expressed, purified ActM. This antibody also interacts with untagged ActM and rabbit skeletal muscle actin (see **Figure 3.4**, left). To assess the physiological concentrations of ActM in *Microcystis aeruginosa* PCC 7806 cells a quantitative Western blot analysis was performed. An extended treatment in a glass-bead grinder was to ensure a thorough cell disruption to release all intracellular ActM from a liquid culture of known cell volume. The treatment was performed in an excess of G-buffer to facilitate the depolymerization of ActM. The resulting extract was loaded on an SDS-PAGE gel together with rabbit actin preparations in a gradient of four known concentrations and analyzed by anti-actin Western blotting (see **Figure 3.4**). To begin with, the chosen method of complete cell disruption produced satisfactory results.

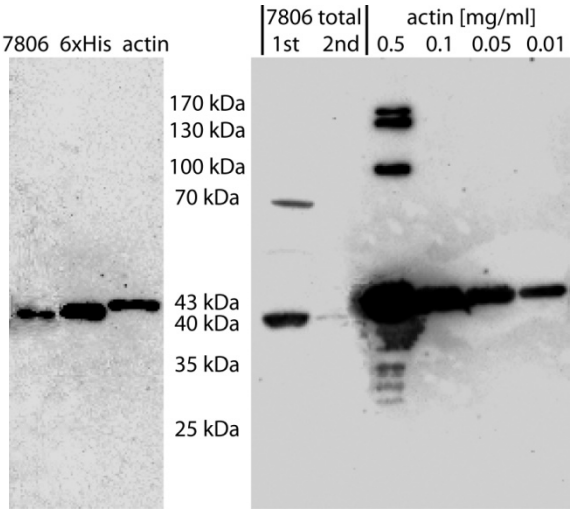

Figure 3.4. Western immunoblots of ActM and rabbit actin.
The left image shows ActM from *Microcystis aeruginosa* PCC 7806 total cell extracts ("7806", 39 kDa), 6xHis-tagged purified ActM ("6xHis", 40 kDa) and rabbit actin ("actin", 43 kDa).
The right image shows a quantitative analysis of ActM (39 kDa) in *Microcystis aeruginosa* PCC 7806 total cell extracts ("1st" + "2nd"). Rabbit actin (43 kDa) was loaded on the same gel in 4 distinct concentrations to estimate intracellular ActM levels.

Comparing two subsequent rounds of cell disruptions, it is clear that the first contains about 95 % of the combined ActM amount, whereas it is near the detection limit in the second (See **Figure 3.4**, right, lanes marked "1st" and "2nd".). The concentration of ActM in the sample loaded can be estimated to be around 0.02 mg/ml. Considering the dilution with the extraction buffer and calculating back to the original cell volume, the physiological concentration was determined to be 0.086 mg/ml. This experiment was repeated three additional times (data not shown), the average ActM concentration calculated was 0.075 mg/ml. Taken together, ActM is present in *Microcystis aeruginosa* PCC 7806 cells at a concentration of roughly 0.08 mg/ml (2.05 µM)

3.1.3.2 DNase I assay

Eukaryotic actin is known as a potent inhibitor of the nuclease activity of DNase I (see 1.1.3.1.3 DNase I, p14). A DNase I inhibition assay was performed to determine whether ActM has conserved this actin hallmark property. Additionally, the suitability of labeled DNase I as a reporter for ActM in future applications could be assessed with this method. Purified and ultra-centrifuged ActM in G-buffer was incubated with a commercially

available DNase I preparation added to a DNA solution and the absorption at 260 nm was measured photometrically over time. As a reference, ultra-pure, monomeric rabbit actin was used in parallel set-ups.

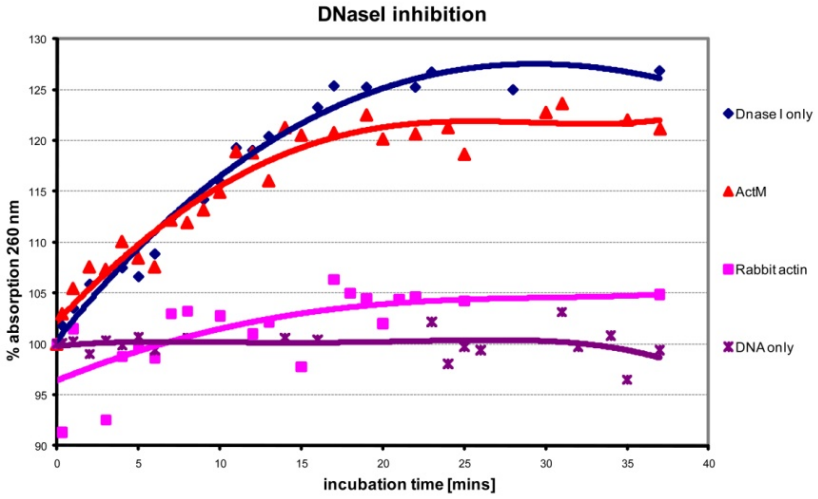

Figure 3.5. DNase I inhibition assay.
Rabbit actin inhibits the nuclease activity of DNase I, whereas ActM does not show this property. "100 % absorption" represents the average of all absorption values measured for a sample containing DNA only.

As expected, rabbit actin efficiently inhibits the DNA cleaving activity of DNase I (see **Figure 3.5**). While DNase I alone produces an immediate increase in 260 nm absorption when added to a DNA solution, the absorption curve generated by a mixture of rabbit actin and DNase I rises only very slowly and reaches its maximum at low absorption values. Initially, the ActM/DNase I mixture curve has a slope very similar to pure DNase I, however, it reaches its maximum at slightly lower values. Nevertheless, this assay shows that ActM has a very low DNase I inhibiting activity.

Since the DNase I molecule contacts the actin molecule at a very specific region on subdomain 2 termed the "DNase binding loop", the conservation of key amino acids can be assessed in a sequence alignment of ActM and eukaryotic actin (see **Figure 3.6**).

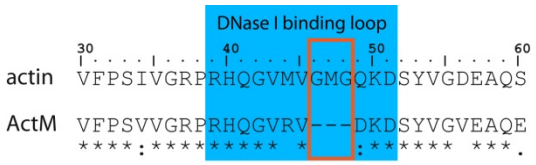

Figure 3.6. Amino acid sequence alignment of the DNase binding loop.
The DNase binding loop is shaded in light blue, a three residue deletion in the ActM sequence is highlighted in red. Numbers refer to the actin eukaryotic molecule. Degree of conservation is indicated by the following symbols: (*) - identical; (:) - highly similar; (.) - similar; ( ) - dissimilar.

Consistent with the results from the DNase I inhibition assay, the DNase binding loop region is severely altered in ActM. The most striking difference is a three residue deletion at positions 46-48. Two additional substitutions have taken place in ActM, one showing no similarity in the residues (M44R), the other, Q49D, exchanging two amino acids with comparable properties.

3.1.3.3 Polymerization and ultracentrifugation

A signature feature of actin is its rapid and near-complete polymerization under physiological salt concentrations. A commonly used, effective way to separate monomeric actin from its polymeric form is the initiation of polymerization in 100 mM KCl F-buffer (see 2.2.4.11 Preparation of polymerized actin, p60) followed by ultracentrifugation at 100,000 x g, leaving F-actin in the pellet (Mabuchi & Spudich, 1980). The results of a polymerization/ultracentrifugation assay comparing ActM with rabbit actin are displayed in **Figure 3.7**.

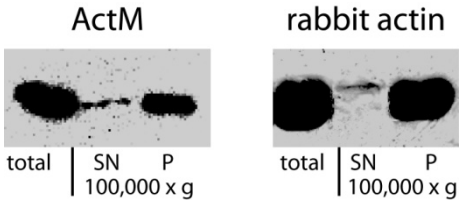

Figure 3.7. Polymerization and ultracentrifugation of rabbit actin and ActM.
A solution of each protein was polymerized in F-buffer ("total") and ultracentrifuged ("100,000 g"). Supernatant ("SN") and pellet ("P") fractions were analyzed by anti-actin immunoblots.

Both ActM and rabbit actin show similar patterns in anti-actin Western blots as both are found predominately in the pellet fraction. This is not only a clear

indication that ActM can indeed polymerize, it also shows that buffer conditions causing the polymerization of eukaryotic actin are sufficient to induce a similar reaction in ActM.

3.1.3.4 Phalloidin staining of ActM and rabbit actin

A common method to visualize actin filaments is the staining with fluorescently labeled phalloidin. This drug very specifically binds to F-actin with a very high affinity, leaving monomeric actin unstained. Based on amino acid sequence alignments, residues known for binding phalloidin (Lorenz et al, 1993; Oda et al, 2005) are conserved in the ActM sequence. Out of 29 sites, 13 (68%) are identical, 4 (21%) are considered strongly similar, 1 (5%) is weakly similar and only 1 has been substituted dissimilarly (see **Figure 3.8**).

Figure 3.8. Conservation of phalloidin binding sites in the ActM sequence.
Residues known to be involved in actin-phalloidin interactions are marked red in a sequence alignment of bovine actin and ActM. Conserved residues are shaded; a non-conserved position is boxed. Information on phalloidin binding residues is from Lorenz et al, 1993 and Oda et al, 2005.

To determine experimentally whether ActM has phalloidin binding properties comparable with eukaryotic actin and to determine the shape and appearance of ActM polymers, a staining assay with fluorescent phalloidin was carried out both with polymerized ActM and rabbit actin (see 2.2.4.12 Phalloidin staining of actin, p60). Stained preparations were observed through a confocal fluorescence microscope (see **Figure 3.9**).

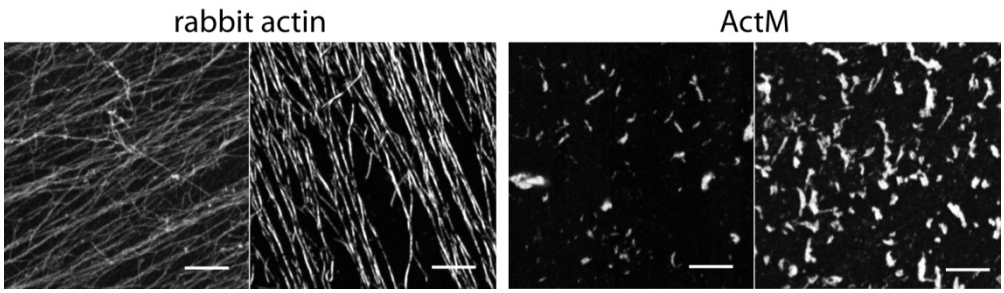

Figure 3.9. Phalloidin staining of polymerized rabbit actin and ActM.
Rabbit actin (left) polymerizes into long filaments forming an interwoven network. ActM polymers (right) frequently appear as short filaments assembling in bundles and sheets. Scale bars: 5 µm.

Polymerized rabbit actin appears in its typical form of a dense filamentous network. Filament lengths are usually more than 10 µm and frequently extend to over 100 µm (**Figure 3.9**, left). While ActM polymers do bind phalloidin and thus become visible, they appear as short filaments of 0.5-2.0 µm that tend to aggregate to give rise to bundles, amorphous plaques and sheet-like structures (**Figure 3.9**, right). The well-known specificity of the phalloidin/F-actin binding confirms the results from the ultracentrifugation experiments showing that ActM and eukaryotic share their ability to polymerize.

3.1.3.5 SAXS analyses of rabbit F-actin and ActM polymers

To gain more detailed structural insight, small angle X-ray scattering (SAXS) of solutions of polymerized ActM was performed in cooperation with Prof. Dr. Andreas Thünemann and Friedmar Delißen at the BAM (Bundesanstalt für Materialforschung und -prüfung, Berlin). Although this method does not allow the determination of total length of F-actin filaments, it provides valuable information on the filament cross sections. Scattering data was subjected to curve fits of model functions (Pedersen, 1997), for comparison, available small-angle scattering data of rabbit F-actin was analyzed using the same data interpretation routines (Cowieson et al, 2008). The results of the SAXS analysis are displayed in **Figure 3.10**.

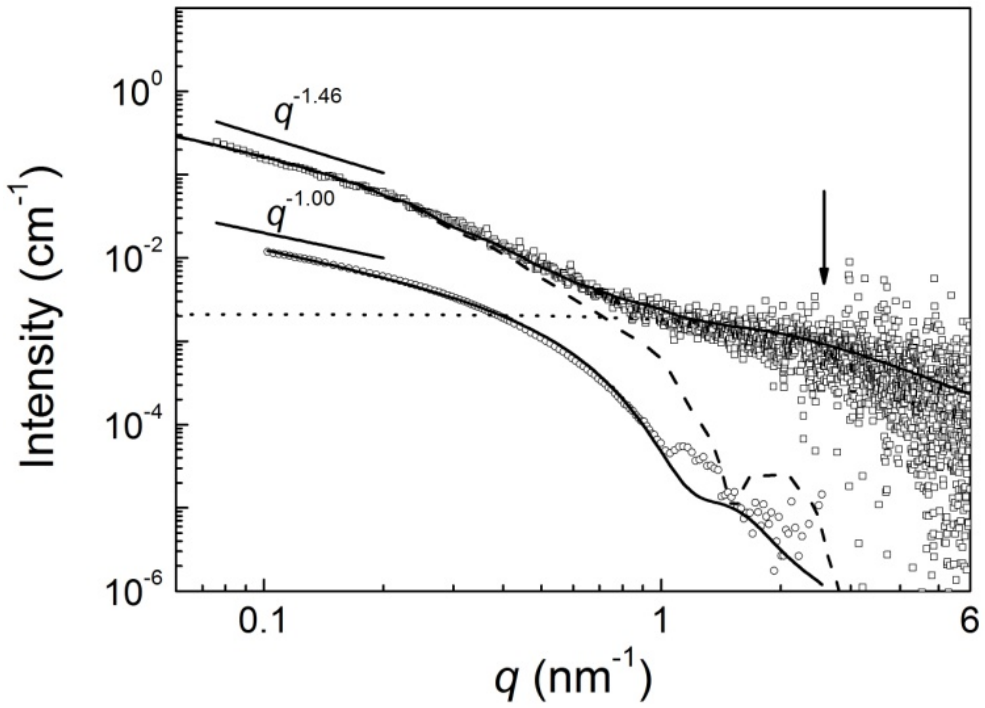

Figure 3.10. SAXS data of polymerized ActM and rabbit actin.
Rabbit actin data is from Cowieson et al, 2008. Best fit curves (solid lines) are from a cylinder function for rabbit actin (circles) and a parallelepiped for ActM (squares). The power-law scalings at low q are indicated as straight lines. The arrow points at the q-region where the scattering of short random-coil structures is visible. Contributions of the parallelepiped and the random coil structure are displayed (dashed and dotted line, respectively).

The data of rabbit actin could be sufficiently fit by using the cylindrical model (Pedersen, 1997) with a filament radius of 3.0 nm (**Figure 3.10**, circles and solid line, respectively). The good fit is not surprising as the cylindrical rod shape model has been typically used to describe small-angle scattering patterns of eukaryotic F-actins and has proven useful in the construction of an F-actin high-resolution structure (Fujii et al, 2010; Norman et al, 2005). Since it was shown previously that the thickness of F-actin is not constant along the filament (Oda et al, 2009), the model was modified and a polydispersity of 0.2 was applied. In a typical curve of a cylindrical rod the intensity decays proportional to q^{-1} at low q-values and shows a steep bending in the higher q-range characteristic for the rod's radius. Here, the rabbit actin curve scales with $q^{-1.00}$ at low q-values indicative of a long cylinder with an estimated radius of 2.6 nm.

The SAXS data of ActM is unambiguous regarding the prevalence of polymeric aggregates in the sample, thus confirming the results obtained in

previous experiments (see above). However, in contrast to rabbit actin, the data could not be fit to the simple cylinder model (see **Figure 3.10**, squares and solid line). The ActM curve scales with $q^{-1.46}$ in the low q-range, indicating a significantly pronounced ribbon-shaped filament structure. This value lies intermediate between the $q^{-1.00}$ scaling of a cylinder and the $q^{-2.00}$ value of an extended sheet (Cowieson et al, 2008). Another conspicuous element is the intensity around $q = 3$ nm^{-1} which is higher than must be expected for a compact filament structure (**Figure 3.10**, arrow). The curve does not show the very steep decay that, according to Porod's law (Glatter & Kratky, 1982) should be proportional to q^{-4}. Therefore, it has to be assumed that small structure entities, tentatively interpreted as random coil structures, with sizes of around 1 nm are also present in the polymer.

The total scattering function of ActM filaments must therefore include the contributions of both the ribbon-shaped filament and the random coil structure. Fitting the resulting scattering function (see 2.2.6.2 Modeling analysis of SAXS data, p65) to the ActM SAXS data, the cross section of the ribbon-shaped polymers were determined to be of a height of $c = 4.2$ nm and a width of $b = 15$ nm. The filaments' length cannot be determined with this method, therefore it was held constant at $a = 500$ nm. From the radius of gyration for the random-coil contribution to the scattering of $R_g = 0.7$ nm the number of amino acids was determined to be in the range of 7.6 to 9.7.

3.1.4 Interaction of ActM and PfnM

3.1.4.1 Co-elution assay

Considering the key role the actin-profilin interaction plays in eukaryotes and the conservation of mutual binding sites in both the ActM and PfnM sequences (Guljamow et al, 2007), the question arose whether ActM and PfnM bind and interact as well. This issue was addressed in a co-elution assay (see 2.2.4.9 Binding and co-elution assays, p59). One of the proteins was reversibly attached to a Ni-NTA-agarose matrix via the 6xHis-tag as if to be purified. Instead of elution, however, the matrix was incubated with a solution containing the putative binding partner and thoroughly washed. The

subsequent elution fraction was analyzed on Western immunoblots with regard to the presence of both putative binding partners. For the validity of this experimental set-up it was imperative that the 6xHis-tag of the protein in the mobile fraction be removed. For this purpose, an N-terminal thrombin cleavage site is encoded between the 6xHis-tag and the translational start of proteins expressed heterologously in the pET15b vector system. The thrombin mediated removal of the 6xHis-tag from purified ActM and PfnM preparations was assessed on Western immunoblots (see **Figure 3.11**).

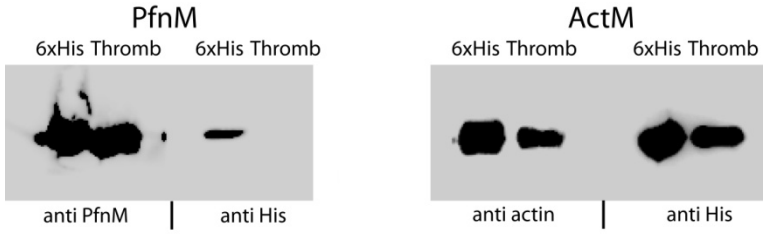

Figure 3.11. Thrombin removal of 6xHis-tag from ActM and PfnM.
The blots compare purified protein preparations before ("6xHis") and after thrombin ("Thromb") incubation. Both protein-specific antibodies ("anti PfnM" and "anti actin") and 6xHis-tag specific antibodies ("anti His") were used to assess protein levels and success of 6xHis-tag removal.

While the anti 6xHis-tag antibody failed to detect a band in thrombin-treated samples of PfnM, the cleavage was unsuccessful in the case of ActM. Variation in reaction conditions did not alter this outcome, therefore it was deemed unfeasible to remove the tag from ActM preparations in this system. As a replacement for ActM, rabbit actin solutions were tested for their ability to bind to PfnM in the co-elution assay. Additionally, native cell extracts from an *E.coli* strain expressing untagged ActM from a fosmid constructed to contain a 40 kb fragment of *Microcystis aeruginosa* PCC 7806 genomic DNA (2.2.3.5 Construction of genomic fosmid libraries, p54) were used as a source for 6xHis-tag free ActM. All actin/ActM containing solutions were kept in G-buffer to prevent polymerization. The results of these experiments can be seen in **Figure 3.12**. In all tested combinations of actin/ActM and PfnM immobilized and added in solution, both potential binding partners are found in considerable amounts in the elution fraction. At the same time, the soluble protein partner was always absent from the final wash steps. This clearly shows that the binding and immobilization of the respective untagged protein

was not mediated by unspecific interactions. Moreover, this outcome strongly suggests that the immobilization of the protein in solution was due to the matrix-bound, putative binding partner. Therefore, it is very likely that PfnM can interact with and bind to both eukaryotic actin and ActM.

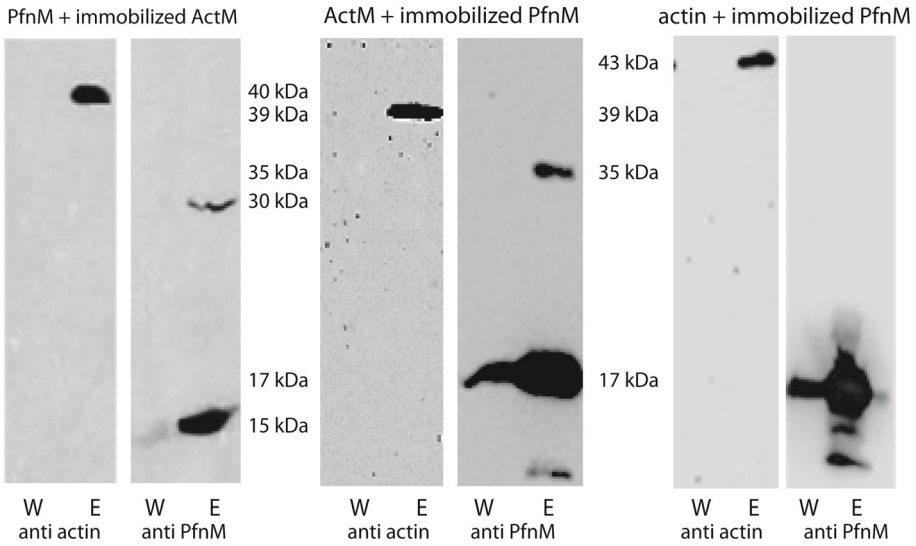

Figure 3.12. Co-elution of ActM/actin and PfnM.
One potential binding partner was immobilized, the other added in solution. Immunodetection of final wash (W) and eluate (E) are shown; the employed antibody is indicated at the bottom. The molecular weights are: 6xHis-ActM/native ActM - 40 kDa/39 kDa; actin - 43 kDa; PfnM - 17 kDa (monomer) 34 kDa (dimer).

3.1.4.2 ActM-PfnM Phalloidin assay

In eukaryotes, profilin signaling to the microfilament network targets both the monomeric and the filamentous form of actin. However, profilin binds only to G-actin, requiring a variety of F-actin interacting proteins as mediators to convey stimuli to filamentous actin. These mediators must be regarded absent from the intracellular space of *Microcystis aeruginosa*. Therefore, after having established that PfnM can bind to monomeric ActM, it was of importance to determine whether PfnM may also be able to bind to polymerized ActM and to assess the possibility that PfnM exerts any influence on the polymerization process. To this end, a modification of the phalloidin-staining experiment was employed. Instead of using only purified ActM for polymerization, PfnM was added to the solution in different molar ratios. PfnM was chemically coupled with the green fluorescent dye FITC, phalloidin had a red fluorescent TRITC-

tag. Polymerized and phalloidin-stained preparations were microscopically observed as before, the results are shown in **Figure 3.13**. The micrographs show that ActM still polymerizes in the presence of PfnM. Additionally, the appearance of the ActM polymers is unaltered in this experimental setup as the binding properties of phalloidin are not visibly influenced by PfnM (compare **Figure 3.9**, p77 and **Figure 3.13**, left). Overview micrographs give the impression of a congruence of ActM polymers and green fluorescent PfnM indicative of a co-localization. This could be confirmed by magnifications of single ActM aggregates as they are decorated with PfnM over their entire surface (**Figure 3.13**, right). Finally, the green fluorescence of decorated ActM aggregates increases with the amount of FITC-labeled PfnM added, suggesting a concentration-dependent binding of PfnM to ActM polymers (**Figure 3.13**, from top to bottom).

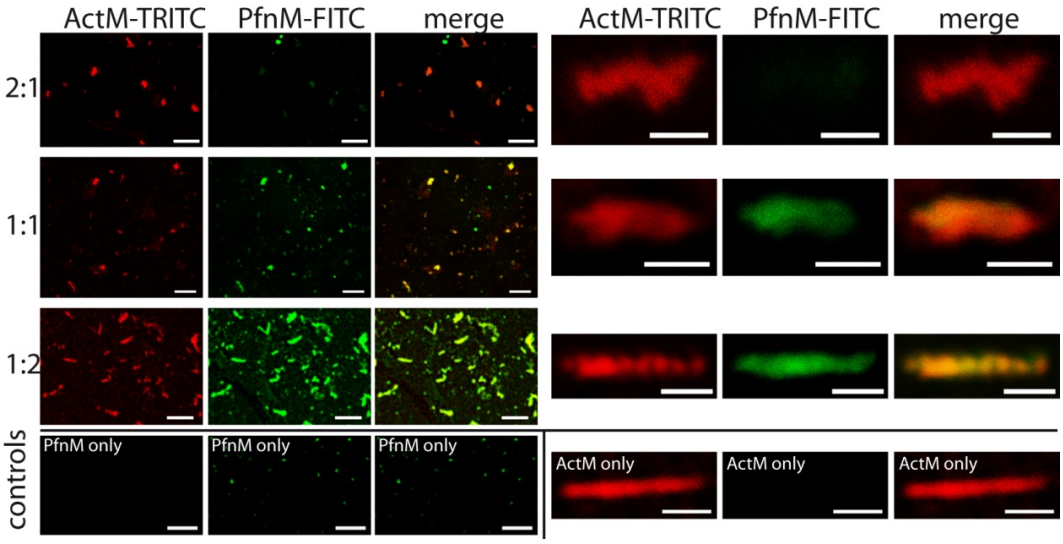

Figure 3.13. Fluorescence microscopy of PfnM binding to ActM polymers.
FITC stained PfnM (green) co-localizes with phalloidin-TRITC stained ActM polymers (red). Single ActM bundles are covered with PfnM. Fluorescence signals increase with increasing PfnM concentrations (top to bottom), molar ratios of ActM:PfnM are indicated to the left. Images on the left hand side show an overview (scale bars: 5 µm), magnifications of corresponding single aggregates are on the right (scale bars: 2 µm). The bottom row shows controls.

Taken together, the phalloidin staining assay performed with mixtures of ActM and PfnM provide strong support to the notion that PfnM, in contrast to eukaryotic profilin, can bind to polymerized ActM. What is more, the decoration of ActM polymers occurs in a concentration dependent manner.

3.1.4.3 Polymerization and ultracentrifugation of ActM and PfnM

To further investigate the binding of PfnM to ActM filaments indicated by the phalloidin assays, solutions containing ActM and PfnM in the ratios of 1:0, 2:1, 1:1, 1:2 and 0:1 were polymerized and subsequently ultracentrifuged at 100,000 x g. The resulting pellet fractions were analyzed by SDS-PAGE with respect to their ActM and PfnM content (see **Figure 3.14**).

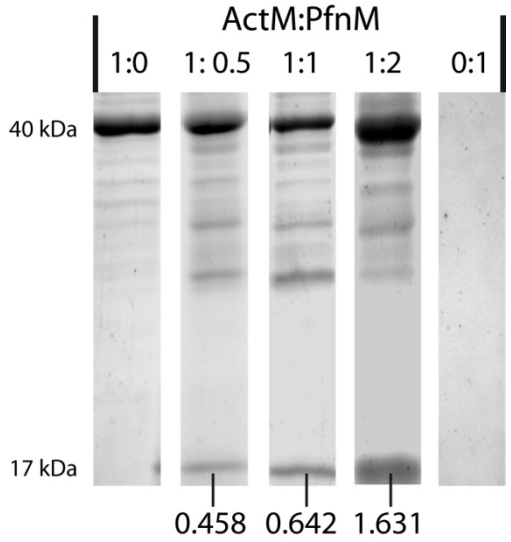

Figure 3.14. Polymerization and ultracentrifugation of ActM and PfnM.
SDS-PAGE of pellet fractions of 5 reactions containing ActM and PfnM in different ratios (indicated at the top) after ultracentrifugation at 100,000 x g. PfnM (17kDa) cosediments with polymerized ActM, the relative amount of PfnM in the pellet (indicated at the bottom) increases with the PfnM amount added before polymerization.

A 17 kDa band was present in all reactions that contained both ActM and PfnM. No such band was observed in set-ups devoid of either ActM of PfnM. This shows that ultracentrifugation of polymerized ActM alone does not result in the appearance of an additional 17 kDa band. Additionally, this proves that purified PfnM cannot be pelleted by ultracentrifugation at 100,000 x g. Rather, the results indicate that PfnM binds to polymerized ActM and can be co-pelleted by ultracentrifugation. To determine the stoichiometry of ActM and PfnM in the pellet fraction the staining intensities of individual bands after Coomassie-staining were measured using the BioRad Image Lab software (see 2.2.4.14 Co-polymerization of ActM and PfnM, p61). Taking into account the differences in molecular weight of ActM and PfnM,

the molar ratios of ActM:PfnM in the pellets were 1:0.458 (for the reaction initially containing ActM and PfnM in a 2:1 ratio), 1:0.642 (1:1) and 1:1.631 (1:2). Confirming previous results, this clearly shows that the binding of PfnM to ActM filaments is concentration-dependent over the range investigated.

3.1.4.4 SAXS assay

To learn more about the nature of the PfnM interaction with polymerized ActM and to assess potential structural implications, SAXS analyses were repeated with ActM-PfnM mixtures equivalent to those used before. The ribbon/parallelepiped model equation (see 3.1.3.5 SAXS analyses of rabbit F-actin and ActM polymers, p77) still sufficiently describes the obtained SAXS data (see **Figure 3.15A**), confirming the unchanged overall polymerization properties of ActM suggested by the ActM-PfnM phalloidin assay. However, when polymerized in molar ActM to PfnM ratios of 1:0, 2:1, 1:1 and 1:2, the dimensions measured for the resulting parallelepiped structure revealed an increasing width from 15 nm, to 23 nm, 28 nm and 38 nm, respectively. The height remained constant at 4.2 nm, as was the random coil contribution to the scattering with $R_g = 0.7$ nm. From this parameters the radius of gyration of the cross section R_c was determined as 4.5 ± 0.1 nm (for the ActM to PfnM ratio of 1:0), 6.8 ± 0.2 nm (2:1), 8.2 ± 0.2 nm (1:1) and 11.0 ± 1.1 nm (2:1).

To check the consistency of the parameters derived from model-based curves, model-free data evaluation methods (Glatter, 1979) were employed (see 2.2.6.3 Model-free analysis of SAXS data, p67). Applying the cross-section Guinier law to the data allows to obtain information related to the cross-sectional dimension of the ActM polymers (Glatter & Kratky, 1982). By this method, the radius of gyration of the cross-section R_c was determined to be 4.5 ± 0.2 nm (ActM to PfnM of 1:0), 6.7 ± 0.3 nm (2:1), 8.1 ± 0.2 nm (1:1) and 9.5 ± 1.0 nm (2:1) (see **Figure 3.15A**, inset). Comparing these values with the model-based parameters shows that both agree within the experimental range of error.

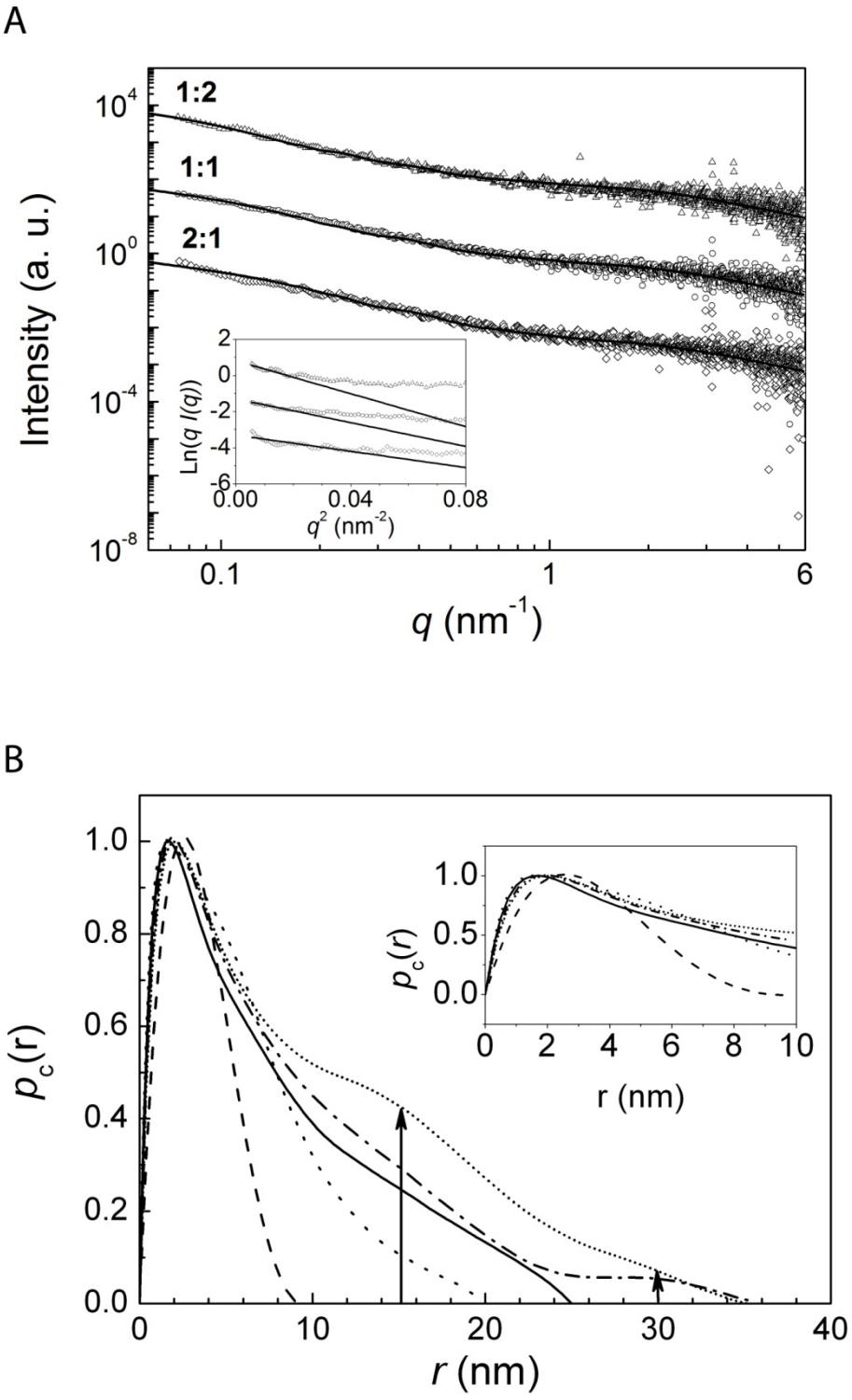

Figure 3.15. SAXS analyses of ActM polymerized in the presence of PfnM.
A: Molar ratios of ActM to PfnM were 2:1, 1:1 and 1:2 (symbols). The best fits according to eq. (1) (see p66) are shown (solid lines). Inset: Cross-section Guinier plots of the same data (symbols) and Guinier fits (solid lines).
B: Pair distance distribution function of PfnM-decorated ActM polymers. Cross section pair distribution functions of rabbit F-actin (dashed line), polymerized ActM (dotted) and polymerized ActM with PfnM in molar ratios of 2:1, 1:1 and 1:2 (solid, dash-dotted, shot dotted line, respectively). Arrows indicate conspicuous peaks attributed to PfnM binding effects. Inset: Magnification of the region around the maxima of the pc(r).

Another model-free method providing information on the filament structure is the pair-distance distribution function (PDDF) of the cross-section, $p_c(r)$. As $p_c(r)$ is interpreted as the electron density weighted number of all possible connections between points within the filament cross-section, it provides detailed information on the cross-section, complementing the Guinier law data. As can be seen in the inset of **Figure 3.15B**, all ActM curves have their peak maxima at ca. 2 nm while it is around 2.6 nm for rabbit F-actin. These values are unsurprising, as they are approximately half the height of the assumed ActM parallelepiped c/2 = 2.1 nm and close to the rabbit F-actin cylinder radius of 2.6 nm (see 3.1.3.5 SAXS analyses of rabbit F-actin and ActM polymers, p77). The maximum dimensions of the filaments are 9 nm (rabbit), 20 nm (1:0), 25 nm (2:1), 35 nm (1:1; 1:2) as derived from the distance where $p_c(r) = 0$. As rabbit F-actin adopts a cylindrical shape, its $p_c(r)$ is symmetric, while the $p_c(r)$ of the ribbon-shaped ActM is highly asymmetric. Two sub-maxima at around 15 nm and 30 nm appear only when PfnM is added to ActM (**Figure 3.15B**, arrows) indicating a contribution of PfnM to ActM polymer shape. Interestingly, the PfnM-mediated increase of the maximum ActM filament width does not occur in multiples of pure ActM polymers, suggesting a direct influence of attached PfnM to the polymer shape.

From the $p_c(r)$ the determination of R_c is possible with higher precision as from the Guinier plot. Accordingly, the values were R_c = 4.9 ± 0.2 nm (1:0), 6.8 ± 0.1 (2:1), 8.1 ± 0.1 (1:1) and 9.1 ± 0.2 (2:1), thus confirming previous results from model-based and Guinier parameters.

Table 3.1. Radius of gyration of polymerized ActM and PfnM determined with different methods.

Ratio ActM : PfnM	R_g[a] [nm] Model	R_g[b] [nm] Guinier	R_g[c] [nm] PDDF
1:0	4.5 ± 0.1	4.5 ± 0.2	4.9 ± 0.2
1:2	6.8 ± 0.2	6.7 ± 0.3	6.8 ± 0.1
1:1	8.2 ± 0.2	8.1 ± 0.2	8.1 ± 0.1
2:1	11.0 ± 1.1	9.5 ± 1.0	9.1 ± 0.2

[a]Calculated from the curve fit parameters b and c. [b]Calculated from cross-section Guinier law. [c]Calculated from the cross section pair distance distribution function pc(r).

In summary, all model-fit calculations and model-free data evaluation methods produce agreeing results in assigning a ribbon-like structure to polymerized ActM that increases in width, but not in height, with increasing amounts of PfnM present during polymerization (see **Table 3.1**, p86).

3.2 Visualization of ActM and PfnM *in vivo*

The visualization of proteins in their native cellular environment can provide valuable information regarding the subcellular localization and possible formation of higher-ordered molecular structures, such as filaments. The fusion of proteins to the fluorescent reporter GFP is a widely used method for *in situ* visualization and was employed here to visualize ActM and PfnM in *E.coli*. In the absence of a reliable system for genetic manipulation and stable heterologous expression of proteins, *in situ* visualizations in *Microcystis aeruginosa* were based on immunofluorescence microscopy.

3.2.1 Immunofluorescence microscopy

Using immunofluorescence microscopy (IFM), ActM was shown previously to concentrate to the cell's periphery in a shell-like manner in *Microcystis aeruginosa* PCC 7806 (Guljamow et al, 2007). With the availability of *E.coli* strains heterologously expressing ActM it was now possible to repeat these experiments in another bacterium to obtain first indications as to whether ActM requires a mechanism specific to *Microcystis aeruginosa* PCC 7806 to adopt the observed shape or if the localization in a layer at the cell envelope is an inherent feature of intracellular ActM polymers. Additionally, IFM studies targeting PfnM were carried out after having obtained an anti-PfnM antiserum (see 3.1.2.1 Antibody generation and Western immunoblots, p71). The results of the IFM analyses with bacterial cells are summarized in **Figure 3.16**. As can be seen on the anti-actin micrographs of *E.coli*, the intracellular distribution of ActM in *E.coli* is comparable to that observed in *Microcystis aeruginosa* in that the protein seems to accumulate at the cells' periphery (**Figure 3.16**, top and middle rows, left).

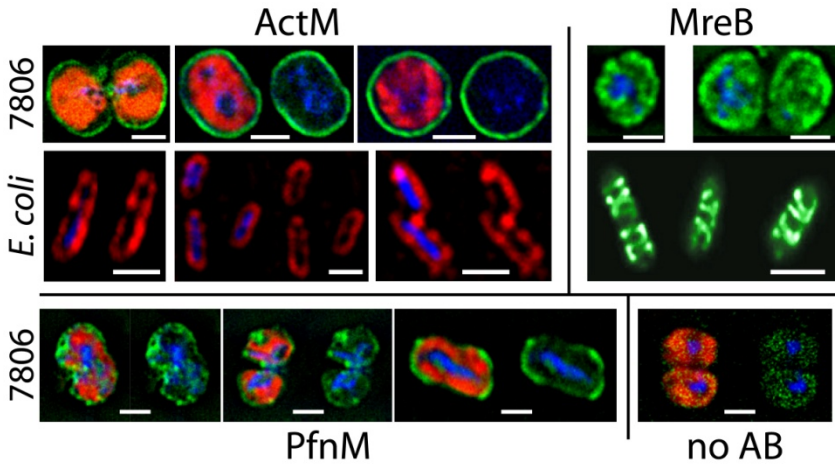

Figure 3.16. Immunofluorescence microscopy of ActM, PfnM and MreB.
The top row images show anti-actin and anti-MreB IFM of *Microcystis aeruginosa* PCC 7806 cells, the protein of interest is shown in green, thylakoid autofluorescence in red and DNA is stained blue. Images are taken from Guljamow et al, 2007.
Middle row images show *E.coli* expressing ActM stained red by anti-actin IFM (left) and *Bacillus subtilis* expressing GFP-Mbl (right; adapted from Cabeen & Jacobs-Wagner, 2010).
Bottom row images show anti-PfnM (green) IFM in *Microcystis aeruginosa* PCC 7806 and controls omitting the antibody ("no AB"). Scale bars: 2 µm.

For comparison, the intracellular localization of MreB both in *Microcystis aeruginosa* and *E.coli* is also displayed, clearly showing distribution patterns different from ActM (**Figure 3.16**, top and middle rows, right).
IFM micrographs displaying PfnM distribution are not as distinguished. While the method did not produce any reliable results in *E.coli* cells expressing PfnM (data not shown), the fluorescent signals in *Microcystis aeruginosa* PCC 7806 indicate a somewhat patchy distribution in some cases (**Figure 3.16**, bottom row, left). However, the anti PfnM IFM frequently did not show any signals unequivocally attributable to PfnM. Therefore, subsequent *in situ* analyses focused on the expression of GFP fusion proteins expressed in *E.coli*.

3.2.2 GFP fusions of ActM and PfnM

To increase the chances of obtaining functional GFP fusion proteins of ActM and PfnM the GFP tag was added in separate approaches to the N-terminus as well as the C-terminus of the target protein (see 2.2.3.2 Generation of GFP-fusion proteins, p52). Since only the C-terminal fusion of GFP to either ActM or PfnM turned out to produce a detectable fluorescent signal, this

orientation was used in all further analyses. **Figure 3.17** gives an overview of the vectors designed for the expression of GFP fusion proteins.

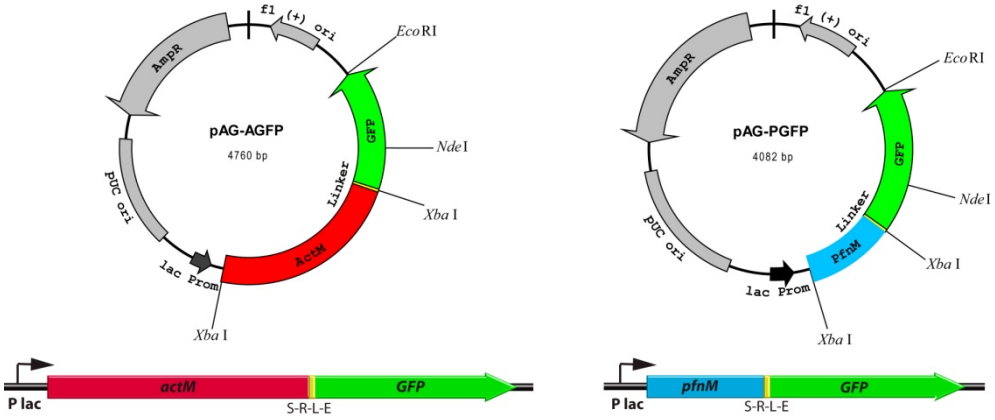

Figure 3.17. Vector maps and linear display of GFP fusion constructs.
The *actM*, *pfnM* and GFP coding genes are shown in red, blue and green, respectively. A flexible S-R-L-E linker sequence is shown in yellow. Further abbreviations: "Amp^R" - ampicillin resistance gene; "f1 (+) ori" - origin of replication; "pUC ori" - origin of replication; "lac Prom" - lac promoter region. The maps only show selected restriction sites.

The respective target gene was ligated into a pMB1/ColE1 compatibility group vector encoding an ampicillin resistance gene. The existing lac promoter was not fully utilized to avoid artifacts stemming from overexpression. In the absence of the inducing agent (IPTG) basal transcription levels were sufficient to produce detectable green fluorescent signal. However, cells had significantly increased doubling times and had to be grown for a minimum of 48 hours to display signal intensities optimal for microscopy.

To create *E.coli* strains for the stable co-expression of a GFP-tagged protein together with its unlabeled binding partner (e.g. ActM-GFP + 6xHis-PfnM and *vice versa*), compatible vectors with p15A-type origin of replication and a chloramphenicol resistance gene were constructed for the T7 mediated expression a 6xHis-tagged proteins (see 2.2.3.4 Generating *E.coli*-strains for co-expression of proteins, p54). The p15A-type vectors and the pMB1/ColE1-group GFP expression vectors can co-exist in the same bacterial host cell (see **Figure 3.18A** and **C**). Successful generation of expression strains and co-expression of proteins was assessed with PCR, restriction analyses (data not shown) and Western blot immunodetection (see **Figure 3.18B** and **D**).

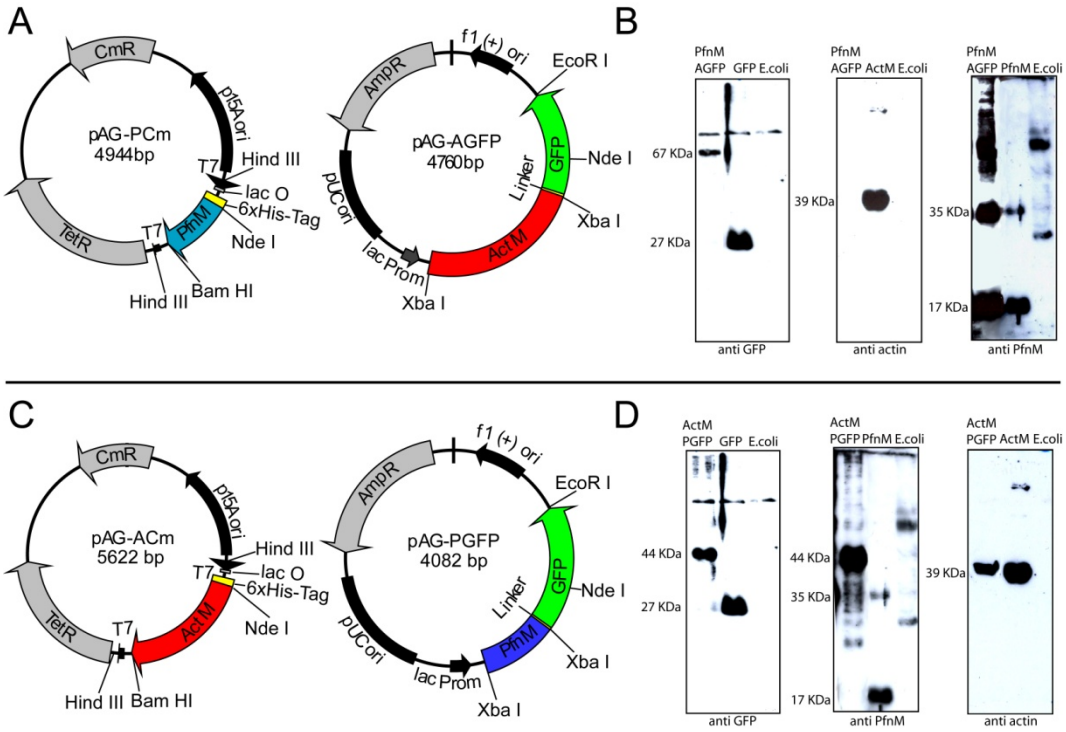

Figure 3.18. Co-expression of proteins in *E.coli* - vector maps and immunodetection.
A: Maps of vectors constructed for the co-expression of ActM-GFP and 6xHis-PfnM.
B: Western blot immunoanalysis of *E.coli* strains co-expressing ActM-GFP and 6xHis-PfnM. Both proteins can be detected; GFP-ActM only reacts with the GFP antibody. Depending on the antibody used, respective positive (middle lanes) and negative controls ("*E.coli*") are shown.
C: Maps of vectors constructed for the co-expression of PfnM-GFP and 6xHis-ActM.
D: Western blot immunoanalysis of *E.coli* strains co-expressing PfnM-GFP and 6xHis-ActM.
Molecular weights: ActM - 40 kDa; PfnM - 17 kDa/34kDa; GFP - 27 kDa; ActM-GFP - 67 kDa; PfnM-GFP - 44 kDa/88 kDa.
Abbreviations: "Amp^R" - ampicillin resistance gene; "Tet^R" - tetracycline resistance gene; "Cm^R" - chloramphenicol resistance gene; "f1 (+) ori"; "pUC ori"; "pBR322 ori" - origins of replication; "lac Prom" - lac promoter region; "lac O" - lac operator region. T7 promoter and terminator regions are indicated "T7" at the N- and the C-terminus of the relevant genes, respectively. The maps only show selected restriction sites.

As can be seen in **Figure 3.19**, ActM-GFP frequently shows an uneven intracellular distribution with the protein being occluded from various intracellular locations in *E.coli*. In accordance with results from IFM analyses (see 3.2.1.1 Immunofluorescence microscopy, p87) accumulation to the peripheral parts of the cell is the most common pattern. However, in some instances ActM-GFP also condenses into elongated shapes of varying width running parallel to the cell's longitudinal axis or traversing the cylindrical cytoplasm. Other images suggest an occlusion of ActM-GFP from cell poles producing a characteristic tetragonal pattern of green fluorescence.

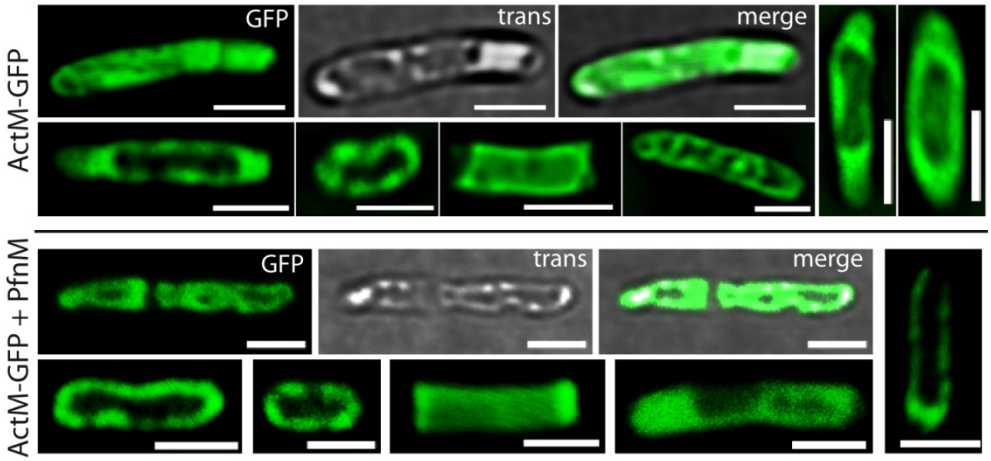

Figure 3.19. ActM-GFP expression in *E.coli*.
The distribution pattern in cells expressing ActM-GFP alone (top) is indistinguishable from cells co-expressing PfnM (bottom). If not stated otherwise, images show GFP channel, micrographs displaying the transmission image ("trans") and an overlay of both ("merge") are marked. Scale bars: 2 µm.

The heterogeneity of the observed ActM-GFP distribution patterns hints at the formation of higher-ordered accumulations of the protein whose size prevents the free diffusion through the cytoplasm. The co-expression of PfnM has no apparent influence on these accumulations as the observed ActM-GFP patterns remain unaltered in the respective cells (**Figure 3.19**, bottom).

Contrary to ActM-GFP, PfnM-GFP does not show complex distribution patterns (see **Figure 3.20**, top). Rather, it is found in either a homogenous cytosolic dispersion or a concentration in polar foci, frequently also a combination of both. The co-expression of ActM-GFP, however, gives rise to a characteristic large intracellular structure that appears ring-like in the micrographs corresponding to a hollow enclosure in three-dimensional space (see **Figure 3.20**, middle). This "enclosure" does not show a preferential localization towards the mid-cell or polar regions. It usually spans the cell's whole width making extensive contact with its inner boundaries. Consequently, the diameter of the enclosure equals the width of *E.coli* cells of about 1-1.5 µm. This structural entity is absent from any other *E.coli* strain expressing GFP fusion proteins investigated here, therefore it is highly probable that this structure is a direct consequence of the specific interaction between PfnM-GFP and ActM.

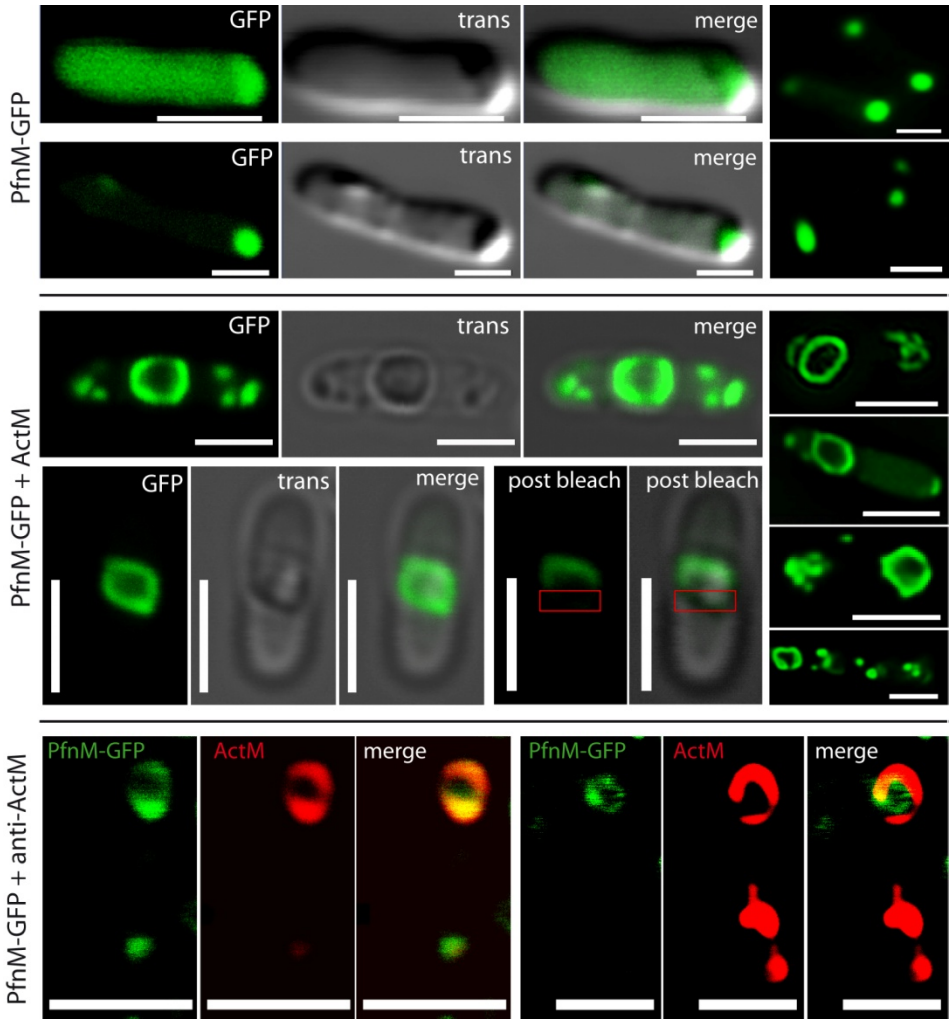

Figure 3.20. PfnM-GFP expression in *E.coli*.
In *E.coli*, PfnM-GFP distributes evenly in the cytoplasm or is localized to the cell poles (top). Co-expression with ActM gives rise to a large, intracellular hollow compartment (middle). This enclosure is not dynamically rearranged, as fluorescence does not recover after bleaching ("post bleach"). Immunodetection of ActM in the hollow enclosures found in *E.coli* cells expressing both ActM and PfnM-GFP reveals a co-localization (bottom). The displayed microscopic channel is indicated ("PfnM-GFP", "ActM" (TRITC) "trans" and "merge"); it is GFP if not stated otherwise. Scale bars: 2 µm.

According to time lapse microscopic analyses, the enclosure does not show any dynamic properties and appears stable and rigid. When green fluorescence is partially bleached from the enclosure with high laser intensities, the signal does not recover over a stretch of 30 minutes (see **Figure 3.20**, middle, "post bleach").

To determine where ActM is localized in cells bearing the PfnM-GFP-rich enclosure, IFM using a polyclonal anti-actin antibody was performed with cells co-expressing PfnM-GFP and ActM. Indeed, in cells displaying the aforementioned structure formed by PfnM-GFP, ActM is found in the same

characteristic ring-shaped pattern along the outline of the enclosure (see **Figure 3.20**, middle). The respective fluorescence signals originating from PfnM-GFP and anti-actin immunostaining overlap considerably indicating a co-localization of PfnM-GFP and ActM in the intracellular enclosure.

To assess whether GFP-tagged proteins can bind to their respective non-tagged binding partner, a co-elution assay was performed as before (see 3.1.4.1 Co-elution assay, p79). Since the GFP fusion proteins did not carry a 6xHis-tag, only the non-GFP proteins could be reversibly attached to the Ni-NTA-agarose matrix and incubated with the GFP fusions in solution. **Figure 3.21** shows the results of these experiments.

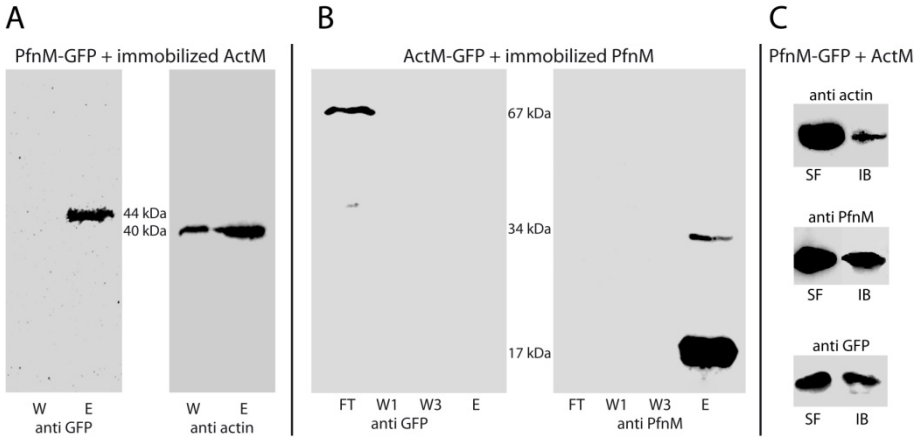

Figure 3.21. Co-elution and solubility assay with GFP fusion proteins.
A: PfnM-GFP co-elutes with ActM, indicating a specific binding of both proteins. Final wash fractions ("W") and elution fractions ("E") are shown. Molecular weight marker bands and antibodies used are marked.
B: ActM-GFP is found only in the flow-through fraction, hence, it does not co-elute with PfnM.
C: In co-expressing cells, both PfnM-GFP and ActM are found predominantly in the soluble cytosolic fraction ("SF") as opposed to aggregating in inclusion bodies ("IB"). Applied antibodies are indicated.

In accordance with the *in situ* findings, ActM-GFP did not co-elute with immobilized PfnM. In contrast to that, a binding and interaction of PfnM-GFP and immobilized ActM can be inferred from the data (see **Figure 3.21A**).

In an experiment aimed at investigating the possibility to have faced a mere artifact of unspecific aggregation and deposition in inclusion bodies (Rokney et al, 2009a), the amount of ActM and PfnM-GFP found in the soluble and the insoluble fraction of co-expressing cells was estimated on Western immunoblots (see 2.2.4.1 Preparation of proteins from bacterial cells, p55). As

Figure 3.21C shows, soluble ActM represents nearly all of the cellular ActM content and a substantial part of PfnM-GFP is found in the soluble fraction as well. The frequently observed small, compact foci of GFP fluorescence in PfnM-GFP/ActM expressing cells may be attributed to the measured insoluble protein fraction (see **Figure 3.20,** middle).

In conclusion, the GFP *in situ* analyses show that ActM localizes towards an intracellular enclosure visualized by PfnM-GFP. The previously discovered tendency of ActM to form extended polymers makes ActM the prime candidate for the structure-bearing element in these enclosures. In addition to that, the data substantiate the assumption that PfnM binding plays an important role in assembling and maintaining these enclosures.

3.3 Presence of ActM and PfnM in field samples

Previous work has shown that genes for ActM and PfnM are present in samples taken from the habitat the original PCC 7806 strain of *Microcystis aeruginosa* was collected from (Guljamow et al, 2007). This "Braakman" habitat is situated near the south-western Atlantic coast of the Netherlands and consists of three separate freshwater reservoirs ("sparbekkens") currently maintained and monitored by the "Evides" company of Rotterdam, NL (see **Figure 3.22**). In early analyses, whole water samples were taken from one sparbekken and subsequently transferred to glass fiber filters. Additionally, liquid samples enriched for cell aggregations using a filter net with a defined mesh-size were taken and fixed by the addition of ethanol (see 2.2.2 Collection of field samples, p44). From these samples, metagenomic DNA was isolated and PCR was performed.

Figure 3.22. Satellite image of Braakman sparbekkens.
The three separate reservoirs are numbered. Reproduced from "google.maps", GPS coordinates: 51.300819, 3.739035. Scale bar: 500 m.

In subsequent years, the sampling was extended to all three sparbekkens. Moreover, samples were not ethanol-fixed and transferred from the Netherlands to the Berlin lab within a day and immediately processed. Two main types of analyses were performed with the material: molecular biological metagenomic experiments and *in situ* microscopic work.

3.3.1 Immunofluorescence microscopy with Braakman colonies

Since anti-actin IFM has been successfully applied with cultured cyanobacterial samples, it was obvious to subject the cyanobacterial Braakman samples to the same procedure. **Figure 3.23** displays some representative images created by this method.

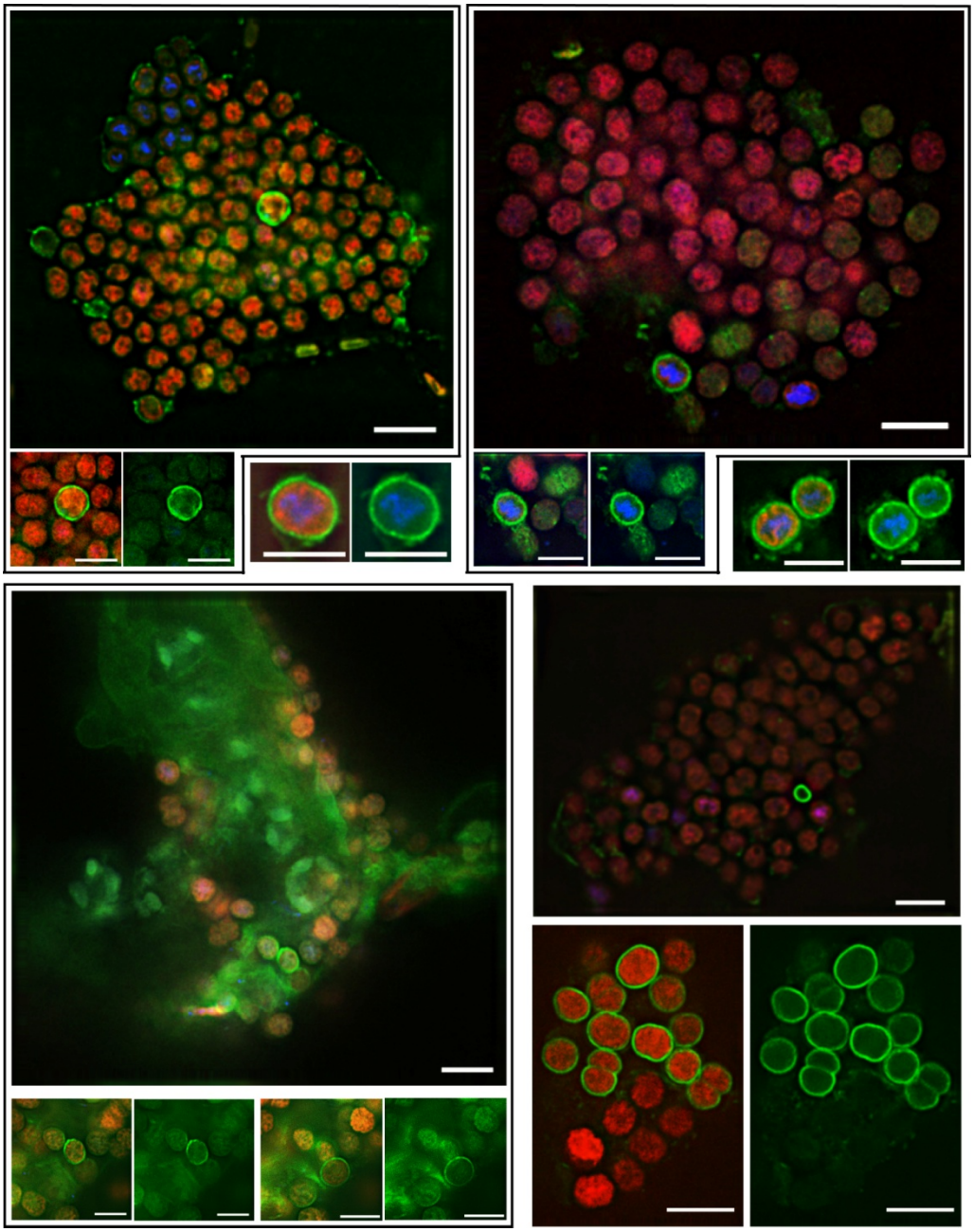

Figure 3.23. Anti-actin immunofluorescence microscopy of Braakman colony samples.
Large overview images show the heterogeneous distribution of ActM (green) to singular cells within one agglomeration of cells (or a whole colony). Enlarged images of single cells are grouped with their respective overview image. Scale bars in colony images: 10 µm. Scale bars in enlargements (including the image at the bottom right): 5 µm.

As before, an anti-actin primary antibody was used in combination with a green fluorescent FITC-coupled secondary antibody. Additionally, DNA was stained blue using the Hoechst stain (see 2.2.5.2 Immunostaining of fixed cyanobacterial cells, p63). As with PCC 7806, the typical ActM rings oriented towards the cell's periphery are visible in *Microcystis aeruginosa* cells identified in the Braakman samples. This confirms initial results identifying the *actM-pfnM* region in Braakman DNA by PCR. However, in addition to that, a remarkable observation can be made with these micrographs: Not only is the ActM signal absent from some cells that appear to be in close contact with ActM bearing cells. In many instances only a few cells, sometimes even only one, in a whole colony were found to show the ActM signal. This is unusual in that cells of a colony are believed to have a clonal relationship and should therefore all carry the same genes. However, with the IFM method it is not possible to attribute variations in protein levels to either differences in gene content or gene expression.

To address that question the adaptation to the special conditions imposed by field samples of two methods well established for laboratory bacterial cultures was attempted. The first method is called RING-FISH (recognition of individual genes-fluorescence *in situ* hybridization; see 2.2.5.3 RING-FISH of bacterial cells, p63). It utilizes the base-pairing of fluorescently labeled, specific single-stranded nucleic acid probes to a relatively short, distinct genomic coding sequence. The main obstacle in visualizing individual protein coding genes with the FISH method is their comparably low copy number that translates to low fluorescence intensities. This can be overcome by supplying the probe in excess and setting buffer conditions in a way so as to enable the formation of secondary structures leading to a complex network of self-interacting probes anchored to the target sequence. This network is usually visible as fluorescent halos, or rings, encompassing the sample cells (Amann & Fuchs, 2008; Zwirglmaier, 2005). Here, the method could be adapted to cyanobacterial culture samples successfully as far as it produced a specific fluorescent signal under defined conditions (data not shown). However, these conditions required the available target gene copies to concentrate to confined loci within the intracellular space, effectively allowing

only for the staining of cells immediately after DNA replication and prior to cytokinesis. Cells in other stages of the cell cycle could not be stained. Despite intensive efforts in adjusting parameters crucial for this method, in particular the incubation-buffer formamide concentration and the temperature and duration of the incubation with the labeled probes, the desired enhancement of sensitivity could not be established. Therefore, this method was deemed unsuitable for this particular problem.

A final attempt to quantify the amount of *actM* and *pfnM* genes in Braakman DNA extracts and in single isolated Braakman *Microcystis aeruginosa* colonies was based on the quantitative PCR method (qPCR) with a *Microcystis aeruginosa* specific intergenic region of the phycocyanin locus serving as a reference (Kurmayer & Kutzenberger, 2003). Unfortunately, neither approach produced consistent and reproducible results, therefore, no reliable assertions could be made based on these data. Most probably the wide range of uncontrollable factors brought about by the heterogeneity of the field sample composition posed too big an obstacle for the highly sensitive and intricate method qPCR.

3.3.2 Metagenomic analyses

3.3.2.1 DNA extraction and PCR

The quality of the DNA isolated from the initial samples with a standard TES-buffer based protocol for bacterial cells left a lot to be desired. The main drawbacks were the high degree of fragmentation of DNA extracted from fixed colony samples and the chemical impurity of DNA from filter samples (see **Figure 3.24A**). Though successful, PCR with primers targeting a region overlapping the *actM* and *pfnM* genes yielded only faint bands. To improve the quality of the extracted metagenomic DNA, an extraction protocol optimized for environmental samples containing high amounts of secondary metabolites and other chemical contaminants was used with the subsequent samples. Briefly, the buffer system was changed to contain CTAB and PVP to remove polyphenoles and the extraction procedure included a high salt wash to eliminate polysaccharide impurities (see 2.2.3.2 Preparation of

metagenomic DNA from field samples, p45). **Figure 3.24B** shows the stepwise purification of the DNA samples from all three sparbekkens. Initial extraction products show a considerable degree of chemical impurity, manifested in aberrant running properties on agarose gels (see **Figure 3.24B**, top left). High salt treatment reverses the migration direction; this is only abolished by two subsequent ethanol washes.

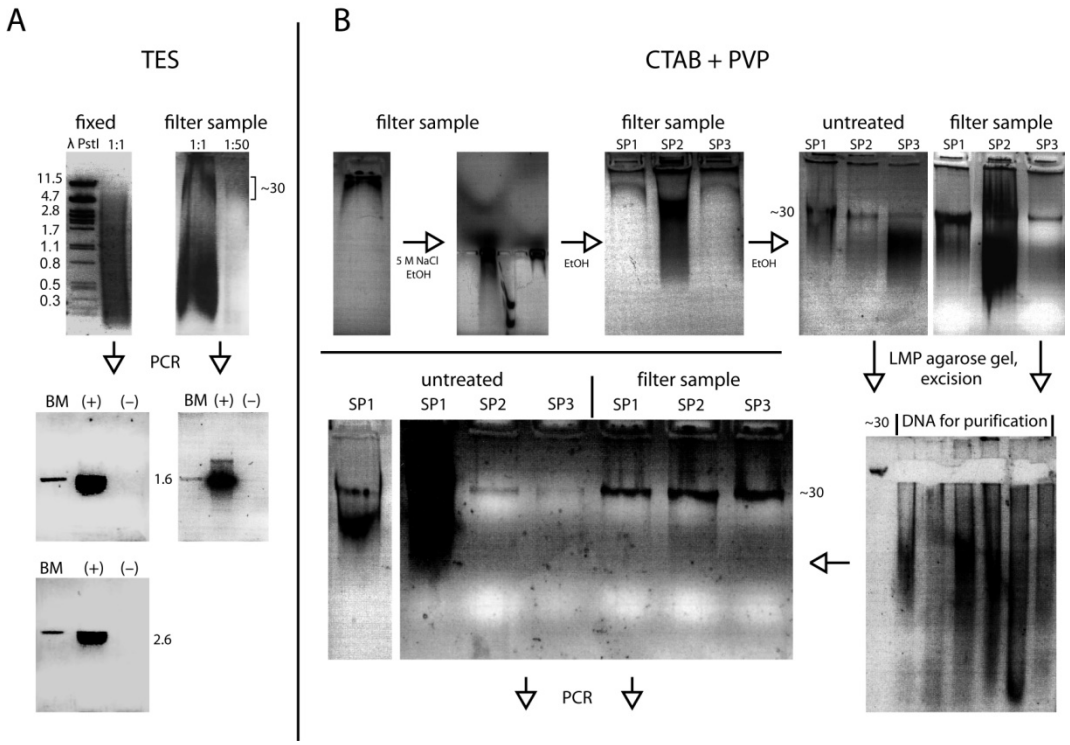

Figure 3.24. Two methods to extract DNA from environmental samples.
A: Tris-EDTA-Sucrose ("TES") based buffer system. The DNA from fixed filter samples ("fixed") is fragmented, the impure DNA from filter samples runs aberrantly on an agarose gel. The yield of *actM-pfnM* directed PCR is very low. Numbers indicate DNA fragment size in kb.
B: CTAB + PVP based buffer system. A high salt step ("5 M NaCl") and three ethanol washings ("EtOH") dramatically enhance DNA quality. Final grade of purity and size selection was achieved by gel excision and elution. All intermediate purification steps are shown. "SP" - sparbekken. Numbers give DNA size in kb.

Metagenomic DNA was further purified and selected for high molecular weight fragments through low-melting-point agarose gel excision and elution. The resultant six DNA samples (one each from each sparbekken and sampling method) had an improved quality and were used in subsequent analyses.

The first analysis performed with the enhanced Braakman DNA samples consisted of extensive PCR experiments employing a wide array of overlapping primers targeting the *actM-pfnM* genomic island region.

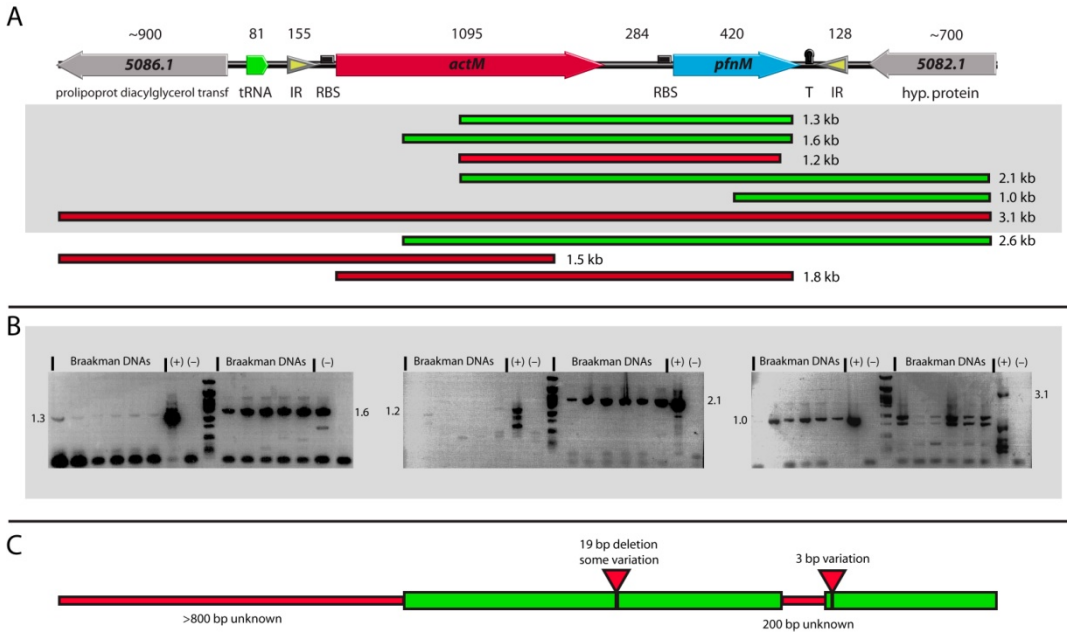

Figure 3.25. Overview of PCR and sequencing analyses of Braakman DNA samples.
A: Graphic representation of fragments of the *actM-pfnM* genomic region targeted by specific primers. The horizontal bars are displayed in relation to their location in the genomic region (top), their lengths are given in kb. Green and red bars indicate successful and unsuccessful amplification, respectively. PCR results of shaded fragments are shown in **B.** Abbreviations: IR - inverted repeats; RBS - ribosome binding site; T - transcription terminator. Numbers give lengths of elements in bp.
B: Agarose gel electrophoresis images of six targeted amplicons using Braakman DNAs (see grey box in **A**.). Two (1.2 and 3.1) did not produce expected fragment lengths. (+) - PCC 7806 DNA; (-) - water control, number give kb size.
C: Collective results of sequencing of generated amplicons from Braakman DNAs. The graphic is aligned to the genomic region in **A**. Green regions show stretches of sequence identity, red regions indicate areas of unknown sequences. Red triangles identify deviations from the PCC 7806 sequence.

Figure 3.25 shows an overview of the results obtained in the PCR analyses. Five out of nine primer pairs yielded fragments of the expected size, the region upstream of position 225 in the *actM* gene could not be amplified with any primer tested. Interestingly, while a primer designed to bind to the extreme 3' part of *pfnM* could be successfully employed in PCR amplifications, another primer, designed to bind to a position about 100 nucleotides upstream failed to produce any PCR fragments. It was this 3' region of *pfnM* that gave ambivalent results in subsequent cloning and sequencing analyses. Some of the sequenced fragments of that region showed a complete congruence with the respective fragment from PCC 7806, whereas others contained a ca. 200 bp fragment that showed no similarity to any sequence in the NCBI database (see **Figure 3.25C**). There were also some minor variations and deletions in the *actM-pfnM* intergenic region and

downstream of the inverted repeat flanking the right side (as in the orientation in **Figure 3.25A**) of the genomic island. No sequences were available for the 5' region that failed to bind any designed primers.
In summary, the presence of stretches of coding nucleotide sequence identical to the *actM-pfnM* genomic island of *Microcystis aeruginosa* PCC 7806 could be shown in the DNA extraction of the Braakman samples. However, a number of unknown sequences, particularly in the 5' regions and the wider flanking areas remained. The differences found suggest the distribution of the genomic island to genomes other than that of *Microcystis aeruginosa*. In order identify the organism(s) carrying the *actM-pfnM* genes in the wild, the determination of the sequence of the flanking regions was the focus of subsequent experiments.

3.3.2.2 Analyzing the regions flanking the genomic island

The size-selected DNA purified by agarose gel elution was used as the template for the construction of a fosmid library. Tentatively assuming a minimal variety of 10 organisms with genome sizes comparable to that of *E.coli* (4.7 Mb), a minimum of 5400 bacterial clones was required to find any given DNA sequence with a 99% chance in a library of 40 kb inserts (see 2.2.3.5 Construction of genomic fosmid libraries, p54). However, after multiple attempts and various protocol modifications the total number of clones obtained did not exceed 100. Needless to say that none of them carried the desired genomic island fragment.
A similar approach aimed at producing a plasmid library with smaller DNA fragments yielded similar unsatisfactory results.
Another method of obtaining information about unknown sequences flanking a well characterized region is called inverse PCR (see 2.2.3.9 Inverse PCR, p48). Briefly, the principle of this method is the fragmentation of the DNA sample with a restriction enzyme that does not target the known sequence. Subsequent ligation is carried out in conditions favoring the circularization of the fragments rather than their linear reassembly. In the final PCR step, amplification is initiated from primers binding to known the sequence region (Sambrook et al, 1989). Here, parallel experiments were carried out with the

restriction enzymes *Xba I* and *Bgl II*. To determine the template concentration optimal for circularization separate ligation reactions contained 3 dilutions of template DNA, 1:1, 1:8 and 1:64. Unfortunately, none of the setups produced any utilizable results as no clear band suitable for excision and sequencing could be identified.

In a last approach targeting the flanking sequences, the streptavidin mediated pull-down of biotin labeled DNA fragments was attempted. First, a single strand replication directed outwards of the known region was initiated using a single biotin labeled primer. Biotin labeled DNA fragments were then mixed with streptavidin coated magnetic beads. Streptavidin very specifically binds to biotin thereby immobilizing the labeled fragments to the beads. These beads were then subjected to a strong magnetic field and the remaining supernatant was removed. In two different setups the suspension containing the beads was either used directly for sequencing or was first subjected to DNA isolation and purification. Either way, no sequences whatsoever were obtained from these experiments.

In conclusion, the application of four different sophisticated methods has failed in uncovering the nucleotide sequence of the regions flanking the *actM-pfiM* coding region which was shown to be present in environmental samples. This signifies the problems encountered when facing a very heterogeneous sample marked by many unknown compositional parameters.

4 Discussion

Sparked by the discovery of prokaryotic cytoskeletal elements, the extensive research in the emerging field of bacterial cell biology has established the current notion of a bacterial intracellular space marked by a high complexity. In the wake of these revelations, the historic image depicting bacteria as "vessels" of a primitive form of life merely stabilized by a rigid cell wall, whose interior lacks internal structuring and cannot overcome the all-dominant principles of random diffusion has quickly outworn itself. The characterization of bacterial homologs of actin, one of the major factors underlying eukaryotic complexity and versatility, has not only confirmed many known key features typical for this family of proteins, it has also become clear that their structural plasticity is reflected in their involvement in a number of essential bacterial cellular processes (Cabeen & Jacobs-Wagner, 2010; Shaevitz & Gitai, 2010). Investigating the eukaryote-type actin ActM that, together with the actin binding protein homolog PfnM, has been transferred horizontally to the cyanobacterium *Microcystis aeruginosa* promises to further expand the broad functional spectrum of actins. Furthermore, the rare opportunity has arisen to analyze the adaptation of one of evolution's most conserved proteins to a foreign cellular environment. Despite having entered the cyanobacterial lineage only rather recently, both ActM and PfnM show a significant degree of sequence amelioration indicative of the evolutionary forces acting on both proteins (Guljamow et al, 2007). Therefore, to enable a comprehensive comparison of ActM with known actins, the first part of the present study concentrated on its biochemical and biophysical characterization. At the same time, the contribution of PfnM to the biological function of this evolutionary linked pair of proteins was considered. The experiments performed in this study's second part were addressing questions regarding evolutionary, metagenomic and ecological aspects of both proteins in a naturally occurring complex bacterial population.

4.1 ActM and PfnM have distinct and unique properties

At the outset of this work, the only known difference between ActM and eukaryotic actin was the amino acid sequence variation and the resulting lower molecular weight of ActM of 39 kDa compared to 43 kDa for actin (Guljamow et al, 2007). This difference was confirmed in this work with ActM heterologously expressed in *E.coli* (see 3.1.1 Heterologous expression of ActM and PfnM, p69). Heterologous expression and purification also allowed the first identification of PfnM on protein gels and blots, confirming the predicted size of 15 kDa. Fortunately, both ActM and PfnM turned out to be proteins that, after minor modifications in the expression routines, could conveniently and reliably be produced in large amounts of high purity. This was vitally important as it paved the way for subsequent work into the characterization of both proteins.

For instance, the hypothesis inferred from a deletion in the ActM amino acid sequence that this protein has lost the signature actin property of inhibiting the nuclease activity of DNase I could be confirmed with purified ActM (see 3.1.3.2 DNase I assay, p73). Since ActM would not encounter the eukaryotic DNase I in a bacterium, this is unsurprising. Interestingly, actins from some unicellular eukaryotes also lack the DNase I inhibition activity (Hirono et al, 1989; Kapoor et al, 2008). These organisms are also not expected to be exposed to DNase I as this enzyme is predominately found in the extracellular space in multicellular eukaryotes. At any rate, the fact that the actin ancestral to ActM has tolerated the loss of the DNase I binding capacity without an apparent major functional impairment supports the notion that the actin-DNase I interaction in eukaryotes indeed is of physiological relevance.

The most immediate question - regarding the polymerization properties of ActM - drew extensive attention in the course of this work. Indeed, this turned out to be an area of significant overlap in the properties of actin and ActM. Both proteins were shown to polymerize almost completely within minutes under the same conditions. The classic polymerization-inducing F-buffer widely used in the field of eukaryotic actin biochemistry was sufficient

to polymerize ActM. Analogous to eukaryotic actin, F-ActM could be sedimented by ultracentrifugation at 100,000 x g, leaving only very low amounts of unpolymerized protein in the supernatant (see 3.1.3.3 Polymerization and ultracentrifugation, p75). The intracellular ActM concentration of about 0.08 mg/ml (2.05 µM) estimated for *Microcystis aeruginosa* is slightly higher than known critical concentrations for polymerization of eukaryotic actin. Depending on the organism, under physiological conditions these threshold concentrations above which polymerization proceeds spontaneously were quantified as "less than 0.05 mg/ml (1.16 µM)" (Korn, 1978; Mabuchi & Spudich, 1980), 0.35 µM (0.015 mg/ml) (Pantaloni et al, 1984) or even as low as 0.1 µM (0.004 mg/ml) (Lodish et al, 2000). Taken together, these results show that ActM has the capacity to form polymers *in vitro* and that it very likely also appears in the aggregated state *in vivo*.

The phalloidin binding experiments proved to be an invaluable tool for comparing polymers of ActM and actin. In contrast to the other known bacterial actins, F-ActM could be stained with fluorescent phalloidin, employing the same technique commonly used for eukaryotic actin. The polymers visualized in that way, however, differ in shape from elongated actin filaments as they are much shorter, tending to form wider aggregates. The observed dimensions can be interpreted as an adaptation to the confined space of a bacterial cell whose length rarely exceeds 5 µm. In accordance with that, filaments formed *in vitro* by bacterial actins characterized to date are typically in the same size range reaching average lengths of 1-2 µm (see 1.2 Prokaryotic actins, p18 and **Figure 4.1**).

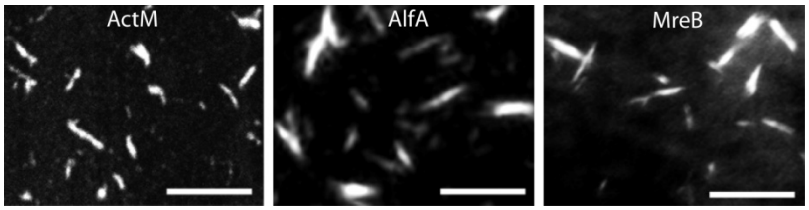

Figure 4.1. Light micrographs of filaments from ActM, AlfA and MreB.
The images show Alexa 488-phalloidin-stained ActM (this work), TIRF images of Cy3-labeled AlfA (Polka et al, 2009) and Alexa 488-stained MreB (Popp et al, 2010c). Scale bars: 5 µm.

Analyzing the finer structural details of ActM polymers by SAXS revealed more clear differences to eukaryotic actin. While the "large" aggregates observed by fluorescence microscopy are inaccessible with this method, the dimensions of the substructures invisible in the phalloidin stains can be determined with SAXS. The results indicate that ActM polymers deviate from the eukaryotic archetype by adopting a ribbon-like shape rather than being cylindrical. Whereas the gross dimensions of a single filament are comparable for both eukaryotic actin and ActM, the maximum dimension of 20 nm determined by the PDDF analysis combined with the constant height of 4.2 nm may be indicative of a subspecies of filaments that have aligned laterally to form wider superstructures (see 3.1.4.4 SAXS assay, p84 and **Figure 3.15**). Based on that, it can be speculated that ActM filaments may have an increased bundling tendency compared to eukaryotic F-actin. Finally, an ~8 amino acid random-coil structure absent from eukaryotic actin was found to contribute significantly to the shape of ActM filaments. However, the potential biological relevance of this finding needs to be addressed in further experiments.

Another obvious question evoked by dealing with homologs of two proteins known for their interaction was addressed by the *in vitro* ActM/PfnM binding and co-elution assays (see 3.1.4.1 Co-elution assay, p79). As postulated in view of the sequence conservation of mutual binding sites (Guljamow et al, 2007), ActM and PfnM were shown to bind each other. Additionally, the structural similarities of both actin/ActM and profilin/PfnM are probably especially pronounced in their contact region as PfnM was also found to co-elute with eukaryotic actin.

While the ActM-PfnM interaction itself was not surprising, the results of the phalloidin experiments conducted with mixtures of both proteins had a remarkable outcome: PfnM was found attached to polymers of ActM (see **Figure 3.13**, p82). This finding is unique in that profilin is usually described as a strictly actin monomer-binding protein (Yarmola & Bubb, 2009; Yarmola et al, 2008). It only binds transiently to actin filaments during its function of shuttling actin monomers to elongating filament ends. In these instances one

profilin molecule is bound per filament until the conformational change induced in the added monomer by the newly established actin-actin contact promotes the dissociation of profilin from the filament. In case of PfnM and ActM filaments, however, the aggregates observed microscopically are decorated by PfnM along their entire surface. In addition to that, the amount of PfnM bound to F-ActM apparently increased with PfnM levels over the ActM:PfnM ratios investigated.

While the latter effect can only be roughly estimated with fluorescence microscopy, it becomes apparent in the SAXS structural data and in the co-polymerization and sedimentation assay. The increasing radius of gyration derived from the scattering analyses was verified with three methods and clearly shows that the cross section of ActM filaments expands with the amount of PfnM added (see 3.1.4.4 SAXS assay, p84). This process had not reached saturation even when PfnM was present in a 2:1 molar excess. However, the analyses based on the radius of gyration do not prove that PfnM remains attached to ActM polymers. Strong support for the actual binding of PfnM to F-ActM came from the PDDF analysis of the SAXS data (see 3.1.4.4 SAXS assay, p84 and **Figure 3.15**). Again, a PfnM-dependent increase of the maximum dimensions of ActM polymers was observed and can be interpreted as augmented bundling of single filaments mediated by PfnM. The conspicuous appearance of pair-distance values at $r = n \cdot 15$ nm upon the addition of PfnM and their PfnM-dependent rise in probability is an indication of the emergence of a new, wider species of filaments (see **Figure 3.15**, arrows), regardless whether PfnM is bound or not. However, the data further show a very low frequency of structures measuring multiples of single ActM polymers whose increase is less pronounced than should be expected for the formation of sheets and bundles solely composed of ActM. This is a clear indication that significant amounts of bound PfnM are responsible for the observed increase in F-ActM width. The SAXS data is consistent with the results stemming from quantifying the relative amounts of ActM and PfnM in pellets generated by co-polymerization and ultracentrifugation (see 3.1.4.3 Polymerization and ultracentrifugation of ActM and PfnM, p83). These

experiments have confirmed that PfnM binds to ActM polymers in a concentration dependent manner and that this interaction is not saturated when PfnM is present in twofold molar excess. Combining the results of three different experimental approaches this work has accumulated robust evidence for the binding of significant amounts of PfnM to polymerized ActM, a property unknown from eukaryotic profilins. What with the absence of the usual eukaryotic actin filament bundling and cross-linking factors it can be speculated that PfnM may have modified its actin binding capacities and expanded its function in *Microcystis aeruginosa* to evolve into an ActM-filament binding and bundling protein.

The co-polymer hypothesis entails a number of implications. Primarily, the molecular structure of the eukaryotic actin filament does not allow for the presence of profilin attached to the known actin-profilin interface. Therefore, the three-dimensional orientation of PfnM towards the subunits of the ActM filament must differ from their eukaryotic ancestors. Two possibilities are conceivable to achieve this: Either the PfnM-ActM contact regions have undergone alterations so as to alleviate sterical hindrances present once ActM-ActM contacts are established upon polymerization. This would probably allow the PfnM molecule to remain filament-bound. Alternatively, the ActM subunit interactions in the filament have changed to the same end. This scenario most probably would result in an altered overall structure of the ActM filament compared with the eukaryotic F-actin helix. Indeed, the data presented here favor the second possibility. Not only does PfnM bind eukaryotic actin (see 3.1.4.1 Co-elution assay, p79), thus suggesting a high conservation of the contact interface, but also do ActM polymers have a pronounced ribbon shape that differs significantly from F-actin. In this respect it is worth mentioning an interesting observation made during the scientific search for a molecular model of F-actin: Crystals composed of actin-profilin heterodimers display actin-actin contacts that define a ribbon-shaped polymer with profilin molecules interdigitating between actin subunits (Egelman, 1994; Schutt et al, 1993). Although these ribbons do not represent naturally occurring F-actin and the ribbon model was ultimately rejected,

these data have shown that "forcing" the eukaryotic actin filament to adopt a ribbon shape can create the space required to accommodate profilin molecules. With "inventing" the ActM-ribbon, evolution may have arrived at a very similar solution to the problem of establishing ActM-PfnM co-polymers. Of course, the molecular background of the assertions that follow from these speculations can be tested with current analytical tools. Obtaining high-resolution structural information to elucidate the exact binding geometry of PfnM to ActM filaments should therefore be the objective of future work.

4.2 Biological relevance of ActM and PfnM

The potential functional relevance of the observed wide aggregates composed of both ActM and PfnM is best assessed in live bacterial cells. Considering failed previous attempts to establish mutant cells (Guljamow, 2006) and in absence of a system for the stable heterologous expression of foreign proteins in *Microcystis aeruginosa*, live-cell analyses with GFP fusions of ActM and PfnM were conducted in *E.coli*. These investigations aimed at elucidating questions regarding appearance, dynamics and localization of putative aggregates. Insight into these areas promised to provide a foundation from which to deduce information on the function of ActM and PfnM.

With the help of GFP-fusion proteins earlier findings from immunofluorescence microscopy of *Microcystis aeruginosa* suggesting the presence of a large intracellular shell-like assembly could be replicated in *E.coli* (see 3.2.1.2GFP fusions of ActM and PfnM, p88; compare **Figure 3.16**, p88 and **Figure 3.19**, p91). Agreeing with the *in vitro* experiments on ActM polymerization, ActM-GFP spontaneously forms agglomerations that are not freely diffusible inside *E.coli* cells. These apparent ActM assemblies frequently localize towards the cell's periphery in a way reminiscent of the ActM distribution in *Microcystis aeruginosa*. Protein complexes of a size from ~140 kDa were recently found to be restricted in their cytoplasmic mobility in *E.coli* (Nenninger et al, 2010). Therefore, ActM-GFP (sized ~65 kDa) at least forms dimeric aggregates, especially in the observed cases where ActM-GFP is

evenly distributed and only excluded from some cellular regions (see **Figure 3.19**, p91). Appearing in distinct shapes such as narrow peripheral layers or traversing bands, ActM-GFP is most likely specifically aggregated into polymeric structures. Unfortunately, GFP-labeled ActM must be regarded unsuitable to faithfully reflect the behavior of the untagged protein in all instances. This especially applies to the studies conducted with *E.coli* cells co-expressing ActM-GFP and PfnM. Considering the finding that no ActM-GFP-PfnM interaction could be detected in co-elution assays (see **Figure 3.21A**, p93), it is invalid to infer from the obtained micrographs that PfnM generally has no effect on *in vivo* ActM-GFP localization. A reason for the abolished PfnM binding may be found in the documented structural flexibility of the actin molecule possibly causing the attachment of protein tags to restructure the surface of ActM thus influencing further protein-protein interactions (Otterbein et al, 2001). Unfortunately, this problem could not be circumvented by fusing GFP to the N-terminus of the ActM protein.

However, PfnM-GFP was shown to bind ActM in the co-elution assay (see **Figure 3.21B**, p93), therefore, the strongest indications of the combined capacity of ActM and PfnM to form structures of potential functional relevance stem from experiments with PfnM-GFP. *E.coli* cells co-expressing PfnM-GFP and ActM typically display large, spherical, hollow structures. An assessment of the solubility of the proteins heterologously expressed by these cells has remedied concerns of having observed unspecific aggregation and deposition in inclusion bodies (**Figure 3.21C**, p93). As the observed structures are absent from cells expressing PfnM alone and the ability of ActM and PfnM to form laterally aligned, wide co-polymers was shown *in vitro*, it was tempting to speculate that ActM is also present in the observed enclosures.

Using a polyclonal anti-actin antibody in IFM experiments with cells co-expressing PfnM-GFP and ActM, the latter was found in the characteristic ring-shaped pattern overlapping with PfnM-GFP in the observed structures (see **Figure 3.20**, p92). Therefore, combining the data from the *in vitro* work with the results from the GFP fusion microscopy there are strong arguments

for the requirement of both ActM and PfnM in forming hollow, shell-like enclosures containing wide co-polymers composed of ActM and PfnM. The extended sheets formed as a result of the lateral alignment of ActM ribbons in the presence of PfnM can be regarded as more favorable for the formation of a continuous proteinaceous layer than individual filaments would be. The irregular shapes visible in cells expressing ActM alone seem to support that notion. Without the bundling and stabilizing effects of PfnM, the strong curvature observed in the spherical enclosures might be less likely to be established by ActM-GFP filaments alone. Rather, the intracellular localization of single filaments is probably governed by extrusion and displacement effects created by the various components of the *E.coli* cell. The observed concentration of ActM at the inner face of the cell envelope may very plausibly be the result of undirected linear polymerization along an immobile structure, eventually generating a shell-like pattern. Any physical obstacle a growing polymer would encounter along a guiding scaffold might conceivably cause a deflection of the direction of elongation leading to the observed patterns of traversing bands or discontinuous shells.

4.3 Towards the function of ActM and PfnM

Extensive efforts and multiple experimental approaches notwithstanding, a clear natural function of ActM and PfnM has not yet become apparent. Hence, the roles these proteins play in *Microcystis aeruginosa*, their benefits to the host and the reasons for their persistence especially in natural populations remain speculative. Taking from the differences in intracellular localization, a functional overlap of ActM with the host actin homolog MreB seems unlikely (see **Figure 3.16**, p88). In *Microcystis aeruginosa,* MreB appears in random strings and patches throughout the cytoplasm and does not concentrate at the cell's periphery. A straightforward interpretation of the presence of a protein layer underlying the cell envelope suggests a role for ActM in cell stabilization. The observed structures appear suited to provide mechanical support as they were found to be rigid and non-dynamic in FRAP

experiments (see **Figure 3.20**, p92). However, it can only be speculated under which circumstances free-living *Microcystis* (or any other bacterium) would benefit from an elevated resistance to mechanical stress. *Microcystis,* for instance, is well known for its ability to migrate vertically through the water column as a reaction to unfavorable light conditions or the trophic state of the environment (Ibelings et al, 1991; Thomas & Walsby, 1985). Increasing the resistance to mechanical stress would conceivably expand the range of variations in hydrostatic pressure the cell could tolerate thus enabling it to advance into otherwise inaccessible water depths. Moreover, a stabilizing proteinaceous layer may increase the cell's resistance to environmental changes in salinity and osmolarity. There are preliminary indications that PCC 7806 may indeed be more resistant to osmotic stress than other strains of *Microcystis aeruginosa* as its genome contains an unusual number of open reading frames that are very similar to key sucrose biosynthesis genes. In many cyanobacteria sucrose functions as an osmoregulatory compound whose intracellular levels increase under osmotic stress (Blumwald et al, 1983; Mackay et al, 1984; Marin et al, 2006; Mikkat et al, 1997; Reed & Stewart, 1985; Suzuki et al, 2010). The principal enzymes of the sucrose biosynthesis pathway are the commonly found combination of sucrose-phosphate synthases (*spsA/B*) with their specific sucrose-phosphate phosphatase (*sppA*). An additional sucrose synthase (*susA*) was so far only found in the filamentous cyanobacterium *Anabaena* sp. PCC 7120 (Cumino et al, 2002; Lunn et al, 1999; Porchia & Salerno, 1996). While PCC 7806 encodes four ORFs (IPF numbers 1563.1, 1564.1, 1565.1 and 1566.1) with sequence identities of around 65% to the aforementioned sucrose biosynthesis genes, none of them is found in the genome of *Microcystis aeruginosa* NIES 843 or any other *Microcystis* strain in the database. This remarkable observation provides an incentive for promising future studies.

Bacteria in general and cyanobacteria in particular are known for their quick adaptation and response to changes in environmental conditions (Tandeau de Marsac, 1977; Walsby & Hayes, 1989). Therefore, given the known rapid responsiveness of actin and profilin to extracellular stimuli in eukaryotes, it is

of outstanding interest to assess to what extent the expression of ActM and PfnM and their concerted formation of a stabilizing shell might be the reaction to changes in external conditions. Again, this promises to be at the focus of fruitful future research.

A number of arguments hint at the involvement of both proteins in bacteriophage related processes. First, ActM and PfnM are encoded in a mobile genetic element common for bacteriophage mediated genetic transfer and are not unlikely to have entered *Microcystis aeruginosa* on a shuttling cyanophage (Coleman et al, 2006; Lindell et al, 2007; Sullivan et al, 2006). While the initial integration of the ancestral *actM* and *pfnM* genes into a bacterial genome has probably occurred after the uptake of stretches of eukaryotic DNA (Guljamow, 2006; Guljamow et al, 2007), the clustering in a typical genomic islands argues both for the adoption of a function and for continuous events of mobilization. Probably, after serial passages through various bacterial genomes accompanied by reshaping and amelioration of the coding sequence, the genomic island eventually has entered the *Microcystis aeruginosa* lineage. It has been shown previously that cyanophages can carry genes that confer a selective advantage to their hosts (Brabban et al, 2005; Bryan et al, 2008; Mühling et al, 2005; Paul, 2008; Paul & Sullivan, 2005). Additionally, bacterial viruses frequently employ mechanisms facilitating the exit of their progeny from host cells or prevent the superinfection with a competing phage (Berngruber et al, 2010; Lee et al, 2005; Russel, 1995). Conceivably, ActM and PfnM and more particularly, their formation of an extensive peripheral protein layer, may play a role in any of these possibly existing mechanisms in the replication-cycle of a putative phage. A second observation possibly arguing in favor of virus-related functions of ActM and PfnM are the well-studied profilins encoded in many viral genomes (Blasco et al, 1991; Gubser et al, 2004; Polet et al, 2007; Upton et al, 2003). Moreover, a large number of "eukaryotic" viruses are strictly dependent on actin and profilin for their genome replication and intercellular spreading of viral particles (Bitko et al, 2003; Burke et al, 2000; Butler-Cole et al, 2007; Harpen

et al, 2009). These beneficial roles actin and profilin play in the propagation of viruses may have contributed to the manifestation of ActM and PfnM in the metagenome of microbial communities.

The experiments performed on the field samples from the original habitat of *Microcystis aeruginosa* PCC 7806 were to shed light on many of these aspects. The most exciting findings of this area of the work stem from the immunofluorescence microscopy probing for the presence of ActM in *Microcystis aeruginosa* colonies. While the successful identification of cells displaying the typical ActM ring-shaped signal was of extraordinary significance, the heterogeneous intercellular distribution of ActM in *Microcystis aeruginosa* colonies (see **Figure 3.23**, p96) entailed some very intriguing implications. Clearly, the heterogeneity of the ActM-derived signal was not an artifact resulting from incoherent cell permeabilization, as the images show many differently stained cells in very close proximity. It is highly unlikely that the conditions for permeabilization and antibody access vary within just a few micrometers. Rather, the results suggest a variation in ActM content in close communities of *Microcystis aeruginosa*. This strengthens the assumption that the appearance of the ActM-PfnM shell is regulated, possibly in response to internal or external stimuli. This interpretation also includes the infection of individual cells with a bacteriophage. Alternatively, although generally considered to be of common clonal descent, individual cells in a *Microcystis aeruginosa* colony may show differences in their genetic outfit.

Especially the latter, rather unconventional proposition unquestionably calls for further careful and thorough analyses. Unfortunately, while the presence of *actM* and *pfnM* shown in previous experiments (Guljamow et al, 2007) could be verified here, neither microscopic nor molecular-biological methods employed in the course of this work were successful in providing arguments for any of these fascinating possibilities. One reason for that may be found in the heterogeneity of taxa of organisms in the field samples. The total DNA extracted from these samples is expected to contain a high number of individual genomes, to a large degree these will be of bacterial origin,

however, eukaryotic and viral genomes are also likely to be found. The *actM-pfnM* region will only constitute a minute sub-fraction of that metagenome and its amount may well be near the PCR detection limit. Assuming that the *actM-pfnM* genomic island is present in more than one group of organisms, its flanking regions are expected to reflect the heterogeneity of the whole sample. Thus, they will not be conserved throughout the metagenome and will be even less accessible to detection and analysis than the genomic island itself. None of the techniques employed for the detection of the flanking regions - fosmid and plasmid libraries, inverse PCR, and biotin pull-down - has a sensitivity comparable to PCR as none of them can accomplish the exponential amplification of an unknown target sequence directly. Both the construction of libraries and the inverse PCR method rely on sensitivity-determining initial enzymatic reactions (restriction enzyme cleavage, end repairing and ligation) prior to PCR detection. If anything, these reactions will only decrease the amount of target sequence impeding successful amplification. The biotin pull-down assay includes a step of unspecific random DNA enrichment and a non-exponential, specific replication in a single-primer set-up. Both steps are expected to increase the total number of available flanking-region DNA molecules. Additionally, the subsequent streptavidin/biotin mediated magnetic pull-down of these molecules constitutes a further step of enrichment. However, a two-primer based, exponential PCR amplification of the target sequences is not possible with this method. In addition to that, the chaining and balancing of many sophisticated molecular techniques increase the susceptibility of this method towards external interference. Therefore, the biotin pull-down approach also proved to be unsuitable to yield enough DNA material for the identification of the flanking regions.

As an alternative explanation for the difficulties encountered in accessing the *actM-pfnM* flanking regions in the metagenome samples, contamination with fragmented laboratory DNA, such as PCR products, must be discussed. However, a number of observations argue against this possibility. As water controls were analyzed in all PCR experiments and only those with satisfying

control results were used for further analysis, the contamination of the reagents is very unlikely. A contamination of the DNA preparations with laboratory DNA (which is undetectable by PCR water controls) would have led to PCR fragments with 100% sequence identity to the genome of *Microcystis aeruginosa* PCC 7806. As the obtained sequences showed variations not observed before and some regions within the *actM-pfiM* region could not be amplified with primers derived from known sequences, cross-contamination of the DNA samples can be ruled out.

Another factor hampering laboratory work with metagenomic samples is their chemical heterogeneity. Although a DNA extraction protocol was used that apparently succeeded in minimizing impurities with some secondary metabolites (see 3.3.2.1 DNA extraction and PCR, p98 and **Figure 3.24**, p99), the samples are still expected to contain a wide range of possibly inhibitory compounds. These may irreversibly interact with DNA molecules, influence photometric measurements or prevent the successful execution of downstream enzymatic reactions (Porebski et al, 1997; Sangwan et al, 1998; Tel-zur et al, 1999; Varma et al, 2007b). The inconsistent results obtained in the quantitative PCR experiments are most likely attributable to these effects. Additionally, these factors may also have heavily influenced any of the employed methods discussed above.

4.4 Concluding remarks and future outlook

The major conclusion to be drawn from the work presented here is that despite being a very slowly evolving protein in eukaryotes, actin still displays a remarkable adaptive flexibility once it faces a foreign cellular environment. The experimental data substantiate the notion that the high degree of conservation of eukaryotic cytoskeletal proteins in general is not an inherent feature of their amino acid sequence itself, rather, it is maintained by constrains exerted by the vast multitude of interacting factors (Erickson, 2007; Jenkins et al, 2002). Being placed in an environment devoid of these binding partners and subjected to adaptive pressure, actin and profilin have

readily developed properties not found in their ancestral eukaryotic proteins. ActM, for instance, combines characteristics known from other bacterial actins: its filaments show a bacterial-type length restriction; similar to MreB, these filaments are flattened and ribbon-shaped (Amos et al, 2004; van den Ent et al, 2001b). The bundling of individual filaments into higher-ordered aggregates is known from AlfA and MreB (Esue et al, 2005; Polka et al, 2009; Popp et al, 2010c). In contrast to most actins, ActM filaments do not show pronounced dynamic properties and form an immobile intracellular structure, a trait however, ActM shares with MamK (Komeili et al, 2006). In cooperation with PfnM, this combination of ActM properties has led to the emergence of a unique intracellular entity in form of a rigid proteinaceous shell. The formation of a comparable structure is unprecedented among actins and adds to the spectrum of key functions fulfilled by members of this family of proteins.

In light of the importance of ABPs in eukaryotic actin evolution and the singular role PfnM – the only known *bona fide* ABP homolog in prokaryotes – plays in the formation of distinct ActM aggregates, it is highly probable that in a co-evolutionary process PfnM and ActM have directly influenced the reshaping of each other's sequence.

Clearly, this work provides ample incentive for extensive future work in this field. Among others, a more detailed analysis of ActM polymer aggregates by electron microscopy is of most outstanding interest. Thin sectioning experiments promise to provide insight into the orientation of single ActM filaments in the structures observed microscopically both *in vitro* and in bacterial cells. High-resolution structural data, obtained either by cryo-EM or X-ray crystallography will help to resolve the open questions regarding the molecular structure of ActM monomers, filaments and PfnM co-polymers. Undoubtedly, the remarkable case of the vagrant eukaryotic cytoskeletal elements that chanced upon a cyanobacterium makes for some intriguing, challenging, and thus rewarding, future scientific endeavors.

5 Appendix

5.1 List of figures

5.2 List of tables

6 References

Amann R, Fuchs BM (2008) Single-cell identification in microbial communities by improved fluorescence in situ hybridization techniques. *Nat Rev Microbiol* **6:** 339-348

Amos LA, van den Ent F, Löwe J (2004) Structural/functional homology between the bacterial and eukaryotic cytoskeletons. *Curr Opin Cell Biol* **16:** 24-31

An SS, Mopps B, Weber K, Bhattacharya D (1999) The origin and evolution of green algal and plant actins. *Mol Biol Evol* **16:** 275-285

Andersson JO (2005) Lateral gene transfer in eukaryotes. *Cell Mol Life Sci* **62:** 1182-1197

Bartles JR (2000) Parallel actin bundles and their multiple actin-bundling proteins. *Curr Opin Cell Biol* **12:** 72-78

Bear JE, Svitkina TM, Krause M, Schafer DA, Loureiro JJ, Strasser GA, Maly IV, Chaga OY, Cooper JA, Borisy GG, Gertler FB (2002) Antagonism between Ena/VASP proteins and actin filament capping regulates fibroblast motility. *Cell* **109:** 509-521

Becker E, Herrera NC, Gunderson FQ, Derman AI, Dance AL, Sims J, Larsen RA, Pogliano J (2006) DNA segregation by the bacterial actin AlfA during Bacillus subtilis growth and development. *Embo J* **25:** 5919-5931

Ben-Yehuda S, Losick R (2002) Asymmetric cell division in B. subtilis involves a spiral-like intermediate of the cytokinetic protein FtsZ. *Cell* **109:** 257-266

Berngruber TW, Weissing FJ, Gandon S (2010) Inhibition of superinfection and the evolution of viral latency. *J Virol* **84:** 10200-10208

Bhattacharya D, Weber K (1997) The actin gene of the glaucocystophyte Cyanophora paradoxa: analysis of the coding region and introns, and an actin phylogeny of eukaryotes. *Curr Genet* **31:** 439-446

Bitko V, Oldenburg A, Garmon NE, Barik S (2003) Profilin is required for viral morphogenesis, syncytium formation, and cell-specific stress fiber induction by respiratory syncytial virus. *BMC Microbiol* **3:** 9

Blanchoin L, Pollard TD, Hitchcock-DeGregori SE (2001) Inhibition of the Arp2/3 complex-nucleated actin polymerization and branch formation by tropomyosin. *Curr Biol* **11:** 1300-1304

Blasco R, Cole NB, Moss B (1991) Sequence analysis, expression, and deletion of a vaccinia virus gene encoding a homolog of profilin, a eukaryotic actin-binding protein. *J Virol* **65:** 4598-4608

Blikstad I, Markey F, Carlsson L, Persson T, Lindberg U (1978) Selective assay of monomeric and filamentous actin in cell extracts, using inhibition of deoxyribonuclease I. *Cell* **15:** 935-943

Blumwald E, Mehlhorn RJ, Packer L (1983) Studies of osmoregulation in salt adaptation of cyanobacteria with ESR spin-probe techniques. *Proc Natl Acad Sci U S A* **80:** 2599-2602

Boldogh IR, Pon LA (2006) Interactions of mitochondria with the actin cytoskeleton. *Biochim Biophys Acta* **1763:** 450-462

Bork P, Sander C, Valencia A (1992) An ATPase domain common to prokaryotic cell cycle proteins, sugar kinases, actin, and hsp70 heat shock proteins. *Proc Natl Acad Sci U S A* **89:** 7290-7294

Bowman GR, Comolli LR, Zhu J, Eckart M, Koenig M, Downing KH, Moerner WE, Earnest T, Shapiro L (2008) A polymeric protein anchors the chromosomal origin/ParB complex at a bacterial cell pole. *Cell* **134:** 945-955

Brabban AD, Hite E, Callaway TR (2005) Evolution of foodborne pathogens via temperate bacteriophage-mediated gene transfer. *Foodborne Pathog Dis* **2:** 287-303

Bradford MM (1976) A rapid and sensitive method for the quantitation of microgram quantities of protein utilizing the principle of protein-dye binding. *Anal Biochem* **72:** 248-254

Brown JR, Italia MJ, Douady C, Stanhope MJ. (2002) Horizontal Gene Transfer and the Universal Tree of Life. In Syvanen M, Kado CI (eds.), *Horizontal Gene Transfer*. Academic Press, London, pp. 305-349.

Bryan MJ, Burroughs NJ, Spence EM, Clokie MR, Mann NH, Bryan SJ (2008) Evidence for the intense exchange of MazG in marine cyanophages by horizontal gene transfer. *PLoS One* **3:** e2048

Bullock JC, Fernandez JM, Short JM (1987) XL1-blue: A high efficiency plasmid transforming recA Escherichia coli strain with ß-galactosidase selection. *BIOTECHNIQUES* **5:** 376-379.

Burke E, Mahoney NM, Almo SC, Barik S (2000) Profilin is required for optimal actin-dependent transcription of respiratory syncytial virus genome RNA. *J Virol* **74:** 669-675

Butler-Cole C, Wagner MJ, Da Silva M, Brown GD, Burke RD, Upton C (2007) An ectromelia virus profilin homolog interacts with cellular tropomyosin and viral A-type inclusion protein. *Virol J* **4:** 76

Cabeen MT, Jacobs-Wagner C (2010) The bacterial cytoskeleton. *Annu Rev Genet* **44:** 365-392

Carballido-Lopez R, Errington J (2003a) The bacterial cytoskeleton: in vivo dynamics of the actin-like protein Mbl of Bacillus subtilis. *Dev Cell* **4:** 19-28

Carballido-Lopez R, Errington J (2003b) A dynamic bacterial cytoskeleton. *Trends Cell Biol* **13:** 577-583

Carlsson L, Nystrom LE, Sundkvist I, Markey F, Lindberg U (1977) Actin polymerizability is influenced by profilin, a low molecular weight protein in non-muscle cells. *J Mol Biol* **115:** 465-483

Chang KS, Zimmer WE, Jr., Bergsma DJ, Dodgson JB, Schwartz RJ (1984) Isolation and characterization of six different chicken actin genes. *Mol Cell Biol* **4:** 2498-2508

Chik JK, Lindberg U, Schutt CE (1996) The structure of an open state of beta-actin at 2.65 A resolution. *J Mol Biol* **263:** 607-623

Chou J, Stolz DB, Burke NA, Watkins SC, Wells A (2002) Distribution of gelsolin and phosphoinositol 4,5-bisphosphate in lamellipodia during EGF-induced motility. *Int J Biochem Cell Biol* **34:** 776-790

Claessens MM, Bathe M, Frey E, Bausch AR (2006) Actin-binding proteins sensitively mediate F-actin bundle stiffness. *Nat Mater* **5:** 748-753

Coleman ML, Sullivan MB, Martiny AC, Steglich C, Barry K, Delong EF, Chisholm SW (2006) Genomic islands and the ecology and evolution of Prochlorococcus. *Science* **311:** 1768-1770

Cowieson NP, King G, Cookson D, Ross I, Huber T, Hume DA, Kobe B, Martin JL (2008) Cortactin adopts a globular conformation and bundles actin into sheets. *J Biol Chem* **283:** 16187-16193

Cowles KN, Gitai Z (2010) Surface association and the MreB cytoskeleton regulate pilus production, localization and function in Pseudomonas aeruginosa. *Mol Microbiol* **76:** 1411-1426

Cramer LP, Briggs LJ, Dawe HR (2002) Use of fluorescently labelled deoxyribonuclease I to spatially measure G-actin levels in migrating and non-migrating cells. *Cell Motil Cytoskeleton* **51:** 27-38

Cumino A, Curatti L, Giarrocco L, Salerno GL (2002) Sucrose metabolism: Anabaena sucrose-phosphate synthase and sucrose-phosphate phosphatase define minimal functional domains shuffled during evolution. *FEBS Lett* **517:** 19-23

Da Lage JL, Feller G, Janecek S (2004) Horizontal gene transfer from Eukarya to bacteria and domain shuffling: the alpha-amylase model. *Cell Mol Life Sci* **61:** 97-109

Daniel RA, Errington J (2003) Control of cell morphogenesis in bacteria: two distinct ways to make a rod-shaped cell. *Cell* **113:** 767-776

Dedova IV, Dedov VN, Nosworthy NJ, Hambly BD, dos Remedios CG (2002) Cofilin and DNase I affect the conformation of the small domain of actin. *Biophys J* **82:** 3134-3143

Defeu Soufo HJ, Graumann PL (2004) Dynamic movement of actin-like proteins within bacterial cells. *EMBO Rep* **5:** 789-794

Defeu Soufo HJ, Graumann PL (2005) Bacillus subtilis actin-like protein MreB influences the positioning of the replication machinery and requires membrane proteins MreC/D and other actin-like proteins for proper localization. *BMC Cell Biol* **6:** 10

Defeu Soufo HJ, Graumann PL (2006) Dynamic localization and interaction with other Bacillus subtilis actin-like proteins are important for the function of MreB. *Mol Microbiol* **62:** 1340-1356

Delory GE (1945) A sodium carbonate-bicarbonate buffer for alkaline phosphatases. *Biochem J* **39:** 245

Derman AI, Becker EC, Truong BD, Fujioka A, Tucey TM, Erb ML, Patterson PC, Pogliano J (2009) Phylogenetic analysis identifies many uncharacterized actin-like proteins (Alps) in bacteria: regulated polymerization, dynamic instability and treadmilling in Alp7A. *Mol Microbiol* **73:** 534-552

Diaz-Camino C, Conde R, Ovsenek N, Villanueva MA (2005) Actin expression is induced and three isoforms are differentially expressed during germination in Zea mays. *J Exp Bot* **56:** 557-565

Dittmann E, Neilan BA, Erhard M, von Dohren H, Borner T (1997) Insertional mutagenesis of a peptide synthetase gene that is responsible for hepatotoxin production in the cyanobacterium Microcystis aeruginosa PCC 7806. *Mol Microbiol* **26:** 779-787

Dobrindt U, Hochhut B, Hentschel U, Hacker J (2004) Genomic islands in pathogenic and environmental microorganisms. *Nat Rev Microbiol* **2:** 414-424

Doi M, Wachi M, Ishino F, Tomioka S, Ito M, Sakagami Y, Suzuki A, Matsuhashi M (1988) Determinations of the DNA sequence of the mreB gene and of the gene products of the mre region that function in formation of the rod shape of Escherichia coli cells. *J Bacteriol* **170:** 4619-4624

Dominguez R (2004) Actin-binding proteins--a unifying hypothesis. *Trends Biochem Sci* **29:** 572-578

Doolittle RF (2002) Gene Transfers Between Distantly Related Organisms. In *Horizontal Gene Transfer*, Syvanen M, Kado CI (eds), pp 269-275. London, U.K.: Academic Press

Doolittle WF (1999) Phylogenetic classification and the universal tree. *Science* **284:** 2124-2129

dos Remedios CG, Chhabra D, Kekic M, Dedova IV, Tsubakihara M, Berry DA, Nosworthy NJ (2003) Actin binding proteins: regulation of cytoskeletal microfilaments. *Physiol Rev* **83:** 433-473

Douglas SE (1998) Plastid evolution: origins, diversity, trends. *Curr Opin Genet Dev* **8:** 655-661

Drouin G, Moniz de Sa M, Zuker M (1995) The Giardia lamblia actin gene and the phylogeny of eukaryotes. *J Mol Evol* **41:** 841-849

Dye NA, Shapiro L (2007) The push and pull of the bacterial cytoskeleton. *Trends Cell Biol* **17:** 239-245

Eads JC, Mahoney NM, Vorobiev S, Bresnick AR, Wen KK, Rubenstein PA, Haarer BK, Almo SC (1998) Structure determination and characterization of Saccharomyces cerevisiae profilin. *Biochemistry* **37:** 11171-11181

Egelman EH (1994) Actin filament structure. The ghost of ribbons past. *Curr Biol* **4:** 79-81

Engel J, Gunning P, Kedes L (1982) Human cytoplasmic actin proteins are encoded by a multigene family. *Mol Cell Biol* **2:** 674-684

Engel JN, Gunning PW, Kedes L (1981) Isolation and characterization of human actin genes. *Proc Natl Acad Sci U S A* **78:** 4674-4678

Erickson HP (1998) Atomic structures of tubulin and FtsZ. *Trends Cell Biol* **8:** 133-137

Erickson HP (2007) Evolution of the cytoskeleton. *BioEssays* **29:** 668-677

Estrada P, Kim J, Coleman J, Walker L, Dunn B, Takizawa P, Novick P, Ferro-Novick S (2003) Myo4p and She3p are required for cortical ER inheritance in Saccharomyces cerevisiae. *J Cell Biol* **163:** 1255-1266

Esue O, Cordero M, Wirtz D, Tseng Y (2005) The assembly of MreB, a prokaryotic homolog of actin. *J Biol Chem* **280:** 2628-2635

Evangelista M, Zigmond S, Boone C (2003) Formins: signaling effectors for assembly and polarization of actin filaments. *J Cell Sci* **116:** 2603-2611

Field CB, Behrenfeld MJ, Randerson JT, Falkowski P (1998) Primary production of the biosphere: integrating terrestrial and oceanic components. *Science* **281:** 237-240

Figge RM, Divakaruni AV, Gober JW (2004) MreB, the cell shape-determining bacterial actin homologue, co-ordinates cell wall morphogenesis in Caulobacter crescentus. *Mol Microbiol* **51:** 1321-1332

Frangeul L, Quillardet P, Castets AM, Humbert JF, Matthijs HC, Cortez D, Tolonen A, Zhang CC, Gribaldo S, Kehr JC, Zilliges Y, Ziemert N, Becker S, Talla E, Latifi A, Billault A, Lepelletier A, Dittmann E, Bouchier C, de Marsac NT (2008) Highly plastic genome of Microcystis aeruginosa PCC 7806, a ubiquitous toxic freshwater cyanobacterium. *BMC Genomics* **9:** 274

Frost LS, Leplae R, Summers AO, Toussaint A (2005) Mobile genetic elements: the agents of open source evolution. *Nat Rev Microbiol* **3:** 722-732

Fujii T, Iwane AH, Yanagida T, Namba K (2010) Direct visualization of secondary structures of F-actin by electron cryomicroscopy. *Nature* **467:** 724-728

Garner EC, Campbell CS, Mullins RD (2004) Dynamic instability in a DNA-segregating prokaryotic actin homolog. *Science* **306:** 1021-1025

Garner EC, Campbell CS, Weibel DB, Mullins RD (2007) Reconstitution of DNA segregation driven by assembly of a prokaryotic actin homolog. *Science* **315:** 1270-1274

Gerdes K, Møller-Jensen J, Ebersbach G, Kruse T, Nordstrom K (2004) Bacterial mitotic machineries. *Cell* **116:** 359-366

Gershman LC, Selden LA, Kinosian HJ, Estes JE (1989) Preparation and polymerization properties of monomeric ADP-actin. *Biochim Biophys Acta* **995:** 109-115

Giovannoni SJ, Turner S, Olsen GJ, Barns S, Lane DJ, Pace NR (1988) Evolutionary relationships among cyanobacteria and green chloroplasts. *J Bacteriol* **170:** 3584-3592

Gitai Z, Dye N, Shapiro L (2004) An actin-like gene can determine cell polarity in bacteria. *Proc Natl Acad Sci U S A* **101:** 8643-8648

Gitai Z, Dye NA, Reisenauer A, Wachi M, Shapiro L (2005) MreB actin-mediated segregation of a specific region of a bacterial chromosome. *Cell* **120:** 329-341

Glatter O (1979) Interpretation of Real-Space Information from Small-Angle Scattering Experiments. *Journal of Applied Crystallography* **12:** 166-175

Glatter O (1980) Evaluation of Small-Angle Scattering data from lamellar and cylindrical particles by the inddirect transformation method. *Journal of Applied Crystallography* **13:** 577-584

Glatter O, Kratky O (1982) *Small Angle X-ray Scattering*, London: Academic Press.

Gogarten JP, Townsend JP (2005) Horizontal gene transfer, genome innovation and evolution. *Nat Rev Microbiol* **3:** 679-687

Goldschmidt-Clermont PJ, Machesky LM, Doberstein SK, Pollard TD (1991) Mechanism of the interaction of human platelet profilin with actin. *J Cell Biol* **113:** 1081-1089

Graumann PL (2004) Cytoskeletal elements in bacteria. *Curr Opin Microbiol* **7:** 565-571

Gubser C, Hue S, Kellam P, Smith GL (2004) Poxvirus genomes: a phylogenetic analysis. *J Gen Virol* **85:** 105-117

Guljamow A (2006) Identification and characterization of eukaryote-like actin and profilin in *Microcystis aeruginosa* PCC7806. Diploma thesis.

Guljamow A, Jenke-Kodama H, Saumweber H, Quillardet P, Frangeul L, Castets AM, Bouchier C, Tandeau de Marsac N, Dittmann E (2007) Horizontal gene transfer of two cytoskeletal elements from a eukaryote to a cyanobacterium. *Curr Biol* **17:** R757-759

Gustafson KR, Sowder RC, 2nd, Henderson LE, Cardellina JH, 2nd, McMahon JB, Rajamani U, Pannell LK, Boyd MR (1997) Isolation, primary sequence determination, and disulfide bond structure of cyanovirin-N, an anti-HIV (human immunodeficiency virus) protein from the cyanobacterium Nostoc ellipsosporum. *Biochem Biophys Res Commun* **238:** 223-228

Hanson J, Lowy J (1963) The structure of F-actin and of actin filaments isolated from muscle. *J Mol Biol* **6:** 46-63

Hara F, Yamashiro K, Nemoto N, Ohta Y, Yokobori S, Yasunaga T, Hisanaga S, Yamagishi A (2007) An actin homolog of the archaeon Thermoplasma acidophilum that retains the ancient characteristics of eukaryotic actin. *J Bacteriol* **189:** 2039-2045

Harpen M, Barik T, Musiyenko A, Barik S (2009) Mutational analysis reveals a noncontractile but interactive role of actin and profilin in viral RNA-dependent RNA synthesis. *J Virol* **83:** 10869-10876

Hartwig JH, Bokoch GM, Carpenter CL, Janmey PA, Taylor LA, Toker A, Stossel TP (1995) Thrombin receptor ligation and activated Rac uncap actin filament barbed ends through phosphoinositide synthesis in permeabilized human platelets. *Cell* **82:** 643-653

Hayes MJ, Rescher U, Gerke V, Moss SE (2004) Annexin-actin interactions. *Traffic* **5:** 571-576

Hertzog M, van Heijenoort C, Didry D, Gaudier M, Coutant J, Gigant B, Didelot G, Preat T, Knossow M, Guittet E, Carlier MF (2004) The beta-thymosin/WH2 domain; structural basis for the switch from inhibition to promotion of actin assembly. *Cell* **117:** 611-623

Hirono M, Kumagai Y, Numata O, Watanabe Y (1989) Purification of Tetrahymena actin reveals some unusual properties. *Proc Natl Acad Sci U S A* **86:** 75-79

Hitchcock SE (1980) Actin deoxyroboncuclease I interaction. Depolymerization and nucleotide exchange. *J Biol Chem* **255:** 5668-5673

Hodge T, Cope MJ (2000) A myosin family tree. *J Cell Sci* **113 Pt 19:** 3353-3354

Holmes KC, Popp D, Gebhard W, Kabsch W (1990) Atomic model of the actin filament. *Nature* **347:** 44-49

Hu B, Yang G, Zhao W, Zhang Y, Zhao J (2007) MreB is important for cell shape but not for chromosome segregation of the filamentous cyanobacterium Anabaena sp. PCC 7120. *Mol Microbiol* **63:** 1640-1652

Huskens D, Ferir G, Vermeire K, Kehr JC, Balzarini J, Dittmann E, Schols D (2010) Microvirin, a novel alpha(1,2)-mannose-specific lectin isolated from Microcystis aeruginosa, has anti-HIV-1 activity comparable with that of cyanovirin-N but a much higher safety profile. *J Biol Chem* **285:** 24845-24854

Ibelings BW, Mur LR, Walsby AE (1991) Diurnal changes in buoyancy and vertical distribution in populations of Microcystisin two shallow lakes. *J Plankton Res* **13:** 419-436

Jain R, Rivera MC, Lake JA (1999) Horizontal gene transfer among genomes: the complexity hypothesis. *Proc Natl Acad Sci U S A* **96:** 3801-3806

Jain R, Rivera MC, Moore JE, Lake JA (2002) Horizontal gene transfer in microbial genome evolution. *Theor Popul Biol* **61:** 489-495

Jenke-Kodama H, Muller R, Dittmann E (2008) Evolutionary mechanisms underlying secondary metabolite diversity. *Prog Drug Res* **65:** 119, 121-140

Jenkins C, Samudrala R, Anderson I, Hedlund BP, Petroni G, Michailova N, Pinel N, Overbeek R, Rosati G, Staley JT (2002) Genes for the cytoskeletal protein tubulin in the bacterial genus Prosthecobacter. *Proc Natl Acad Sci U S A* **99:** 17049-17054

Jones LJ, Carballido-Lopez R, Errington J (2001) Control of cell shape in bacteria: helical, actin-like filaments in Bacillus subtilis. *Cell* **104:** 913-922

Kabsch W, Mannherz HG, Suck D, Pai EF, Holmes KC (1990) Atomic structure of the actin:DNase I complex. *Nature* **347:** 37-44

Kabsch W, Vandekerckhove J (1992) Structure and function of actin. *Annu Rev Biophys Biomol Struct* **21:** 49-76

Kandasamy MK, McKinney EC, Meagher RB (1999) The late pollen-specific actins in angiosperms. *Plant J* **18:** 681-691

Kaneko T, Nakajima N, Okamoto S, Suzuki I, Tanabe Y, Tamaoki M, Nakamura Y, Kasai F, Watanabe A, Kawashima K, Kishida Y, Ono A, Shimizu Y, Takahashi C, Minami C, Fujishiro T, Kohara M, Katoh M, Nakazaki N, Nakayama S, Yamada M, Tabata S, Watanabe MM (2007) Complete genomic structure of the bloom-forming toxic cyanobacterium Microcystis aeruginosa NIES-843. *DNA Res* **14:** 247-256

Kapoor P, Sahasrabuddhe AA, Kumar A, Mitra K, Siddiqi MI, Gupta CM (2008) An unconventional form of actin in protozoan hemoflagellate, Leishmania. *J Biol Chem* **283:** 22760-22773

Kehr JC, Zilliges Y, Springer A, Disney MD, Ratner DD, Bouchier C, Seeberger PH, de Marsac NT, Dittmann E (2006) A mannan binding lectin is involved in cell-cell attachment in a toxic strain of Microcystis aeruginosa. *Mol Microbiol* **59:** 893-906

Kim SY, Gitai Z, Kinkhabwala A, Shapiro L, Moerner WE (2006) Single molecules of the bacterial actin MreB undergo directed treadmilling motion in Caulobacter crescentus. *Proc Natl Acad Sci U S A* **103:** 10929-10934

Kinley AW, Weed SA, Weaver AM, Karginov AV, Bissonette E, Cooper JA, Parsons JT (2003) Cortactin interacts with WIP in regulating Arp2/3 activation and membrane protrusion. *Curr Biol* **13:** 384-393

Kohn JE, Millett IS, Jacob J, Zagrovic B, Dillon TM, Cingel N, Dothager RS, Seifert S, Thiyagarajan P, Sosnick TR, Hasan MZ, Pande VS, Ruczinski I, Doniach S, Plaxco KW (2004) Random-coil behavior and the dimensions of chemically unfolded proteins. *Proceedings of the National Academy of Sciences of the United States of America* **101:** 12491-12496

Komeili A, Li Z, Newman DK, Jensen GJ (2006) Magnetosomes are cell membrane invaginations organized by the actin-like protein MamK. *Science* **311:** 242-245

Koonin EV, Makarova KS, Wolf Y, Aravind L. (2002) Horizontal Gene Transfer and its Role in the Evolution of Prokaryotes. In Syvanen M, Kado CI (eds.), *Horizontal Gene Transfer*. Academic Press, London, pp. 277-304.

Korn ED (1978) Biochemistry of actomyosin-dependent cell motility (a review). *Proc Natl Acad Sci U S A* **75:** 588-599

Kruse T, Blagoev B, Lobner-Olesen A, Wachi M, Sasaki K, Iwai N, Mann M, Gerdes K (2006) Actin homolog MreB and RNA polymerase interact and are both required for chromosome segregation in Escherichia coli. *Genes Dev* **20:** 113-124

Kruse T, Bork-Jensen J, Gerdes K (2005) The morphogenetic MreBCD proteins of Escherichia coli form an essential membrane-bound complex. *Mol Microbiol* **55:** 78-89

Kruse T, Møller-Jensen J, Lobner-Olesen A, Gerdes K (2003) Dysfunctional MreB inhibits chromosome segregation in Escherichia coli. *Embo J* **22:** 5283-5292

Kuchibhatla A, Rasheed ASA, Narayanan J, Bellare J, Panda D (2009) An Analysis of FtsZ Assembly Using Small Angle X-ray Scattering and Electron Microscopy. *Langmuir* **25:** 3775-3785

Kurmayer R, Kutzenberger T (2003) Application of real-time PCR for quantification of microcystin genotypes in a population of the toxic cyanobacterium Microcystis sp. *Appl Environ Microbiol* **69:** 6723-6730

Laemmli UK (1970) Cleavage of structural proteins during the assembly of the head of bacteriophage T4. *Nature* **227:** 680-685

Lappalainen P, Kessels MM, Cope MJ, Drubin DG (1998) The ADF homology (ADF-H) domain: a highly exploited actin-binding module. *Mol Biol Cell* **9:** 1951-1959

Lara B, Rico AI, Petruzzelli S, Santona A, Dumas J, Biton J, Vicente M, Mingorance J, Massidda O (2005) Cell division in cocci: localization and properties of the Streptococcus pneumoniae FtsA protein. *Mol Microbiol* **55:** 699-711

Lazarides E, Lindberg U (1974) Actin is the naturally occurring inhibitor of deoxyribonuclease I. *Proc Natl Acad Sci U S A* **71:** 4742-4746

Le Rumeur E, Winder SJ, Hubert JF (2010) Dystrophin: more than just the sum of its parts. *Biochim Biophys Acta* **1804:** 1713-1722

Lee YM, Tscherne DM, Yun SI, Frolov I, Rice CM (2005) Dual mechanisms of pestiviral superinfection exclusion at entry and RNA replication. *J Virol* **79:** 3231-3242

Lepault J, Ranck JL, Erk I, Carlier MF (1994) Small angle X-ray scattering and electron cryomicroscopy study of actin filaments: role of the bound nucleotide in the structure of F-actin. *J Struct Biol* **112:** 79-91

Lindell D, Jaffe JD, Coleman ML, Futschik ME, Axmann IM, Rector T, Kettler G, Sullivan MB, Steen R, Hess WR, Church GM, Chisholm SW (2007) Genome-wide expression dynamics of a marine virus and host reveal features of co-evolution. *Nature* **449:** 83-86

Lodish H, Berk A, Zipursky LS, Matsudaira P, Baltimore D, Darnell J (2000) *Molecular Cell Biology*, 4th edition edn. New York: W. H. Freeman.

Lorenz M, Popp D, Holmes KC (1993) Refinement of the F-actin model against X-ray fiber diffraction data by the use of a directed mutation algorithm. *J Mol Biol* **234:** 826-836

Lunn JE, Price GD, Furbank RT (1999) Cloning and expression of a prokaryotic sucrose-phosphate synthase gene from the cyanobacterium Synechocystis sp. PCC 6803. *Plant Mol Biol* **40:** 297-305

Mabuchi I, Spudich JA (1980) Purification and properties of soluble actin from sea urchin eggs. *J Biochem* **87:** 785-802

Machesky LM, Atkinson SJ, Ampe C, Vandekerckhove J, Pollard TD (1994) Purification of a cortical complex containing two unconventional actins from Acanthamoeba by affinity chromatography on profilin-agarose. *J Cell Biol* **127:** 107-115

Machesky LM, Goldschmidt-Clermont PJ, Pollard TD (1990) The affinities of human platelet and Acanthamoeba profilin isoforms for polyphosphoinositides account for their relative abilities to inhibit phospholipase C. *Cell Regul* **1:** 937-950

Maciver SK, Ternent D, McLaughlin PJ (2000) Domain 2 of gelsolin binds directly to tropomyosin. *FEBS Lett* **473:** 71-75

Mackay MA, Norton RS, Borowitzka LJ (1984) Organic Osmoregulatory Solutes in Cyanobacteria. *J Gen Microbiol* **130:** 2177-2191

Madabhushi R, Marians KJ (2009) Actin homolog MreB affects chromosome segregation by regulating topoisomerase IV in Escherichia coli. *Mol Cell* **33:** 171-180

Madigan MT, Martinko J, Parker J. (2002) Brock Biology of Microorganisms, 10th edititon. Prentice Hall.

Mahoney NM, Janmey PA, Almo SC (1997) Structure of the profilin-poly-L-proline complex involved in morphogenesis and cytoskeletal regulation. *Nat Struct Biol* **4:** 953-960

Malicka-Blaszkiewicz M (1986) DNase I-like activity and actin content in the liver of some vertebrates. *Comp Biochem Physiol B* **84:** 207-209

Marin K, Stirnberg M, Eisenhut M, Kramer R, Hagemann M (2006) Osmotic stress in Synechocystis sp. PCC 6803: low tolerance towards nonionic osmotic stress results from lacking activation of glucosylglycerol accumulation. *Microbiology* **152:** 2023-2030

Martinez-Quiles N, Rohatgi R, Anton IM, Medina M, Saville SP, Miki H, Yamaguchi H, Takenawa T, Hartwig JH, Geha RS, Ramesh N (2001) WIP regulates N-WASP-mediated actin polymerization and filopodium formation. *Nat Cell Biol* **3:** 484-491

Mauriello EM, Mouhamar F, Nan B, Ducret A, Dai D, Zusman DR, Mignot T (2010) Bacterial motility complexes require the actin-like protein, MreB and the Ras homologue, MglA. *Embo J* **29:** 315-326

Mazel D (2006) Integrons: agents of bacterial evolution. *Nat Rev Microbiol* **4:** 608-620

Mazza P, Noens EE, Schirner K, Grantcharova N, Mommaas AM, Koerten HK, Muth G, Flardh K, van Wezel GP, Wohlleben W (2006) MreB of

Streptomyces coelicolor is not essential for vegetative growth but is required for the integrity of aerial hyphae and spores. *Mol Microbiol* **60:** 838-852

McDowell JM, Huang S, McKinney EC, An YQ, Meagher RB (1996) Structure and evolution of the actin gene family in Arabidopsis thaliana. *Genetics* **142:** 587-602

McGough A, Pope B, Chiu W, Weeds A (1997) Cofilin changes the twist of F-actin: implications for actin filament dynamics and cellular function. *J Cell Biol* **138:** 771-781

Meissner S (2010) Physiological functions of microcystin in *Microcystis aeruginosa* PCC 7806. Diploma thesis.

Miki H, Suetsugu S, Takenawa T (1998) WAVE, a novel WASP-family protein involved in actin reorganization induced by Rac. *Embo J* **17:** 6932-6941

Mikkat S, Effmert U, Hagemann M (1997) Uptake and use of the osmoprotective compounds trehalose, glucosylglycerol, and sucrose by the cyanobacterium Synechocystis sp. PCC6803. *Arch Microbiol* **167:** 112-118

Mittelbach P, Porod G (1961) Zur Röntgenkleinwinkelstreuung verdünnter kolloidaler Systeme. Die Berechunung der Streukurven von Parallelepipeden. *Acta Physica Austriaca* **14:** 185-211

Møller-Jensen J, Gerdes K (2004) Dynamic instability of a bacterial engine. *Science* **306:** 987-989

Moller-Jensen J, Jensen RB, Lowe J, Gerdes K (2002) Prokaryotic DNA segregation by an actin-like filament. *Embo J* **21:** 3119-3127

Møller-Jensen J, Jensen RB, Lowe J, Gerdes K (2002) Prokaryotic DNA segregation by an actin-like filament. *Embo J* **21:** 3119-3127

Montoya JP, Holl CM, Zehr JP, Hansen A, Villareal TA, Capone DG (2004) High rates of N2 fixation by unicellular diazotrophs in the oligotrophic Pacific Ocean. *Nature* **430:** 1027-1032

Moore PB, Huxley HE, DeRosier DJ (1970) Three-dimensional reconstruction of F-actin, thin filaments and decorated thin filaments. *J Mol Biol* **50:** 279-295

Mühling M, Fuller NJ, Millard A, Somerfield PJ, Marie D, Wilson WH, Scanlan DJ, Post AF, Joint I, Mann NH (2005) Genetic diversity of marine Synechococcus and co-occurring cyanophage communities: evidence for viral control of phytoplankton. *Environ Microbiol* **7:** 499-508

Mullins RD, Heuser JA, Pollard TD (1998) The interaction of Arp2/3 complex with actin: nucleation, high affinity pointed end capping, and formation of branching networks of filaments. *Proc Natl Acad Sci U S A* **95:** 6181-6186

Mullins RD, Kelleher JF, Pollard TD (1996) Actin' like actin? *Trends Cell Biol* **6:** 208-212

Mullins RD, Stafford WF, Pollard TD (1997) Structure, subunit topology, and actin-binding activity of the Arp2/3 complex from Acanthamoeba. *J Cell Biol* **136:** 331-343

Munoz-Espin D, Daniel R, Kawai Y, Carballido-Lopez R, Castilla-Llorente V, Errington J, Meijer WJ, Salas M (2009) The actin-like MreB cytoskeleton organizes viral DNA replication in bacteria. *Proc Natl Acad Sci U S A*

Neilan BA, Jacobs D, Goodman AE (1995) Genetic diversity and phylogeny of toxic cyanobacteria determined by DNA polymorphisms within the phycocyanin locus. *Appl Environ Microbiol* **61:** 3875-3883

Nenninger A, Mastroianni G, Mullineaux CW (2010) Size dependence of protein diffusion in the cytoplasm of Escherichia coli. *J Bacteriol* **192:** 4535-4540

Norman AI, Ivkov R, Forbes JG, Greer SC (2005) The polymerization of actin: Structural changes from small-angle neutron scattering. *Journal of Chemical Physics* **123:** -

Oda T, Iwasa M, Aihara T, Maeda Y, Narita A (2009) The nature of the globular- to fibrous-actin transition. *Nature* **457:** 441-445

Oda T, Namba K, Maeda Y (2005) Position and orientation of phalloidin in F-actin determined by X-ray fiber diffraction analysis. *Biophys J* **88:** 2727-2736

Orlova A, Garner EC, Galkin VE, Heuser J, Mullins RD, Egelman EH (2007) The structure of bacterial ParM filaments. *Nat Struct Mol Biol* **14:** 921-926

Orlova A, Yu X, Egelman EH (1994) Three-dimensional reconstruction of a co-complex of F-actin with antibody Fab fragments to actin's NH2 terminus. *Biophys J* **66:** 276-285

Orthaber D, Bergmann A, Glatter O (2000) SAXS experiments on absolute scale with Kratky systems using water as a secondary standard. *Journal of Applied Crystallography* **33:** 218-225

Otterbein LR, Graceffa P, Dominguez R (2001) The crystal structure of uncomplexed actin in the ADP state. *Science* **293:** 708-711

Paavilainen VO, Bertling E, Falck S, Lappalainen P (2004) Regulation of cytoskeletal dynamics by actin-monomer-binding proteins. *Trends Cell Biol* **14:** 386-394

Palenik B, Ren Q, Tai V, Paulsen IT (2009) Coastal Synechococcus metagenome reveals major roles for horizontal gene transfer and plasmids in population diversity. *Environ Microbiol* **11:** 349-359

Palmgren S, Vartiainen M, Lappalainen P (2002) Twinfilin, a molecular mailman for actin monomers. *J Cell Sci* **115:** 881-886

Pant K, Chereau D, Hatch V, Dominguez R, Lehman W (2006) Cortactin binding to F-actin revealed by electron microscopy and 3D reconstruction. *J Mol Biol* **359:** 840-847

Pantaloni D, Carlier MF (1993) How profilin promotes actin filament assembly in the presence of thymosin beta 4. *Cell* **75:** 1007-1014

Pantaloni D, Carlier MF, Coue M, Lal AA, Brenner SL, Korn ED (1984) The critical concentration of actin in the presence of ATP increases with the number concentration of filaments and approaches the critical concentration of actin.ADP. *J Biol Chem* **259:** 6274-6283

Pantaloni D, Le Clainche C, Carlier MF (2001) Mechanism of actin-based motility. *Science* **292:** 1502-1506

Paul JH (2008) Prophages in marine bacteria: dangerous molecular time bombs or the key to survival in the seas? *ISME J* **2:** 579-589

Paul JH, Sullivan MB (2005) Marine phage genomics: what have we learned? *Curr Opin Biotechnol* **16:** 299-307

Pedersen JS (1997) Analysis of small-angle scattering data from colloids and polymer solutions: modeling and least-squares fitting. *Advances in Colloid and Interface Science* **70:** 171-210

Peitsch MC, Polzar B, Stephan H, Crompton T, MacDonald HR, Mannherz HG, Tschopp J (1993) Characterization of the endogenous deoxyribonuclease involved in nuclear DNA degradation during apoptosis (programmed cell death). *Embo J* **12:** 371-377

Perelroizen I, Marchand JB, Blanchoin L, Didry D, Carlier MF (1994) Interaction of profilin with G-actin and poly(L-proline). *Biochemistry* **33:** 8472-8478

Peters G (1991) Azolla and other plant-cyanobacteria symbioses: Aspects of form and function. *Plant Soil* **137:** 25-36

Pichoff S, Lutkenhaus J (2005) Tethering the Z ring to the membrane through a conserved membrane targeting sequence in FtsA. *Mol Microbiol* **55:** 1722-1734

Pilhofer M, Rosati G, Ludwig W, Schleifer KH, Petroni G (2007) Coexistence of tubulins and ftsZ in different Prosthecobacter species. *Mol Biol Evol* **24:** 1439-1442

Polet D, Lambrechts A, Vandepoele K, Vandekerckhove J, Ampe C (2007) On the origin and evolution of vertebrate and viral profilins. *FEBS Lett* **581:** 211-217

Polka JK, Kollman JM, Agard DA, Mullins RD (2009) The structure and assembly dynamics of plasmid actin AlfA imply a novel mechanism of DNA segregation. *J Bacteriol* **191:** 6219-6230

Pollard TD. (1999) Introduction to actin and associated proteins. In T. K, R. V (eds.), *Guidebook to the Cytoskeletal and Motor Proteins*. Oxford Univ. Press, Oxford, UK, pp. 3–11.

Pollard TD, Blanchoin L, Mullins RD (2000) Molecular mechanisms controlling actin filament dynamics in nonmuscle cells. *Annu Rev Biophys Biomol Struct* **29:** 545-576

Pollard TD, Borisy GG (2003) Cellular motility driven by assembly and disassembly of actin filaments. *Cell* **112:** 453-465

Pollard TD, Cooper JA (2009) Actin, a central player in cell shape and movement. *Science* **326:** 1208-1212

Pollard TD, Quirk S. (1994) Profilins, ancient actin binding proteins with highly divergent primary structures. In Fambrough DM (ed.), *Molecular Evolution of Physiological Processes*. The Rockefeller University Press, New York.

Ponte P, Gunning P, Blau H, Kedes L (1983) Human actin genes are single copy for alpha-skeletal and alpha-cardiac actin but multicopy for beta- and gamma-cytoskeletal genes: 3' untranslated regions are isotype specific but are conserved in evolution. *Mol Cell Biol* **3:** 1783-1791

Popp D, Narita A, Ghoshdastider U, Maeda K, Maeda Y, Oda T, Fujisawa T, Onishi H, Ito K, Robinson RC (2010a) Polymeric structures and dynamic properties of the bacterial actin AlfA. *J Mol Biol* **397:** 1031-1041

Popp D, Narita A, Ghoshdastider U, Maeda K, Maeda Y, Oda T, Fujisawa T, Onishi H, Ito K, Robinson RC (2010b) Polymeric structures and dynamic properties of the bacterial actin AlfA. *J Mol Biol* **397:** 1031-1041

Popp D, Narita A, Maeda K, Fujisawa T, Ghoshdastider U, Iwasa M, Maeda Y, Robinson RC (2010c) Filament structure, organization, and dynamics in MreB sheets. *J Biol Chem* **285:** 15858-15865

Porchia AC, Salerno GL (1996) Sucrose biosynthesis in a prokaryotic organism: Presence of two sucrose-phosphate synthases in Anabaena with remarkable differences compared with the plant enzymes. *Proc Natl Acad Sci U S A* **93:** 13600-13604

Porebski S, Bailey L, Baum B (1997) Modification of a CTAB DNA extraction protocol for plants containing high polysaccharide and polyphenol components. *Plant Molecular Biology Reporter* **15:** 8-15

Purich DL, Allison RD (1999) *Handbook of Biochemical Kinetics: A Guide to Dynamic Processes in the Molecular Life Sciences*: Academic Press Inc.

Reed RH, Stewart WDP (1985) Osmotic adjustment and organic solute accumulation in unicellular cyanobacteria from freshwater and marine habitats. *Marine Biology* **88:** 1-9

Reinhard M, Giehl K, Abel K, Haffner C, Jarchau T, Hoppe V, Jockusch BM, Walter U (1995) The proline-rich focal adhesion and microfilament protein VASP is a ligand for profilins. *Embo J* **14:** 1583-1589

Rippka R. (1988) Recognition and identification of cyanobacteria. In Packer L, Glazer AN (eds.), *Methods in Enzymology vol 167*. Academic Press Inc., San Diego, pp. 28- 67.

Rippka R, Deruelles J, Waterbury JB, Herdman M, Stanier RY (1979) Generic assignments, strain histories and properties of pure cultures of cyanobacteria. *J Gen Microbiol* **111:** 1-61

Roeben A, Kofler C, Nagy I, Nickell S, Hartl FU, Bracher A (2006) Crystal structure of an archaeal actin homolog. *J Mol Biol* **358:** 145-156

Rogers MB, Patron NJ, Keeling PJ (2007) Horizontal transfer of a eukaryotic plastid-targeted protein gene to cyanobacteria. *BMC Biol* **5:** 26

Rokney A, Shagan M, Kessel M, Smith Y, Rosenshine I, Oppenheim AB (2009a) E. coli transports aggregated proteins to the poles by a specific and energy-dependent process. *J Mol Biol* **392:** 589-601

Rokney A, Shagan M, Kessel M, Smith Y, Rosenshine I, Oppenheim AB (2009b) E. coli transports aggregated proteins to the poles by a specific and energy-dependent process. *J Mol Biol* **392:** 589-601

Russel M (1995) Moving through the membrane with filamentous phages. *Trends Microbiol* **3:** 223-228

Sambrook J, Fritsch EF, Maniatis T (1989) Molecular cloning. A laboratory manual. *Cold Spring Harbour Lab Press*

Sangwan NS, Sangwan RS, Kumar S (1998) Isolation of Genomic DNA from the Antimalarial Plant Artemisia annua. *Plant Molecular Biology Reporter* **16:** 365-365

Savage DF, Afonso B, Chen AH, Silver PA (2010) Spatially ordered dynamics of the bacterial carbon fixation machinery. *Science* **327:** 1258-1261

Scheffel A, Gruska M, Faivre D, Linaroudis A, Plitzko JM, Schuler D (2006) An acidic protein aligns magnetosomes along a filamentous structure in magnetotactic bacteria. *Nature* **440:** 110-114

Scheffers DJ, Jones LJ, Errington J (2004) Several distinct localization patterns for penicillin-binding proteins in Bacillus subtilis. *Mol Microbiol* **51:** 749-764

Schmidt A, Hall MN (1998) Signaling to the actin cytoskeleton. *Annu Rev Cell Dev Biol* **14:** 305-338

Schnablegger H, Antonietti M, Goltner C, Hartmann J, Colfen H, Samori P, Rabe JP, Hager H, Heitz W (1999a) Morphological characterization of the molecular superstructure of polyphenylene ethynylene derivatives. *Journal of Colloid and Interface Science* **212:** 24-32

Schnablegger H, Antonietti M, Goltner C, Stapff IH, Brink-Spalink F, Greiner A (1999b) Investigations on the morphology of poly-1,4-(phenylethyl xylylene) in solution. *Acta Polymerica* **50:** 391-398

Scholey JM, Brust-Mascher I, Mogilner A (2003) Cell division. *Nature* **422:** 746-752

Schroer TA, Fyrberg E, Cooper JA, Waterston RH, Helfman D, Pollard TD, Meyer DI (1994) Actin-related protein nomenclature and classification. *J Cell Biol* **127:** 1777-1778

Schubbe S, Kube M, Scheffel A, Wawer C, Heyen U, Meyerdierks A, Madkour MH, Mayer F, Reinhardt R, Schuler D (2003) Characterization of a spontaneous nonmagnetic mutant of Magnetospirillum gryphiswaldense reveals a large deletion comprising a putative magnetosome island. *J Bacteriol* **185:** 5779-5790

Schutt CE, Myslik JC, Rozycki MD, Goonesekere NC, Lindberg U (1993) The structure of crystalline profilin-beta-actin. *Nature* **365:** 810-816

Schutt CE, Rozycki MD, Chik JK, Lindberg U (1995) Structural studies on the ribbon-to-helix transition in profilin: actin crystals. *Biophys J* **68:** 12S-17S; discussion 17S-18S

Shaevitz JW, Gitai Z (2010) The structure and function of bacterial actin homologs. *Cold Spring Harb Perspect Biol* **2:** a000364

Shebelut CW, Jensen RB, Gitai Z (2009) Growth conditions regulate the requirements for Caulobacter chromosome segregation. *J Bacteriol* **191:** 1097-1100

Shih YL, Kawagishi I, Rothfield L (2005) The MreB and Min cytoskeletal-like systems play independent roles in prokaryotic polar differentiation. *Mol Microbiol* **58:** 917-928

Smets BF, Barkay T (2005) Horizontal gene transfer: perspectives at a crossroads of scientific disciplines. *Nat Rev Microbiol* **3:** 675-678

Sorensen SJ, Bailey M, Hansen LH, Kroer N, Wuertz S (2005) Studying plasmid horizontal transfer in situ: a critical review. *Nat Rev Microbiol* **3:** 700-710

Soufo HJ, Graumann PL (2003) Actin-like proteins MreB and Mbl from Bacillus subtilis are required for bipolar positioning of replication origins. *Curr Biol* **13:** 1916-1920

Srinivasan R, Mishra M, Murata-Hori M, Balasubramanian MK (2007) Filament formation of the Escherichia coli actin-related protein, MreB, in fission yeast. *Curr Biol* **17:** 266-272

Steward WD, Rowell P, Rai AN (1983) Cyanobacteria-eukaryotic plant symbioses. *Ann Microbiol (Paris)* **134B:** 205-228

Straub BF (1942) In *Studies from the Institute of Medical Chemistry University Szeged*, Szent-Györgyi A (ed), Vol. 2, pp 3-15. Basel: S. Karger AG

Studier FW, Moffatt BA (1986) Use of bacteriophage T7 RNA polymerase to direct selective high-level expression of cloned genes. *J Mol Biol* **189:** 113-130

Sullivan MB, Lindell D, Lee JA, Thompson LR, Bielawski JP, Chisholm SW (2006) Prevalence and evolution of core photosystem II genes in marine cyanobacterial viruses and their hosts. *PLoS Biol* **4:** e234

Sun HQ, Yamamoto M, Mejillano M, Yin HL (1999) Gelsolin, a multifunctional actin regulatory protein. *J Biol Chem* **274:** 33179-33182

Suzuki E, Ohkawa H, Moriya K, Matsubara T, Nagaike Y, Iwasaki I, Fujiwara S, Tsuzuki M, Nakamura Y (2010) Carbohydrate metabolism in mutants of the cyanobacterium Synechococcus elongatus PCC 7942 defective in glycogen synthesis. *Appl Environ Microbiol* **76:** 3153-3159

Svitkina TM, Borisy GG (1999) Arp2/3 complex and actin depolymerizing factor/cofilin in dendritic organization and treadmilling of actin filament array in lamellipodia. *J Cell Biol* **145:** 1009-1026

Syvanen M, Kado CI (2002) *Horizontal gene transfer*, 2nd edition edn. London: Academic Press.

Takacs CN, Poggio S, Charbon G, Pucheault M, Vollmer W, Jacobs-Wagner C (2010) MreB drives de novo rod morphogenesis in Caulobacter crescentus via remodeling of the cell wall. *J Bacteriol* **192:** 1671-1684

Takizawa PA, Vale RD (2000) The myosin motor, Myo4p, binds Ash1 mRNA via the adapter protein, She3p. *Proc Natl Acad Sci U S A* **97:** 5273-5278

Tandeau de Marsac N (1977) Occurrence and nature of chromatic adaptation in cyanobacteria. *J Bacteriol* **April 130:** 82-91

Taoka A, Asada R, Wu LF, Fukumori Y (2007) Polymerization of the actin-like protein MamK, which is associated with magnetosomes. *J Bacteriol* **189:** 8737-8740

Tel-zur N, Abbo S, Myslabodski D, Mizrahi Y (1999) Modified CTAB Procedure for DNA Isolation from Epiphytic Cacti of the Genera Hylocereus and Selenicereus (Cactaceae). *Plant Molecular Biology Reporter* **17:** 249-254

Tepfer D, Garcia-Gonzales R, Mansouri H, Seruga M, Message B, Leach F, Perica MC (2003) Homology-dependent DNA transfer from plants to a soil bacterium under laboratory conditions: implications in evolution and horizontal gene transfer. *Transgenic Res* **12:** 425-437

Theriot JA, Mitchison TJ (1991) Actin microfilament dynamics in locomoting cells. *Nature* **352:** 126-131

Thomas CM, Nielsen KM (2005) Mechanisms of, and barriers to, horizontal gene transfer between bacteria. *Nat Rev Microbiol* **3:** 711-721

Thomas RH, Walsby AE (1985) Buoyancy Regulation in a Strain of Microcystis. *J Gen Microbiol* **131:** 799-809

Uehara T, Park JT (2008) Growth of Escherichia coli: significance of peptidoglycan degradation during elongation and septation. *J Bacteriol* **190:** 3914-3922

Upton C, Slack S, Hunter AL, Ehlers A, Roper RL (2003) Poxvirus orthologous clusters: toward defining the minimum essential poxvirus genome. *J Virol* **77:** 7590-7600

Usher KM, Bergman B, Raven JA (2007) Exploring Cyanobacterial Mutualisms. *Annual Review of Ecology, Evolution, and Systematics* **38:** 255-273

Utkilen H, Skulberg OM, Underdal B, Gjolme N, Skulberg R, Kotai J (1996) The rise and fall of a toxigenic population of Microcystis aeruginosa: a decade of

observations in Lake Akersvatnet, Norway. *Phycologia 35*: 189-197

van den Ent F, Amos L, Löwe J (2001a) Bacterial ancestry of actin and tubulin. *Curr Opin Microbiol* **4:** 634-638

van den Ent F, Amos LA, Löwe J (2001b) Prokaryotic origin of the actin cytoskeleton. *Nature* **413:** 39-44

van den Ent F, Johnson CM, Persons L, de Boer P, Lowe J (2010) Bacterial actin MreB assembles in complex with cell shape protein RodZ. *Embo J* **29:** 1081-1090

van den Ent F, Löwe J (2000) Crystal structure of the cell division protein FtsA from Thermotoga maritima. *Embo J* **19:** 5300-5307

van den Ent F, Møller-Jensen J, Amos LA, Gerdes K, Löwe J (2002) F-actin-like filaments formed by plasmid segregation protein ParM. *Embo J* **21:** 6935-6943

Varma A, de Pedro MA, Young KD (2007a) FtsZ directs a second mode of peptidoglycan synthesis in Escherichia coli. *J Bacteriol* **189:** 5692-5704

Varma A, Padh H, Shrivastava N (2007b) Plant genomic DNA isolation: an art or a science. *Biotechnol J* **2:** 386-392

Varma A, Young KD (2009) In Escherichia coli, MreB and FtsZ direct the synthesis of lateral cell wall via independent pathways that require PBP 2. *J Bacteriol* **191:** 3526-3533

Vetterkind S, Miki H, Takenawa T, Klawitz I, Scheidtmann KH, Preuss U (2002) The rat homologue of Wiskott-Aldrich syndrome protein (WASP)-interacting protein (WIP) associates with actin filaments, recruits N-WASP from the nucleus, and mediates mobilization of actin from stress fibers in favor of filopodia formation. *J Biol Chem* **277:** 87-95

Via-Ordorika L, Fastner J, Kurmayer R, Hisbergues M, Dittmann E, Komarek J, Erhard M, Chorus I (2004) Distribution of microcystin-producing and non-microcystin-producing Microcystis sp. in European freshwater bodies: detection of microcystins and microcystin genes in individual colonies. *Syst Appl Microbiol* **27:** 592-602

Vinson VK, Archer SJ, Lattman EE, Pollard TD, Torchia DA (1993) Three-dimensional solution structure of Acanthamoeba profilin-I. *J Cell Biol* **122:** 1277-1283

Vinson VK, De La Cruz EM, Higgs HN, Pollard TD (1998) Interactions of Acanthamoeba profilin with actin and nucleotides bound to actin. *Biochemistry* **37:** 10871-10880

Walcott S, Sun SX (2010) A mechanical model of actin stress fiber formation and substrate elasticity sensing in adherent cells. *Proc Natl Acad Sci U S A* **107:** 7757-7762

Walsby AE, Hayes PK (1989) Gas vesicle proteins. *Biochem J* **264:** 313-322

Wang S, Arellano-Santoyo H, Combs PA, Shaevitz JW (2010) Actin-like cytoskeleton filaments contribute to cell mechanics in bacteria. *Proc Natl Acad Sci U S A* **107:** 9182-9185

Wang YL (1985) Exchange of actin subunits at the leading edge of living fibroblasts: possible role of treadmilling. *J Cell Biol* **101:** 597-602

Welch MD, Mullins RD (2002) Cellular control of actin nucleation. *Annu Rev Cell Dev Biol* **18:** 247-288

Willmotte A. (1994) Molecular evolution and taxonomy of the cyanobacteria. In Bryant DA (ed.), *The molecular biology of cyanobacteria*. Kluwer Academic Publishers, Dordrecht/Boston/London, pp. 1-25.

Winder SJ, Ayscough KR (2005) Actin-binding proteins. *J Cell Sci* **118:** 651-654

Witke W (2004) The role of profilin complexes in cell motility and other cellular processes. *Trends Cell Biol* **14:** 461-469

Woodrum DT, Rich SA, Pollard TD (1975) Evidence for biased bidirectional polymerization of actin filaments using heavy meromyosin prepared by an improved method. *J Cell Biol* **67:** 231-237

Wu D, Hugenholtz P, Mavromatis K, Pukall R, Dalin E, Ivanova NN, Kunin V, Goodwin L, Wu M, Tindall BJ, Hooper SD, Pati A, Lykidis A, Spring S, Anderson IJ, D'Haeseleer P, Zemla A, Singer M, Lapidus A, Nolan M, Copeland A, Han C, Chen F, Cheng JF, Lucas S, Kerfeld C, Lang E, Gronow S, Chain P, Bruce D, Rubin EM, Kyrpides NC, Klenk HP, Eisen JA (2009) A phylogeny-driven genomic encyclopaedia of Bacteria and Archaea. *Nature* **462:** 1056-1060

Xu W, Baribault H, Adamson ED (1998) Vinculin knockout results in heart and brain defects during embryonic development. *Development* **125:** 327-337

Xu Y, Moseley JB, Sagot I, Poy F, Pellman D, Goode BL, Eck MJ (2004) Crystal structures of a Formin Homology-2 domain reveal a tethered dimer architecture. *Cell* **116:** 711-723

Yan K, Pearce KH, Payne DJ (2000) A conserved residue at the extreme C-terminus of FtsZ is critical for the FtsA-FtsZ interaction in Staphylococcus aureus. *Biochem Biophys Res Commun* **270:** 387-392

Yang C, Czech L, Gerboth S, Kojima S, Scita G, Svitkina T (2007) Novel roles of formin mDia2 in lamellipodia and filopodia formation in motile cells. *PLoS Biol* **5:** e317

Yarmola EG, Bubb MR (2009) How depolymerization can promote polymerization: the case of actin and profilin. *BioEssays* **31:** 1150-1160

Yarmola EG, Dranishnikov DA, Bubb MR (2008) Effect of profilin on actin critical concentration: a theoretical analysis. *Biophys J* **95:** 5544-5573

Yonezawa N, Nishida E, Iida K, Yahara I, Sakai H (1990) Inhibition of the interactions of cofilin, destrin, and deoxyribonuclease I with actin by phosphoinositides. *J Biol Chem* **265:** 8382-8386

Zilliges Y, Kehr JC, Mikkat S, Bouchier C, de Marsac NT, Borner T, Dittmann E (2008) An extracellular glycoprotein is implicated in cell-cell contacts in the toxic cyanobacterium Microcystis aeruginosa PCC 7806. *J Bacteriol* **190:** 2871-2879

Zwirglmaier K (2005) Fluorescence in situ hybridisation (FISH)--the next generation. *FEMS Microbiol Lett* **246:** 151-158

Publications, awards, conference contributions

Publications:

Guljamow A, Jenke-Kodama H, Saumweber H, Quillardet P, Frangeul L, Castets AM, Bouchier C, Tandeau de Marsac N, Dittmann E (2007) Horizontal gene transfer of two cytoskeletal elements from a eukaryote to a cyanobacterium. *Curr Biol* **17:** R757-759

Guljamow A, Delissen F, Baumann O, Thünemann AF, Dittmann E (2011) Unique properties of eukaryote-type actin and profilin horizontally transferred to cyanobacteria. *In preparation.*

Awards:

Humboldt-Preis 2007 for outstanding Diploma thesis.

Full grant for selected students 2010 to participate at the "QECG workshop" at Okinawa Institute of Science and Technology, Okinawa, Japan.

Conference contributions:

May 2010

Horizontal gene transfer of eukaryotic cytoskeletal elements within a complex bacterial community. *Poster presentation* at "QECG workshop" at Okinawa Institute of Science and Technology, Okinawa, Japan.

April 2009

Horizontal gene transfer of eukaryotic cytoskeletal elements within a complex bacterial community. *Poster presentation* at "Annual Conference of the Association for General and Applied Microbiology", Bochum, Germany.

April 2008

Horizontal gene transfer of eukaryotic cytoskeletal elements to Microcystis. *Poster presentation* at ESF-EMBO Symposium "Molecular Bioenergetics of Cyanobacteria: Towards Systems Biology Level of Understanding", Sant Feliu de Guixols, Spain.

April 2007

Horizontal gene transfer of two cytoskeletal elements from a eukaryote to a cyanobacterium. *Oral presentation* at "Annual Conference of the Association for General and Applied Microbiology", Osnabrück, Germany.

Acknowledgement

Even though a great number of people have contributed in their own way to the successful completion of this little project, I wish to express my gratitude towards Professor Elke Dittmann for showing trust and confidence in my humble abilities and letting me join her group to work on this most fascinating topic. Time and time again she has been a teacher, motivator and inspirator, drawing from a seemingly inexhaustible source of ideas.

This work would have been impossible without the helpful council, open ears and precious toys of Professor Andreas Thünemann, Friedmar Delißen, Professor Otto Baumann, Professor Harald Saumweber and Henk Castelijns. Without them, it would be gels and lanes and bands *ad infinitum*.

I thank all my colleagues for fighting the daily struggle with me and making lab life way easier. I thank Annika and Katrin for their strict upbringing, Nadine for her ceaseless, often meaningless but never pointless discussions. I am glad that I could always approach Jan-Christoph in matters of highest scientific complexity as well as utmost nonsense. Long before I realized the necessity of it for scientific success, I found Karsten, Reimo, Michi, Lili and Tobias to be the most willing accomplices in diversion and entertainment. A role which the young'uns, Katharina and Sven, also played to perfection. The lab's heart and souls, Jana, Conny and Petra shall not be forgotten here.

Special credits are due for Martin and Nadine for putting up with the raw and unrefined drafts of this here thing of mine.

I appreciate my family's effort of letting me be a scientist whenever I needed to be one, long even after having become one.

Finally, yet at the forefront, my love and appreciation goes out to Meene Kleene Kläre, whose patience, perseverance, deep affection and little tempers I couldn't have done without.

Eigenständigkeitserklärung

Gemäß §6 der Promotionsordnung der Mathematisch-Naturwissenschaftlichen Fakultät I der Humboldt-Universität zu Berlin in der Fassung vom 1. September 2005,

erkläre ich,

dass ich die vorliegende Arbeit selbständig angefertigt und ohne fremde Hilfe verfasst habe, keine außer den angegebenen Hilfsmitteln und Quellen dazu verwendet habe und die den benutzten Werken wörtlich oder inhaltlich entnommenen Stellen als solche kenntlich gemacht habe.

.....
Arthur Guljamow, Berlin, 21.06.2011